

Increase in Surface Temperature and Deep Layer Nitrate in the California Current:
A Spatiotemporal Analysis of Four-Dimensional Hydrographic Data

by

Lindsay Hennes

A Thesis Presented to the
Faculty of the USC Dornsife School of Letters, Arts and Sciences,
University of Southern California
In Partial Fulfillment of the
Requirements for the Degree
Master of Science
(Geographic Information Science and Technology)

May 2020

Table of Contents

List of Figures	vi
List of Tables	viii
Acknowledgements	ix
List of Abbreviations.....	x
Abstract	xi
Chapter 1 Introduction	1
1.1. Three-Dimensional Ocean Data	1
1.2. Southern California Current System Dynamics	3
1.3. Value of the SCCS.....	6
1.4. Climate Change and a Productivity Paradox	7
1.5. Research Goal	9
1.6. Structure of this Thesis	9
Chapter 2 Related Research.....	11
2.1. Phytoplankton and Nitrate	11
2.2. Temperature, Ocean Structure, and Movement	12
2.2.1. Stratification and the Thermocline	14
2.2.2. Light	15
2.2.3. Currents, Upwelling, and Other Sources of Motion and Mixing	15
2.3. Predictions of Decreased Surface Nitrate and Productivity as a Result of Surface Warming	17
2.4. Unexpected Increase in Productivity and Possible Mechanisms	19
2.5. GIS for Analysis of 3D Marine Environment	21
Chapter 3 Methods	26
3.1. Overview: Challenges and Solutions.....	26

3.2. Four-Dimensional Ocean Data.....	29
3.2.1. Data Collection Methods.....	29
3.2.2. Data Preparation	32
3.2.3. Development of Custom Iterative Workflows.....	36
3.3. Empirical Bayesian Kriging 3D	36
3.4. Export to Cross Sections and Data Merging Across Time: Preparation for Space Time Cubes	41
3.4.1. Horizontal Cross Sections	42
3.4.2. Vertical Cross Sections	44
3.5. Space Time Cubes	47
3.5.1. Constructing Horizontal Cross Section Space Time Cubes	48
3.5.2. Constructing Vertical Cross Section Space Time Cubes	49
3.6. Mann Kendall Trends	49
3.7. Visualization of Results	50
Chapter 4 Results	53
4.1. EBK3D.....	53
4.2. Space Time Cubes	55
4.3. Mann Kendall Trends	57
4.3.1. Temperature Trends	61
4.3.2. Nitrate Trends	65
Chapter 5 Discussion and Conclusions	71
5.1. Temperature	71
5.2. Nitrate	72
5.3. Source of the Nitrate Increase	74
5.4. Conclusion	77
References	81

Appendix A Iterative Workflows in ModelBuilder	86
Appendix B Trends Not Used in Main Body of Thesis	89
Appendix C Anomalous Nitrate Data	93
Appendix D Results with “Filmstrips”	94

List of Figures

Figure 1 CalCOFI 75 Station Positions.	2
Figure 2 Summary of SCCS dynamics	4
Figure 3 Illustrations of ocean mechanisms and structures.....	13
Figure 4 Ecological Marine Units (EMUs)	23
Figure 5 A conceptual summary of the workflow	26
Figure 6 CTD sampling.	30
Figure 7 3D Scene with Raw Data Points and CalCOFI Standard Stations.....	35
Figure 8 EBK3D and target points.	39
Figure 9 Example of cross validation	41
Figure 10 First portion of the model to create horizontal cross sections	42
Figure 11 Steps to convert a raster slice.....	43
Figure 12 Point shapefile of a vertical cross section.....	45
Figure 13 Schematic representing the process of creating vertical cross sections.	47
Figure 14 A conceptual view of vertical cross sections.	52
Figure 15 EBK3D results of interpolation of nitrate data	54
Figure 16 Cross validation results for EBK3D.....	55
Figure 17 Space Time Cube at 0m cross section showing temperature	56
Figure 18 Space Time Cube results at Line 93, temperature	57
Figure 19 Temperature trends at the sea surface (0m),.....	58
Figure 20 Nitrate trends on Line 93,.....	60
Figure 21 Horizontal cross sections showing temperature trends	63
Figure 22 Vertical cross sections showing temperature trends	64
Figure 23 Horizontal cross sections showing nitrate trends.....	67
Figure 24 Vertical cross sections showing nitrate trends.....	68

Figure 25 Vertical cross sections of nitrate trends, overlaid	70
Figure 26 Schematic representing mechanisms controlling nitrate transport	74
Figure 27 Research describing the California Current system.	75

List of Tables

Table 1 Datasets used in the completion of this project.....	32
Table 2 Summary of fields kept in <i>Casts</i> and <i>Bottles</i> tables	33
Table 3 Summary of observed Mann Kendall trends in temperature in horizontal cross sections from 1969-2018	62
Table 4 Summary of observed Mann Kendall trends in temperature in vertical cross sections from 1969-2018.....	62
Table 5 Summary of observed Mann Kendall trends in nitrate in horizontal cross sections from 1985-2017.....	66
Table 6 Summary of observed Mann Kendall trends in nitrate in vertical cross sections from 1985-2017	66

Acknowledgements

I would like to acknowledge all the help, advice, and encouragement provided by my mentor, Dr. Karen Kemp. I am very grateful to have had the chance to work with such an accomplished, yet down to earth role model. She provided excellent guidance on how to do great geospatial science, but also unerringly good judgement and kind introductions when I came up with bizarre ocean GIS questions and needed to email the experts. Dr. Kevin Butler was one of these experts, and I am very grateful to him for his advice on statistical tools and methods. Andy Cavatorta also deserves thanks for his valuable advice on the graphic design of presenting 4D data on a 2D page. I would also like to extend my gratitude to my thesis committee members, Dr. Su Jin Lee and Dr. Darren Ruddell for their feedback and advice on this project.

In addition, I would like to acknowledge the research group CalCOFI for providing both the data and the inspiration for this thesis. I was a volunteer on three CalCOFI research cruises several years ago, and that experience helped lead me to where I am today. I hope CalCOFI continues to collect great data at sea for many years to come.

Finally, I could not have survived the journey to thesis completion without the love and support of my family, friends, and boyfriend Ryan. All of these wonderful people patiently waited through my rants about data that was “underwater, in the wrong dimension,” dished out equal parts of gentle and tough-love encouragement, made some marvelous meals, provided hugs and back rubs, and accompanied me on the occasional hiking/sailing/snowboard adventure when I couldn’t look at a screen any longer. Special thanks to my brother Matt, who helped me build the computer that made this project possible. I’m deeply grateful to be surrounded by so many extraordinary people.

List of Abbreviations

3D	Three Dimensional
CC	California Current
CalCOFI	California Cooperative Oceanic Fisheries Investigations
CCE	California Current Ecosystem
CCS	California Current System
CDFW	Department of Fish and Wildlife
CTD	Conductivity Temperature Density (sensor)
CUC	California Undercurrent
dGPS	Differential GPS
EBK	Empirical Bayesian Kriging
EBK3D	Empirical Bayesian Kriging 3D
ENSO	El Nino Southern Oscillation
GIS	Geographic information system
NO ₃	Nitrate
NOAA	National Oceanic and Atmospheric Administration
PDO	Pacific Decadal Oscillation
SCCS	Southern California Current System
SIO	Scripps Institution of Oceanography
SST	Sea Surface Temperature
STC	Space Time Cube
USC	University of Southern California

Abstract

The Southern California Current System (SCCS) has been surveyed for 70 years by the research group CalCOFI, creating one of the longest running hydrographic datasets in the world.

CalCOFI, California Cooperative Oceanic Fisheries Investigations, was initially created in 1949 to monitor sardine fisheries, but since then its mission has expanded to include the study of many more organisms and abiotic hydrographic attributes. The area consistently surveyed by CalCOFI stretches from Point Conception to San Diego and extends approximately 700 km offshore. It encompasses a small portion of the path traversed by the California Current (CC) as it travels southward along the North American west coast. In the SCCS, primary productivity is limited by nitrate availability. In previous decades, episodes of sea surface warming have been associated with a decrease in primary productivity due to a strengthening of the thermocline, which prevents nitrate from moving from the deep layer to the surface. This has led to the belief that increases in sea surface temperature (SST) due to global climate change will cause a decrease in primary production in the SCCS. However, recent research indicates that, despite an increase in SST, primary production is increasing in the SCCS, possibly because nitrate concentration in the deep water is increasing. This project seeks to shed further light on this unexpected trend and determine (1) is SST increasing in the CCS, and (2) is nitrate concentration increasing in the deep water of the CCS? A unique workflow was created using Empirical Bayesian Kriging 3D and the Space Time Cube toolset in ArcGIS Pro to analyze spatial and temporal patterns in temperature and nitrate in CalCOFI's four-dimensional hydrographic dataset. Results show that SST and deep layer nitrate are increasing in parts of the CCS, particularly in the offshore portion of the study area. Comparison of spatial patterns to past research suggests increased nitrate may be delivered by the CC, perhaps due to global changes to circulation in the Pacific.

Chapter 1 Introduction

The oceans cover most of planet Earth, but mile-for-mile, our seas are relatively poorly studied and understood compared to terrestrial habitats. Furthermore, the vast majority of large-scale ocean research focuses on patterns observed in the surface of the ocean, as this is the portion accessible to satellite imaging. However, the ocean is a complex three-dimensional environment, continuously changing across the fourth dimension of time. Understanding three-dimensional patterns in the ocean is important because these processes affect climate and weather patterns, primary productivity, ecosystem structure, and economically important fisheries.

1.1. Three-Dimensional Ocean Data

Acquiring three-dimensional ocean data is rare, because gathering such data requires cost- and effort-intensive in situ measurements by a research vessel (Gnanadesikan et al. 2001). Due to the difficulty of collecting the data, long-term datasets of this nature are rare and valuable. CalCOFI, California Cooperative Oceanic Fisheries Investigations, is a collaboration between California Department of Fish and Wildlife (CDFW), National Oceanic and Atmospheric Administration (NOAA) Fisheries Service, and Scripps Institution of Oceanography (SIO). CalCOFI has been collecting hydrographic data in the California Current System (CCS) since 1949 and their dataset is the longest-running multidisciplinary oceanographic field dataset on record.

Initially created to study California's sardine fisheries, CalCOFI is on its 70th year of data collection as of 2019, with plans to continue indefinitely. Since its inception, the mission of CalCOFI has expanded to include measurement of many more attributes such as nutrients, climate research, management of living resources, and monitoring of invertebrates, seabirds, and marine mammals (Thompson et al. 2018).

Although the area of CalCOFI surveys varied in their early years, extending as far north as Oregon and as far south as the tip of Baja California, the 75 station pattern shown in Figure 1 has been surveyed most consistently, and is considered a standard survey today. Similarly, timing of surveys varied in the early years, taking place as frequently as once a month, and as infrequently as once every 3 years. Since the mid-1980's, however, surveys have consistently taken place once per season, or four times a year, although the precise dates change year-to-year. Datasets like this allow us to examine ocean structure, layering, and nutrient mixing that are invisible to satellite imaging of the surface.

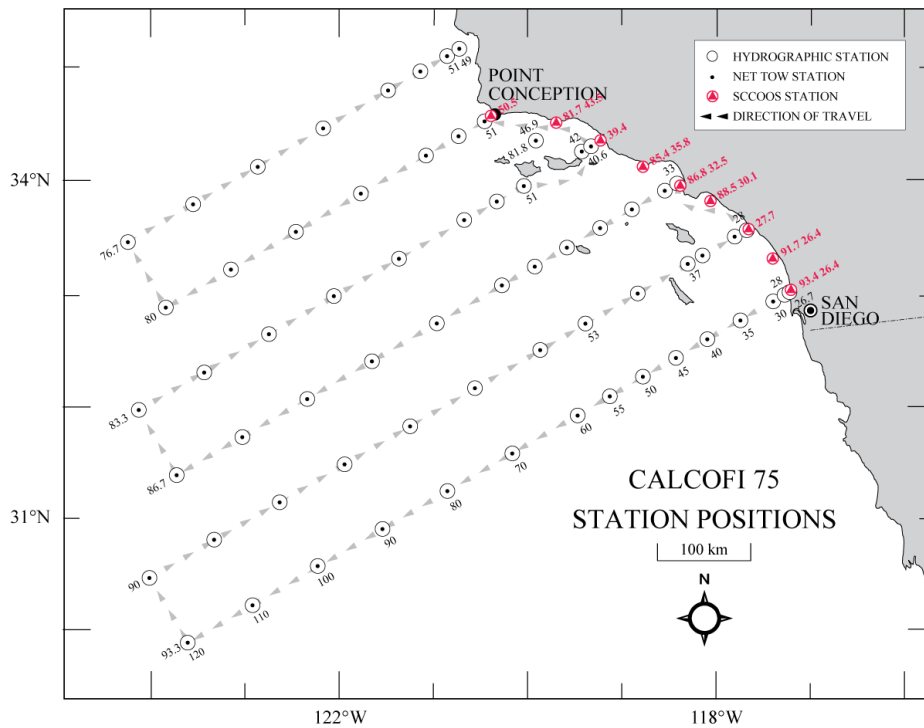


Figure 1 CalCOFI 75 Station Positions. Source: CalCOFI 2019a

Although three-dimensional ocean data is rare, it is critical to our understanding of the physical processes and ecosystems in the ocean. More so than most terrestrial environments, the ocean has a distinctive vertical structure. Although features of the ocean environment vary horizontally across latitude and longitude, most features change much more rapidly in the

vertical direction than the horizontal direction This results in several distinct ecosystems stacked on top of one another and mixing with one another. The CalCOFI dataset provides a unique opportunity to map the vertical structure of the California Current over several decades and observe changes over time.

1.2. Southern California Current System Dynamics

The California Current is the current that carries water southward along the North American west coast from British Columbia to Baja California, where the flow of water turns offshore towards the west. This is a highly productive coastal upwelling ecosystem. The area considered the Southern California Current System (SCCS) is the patch of ocean off the coast of southern California, stretching from San Diego on its southern end to Point Conception on the northern side, and extending to a maximum of approximately 700 km offshore. This area has been studied extensively thanks to the efforts of CalCOFI.

Figure 2 depicts a summarized version of the causal relationships between temperature, ocean structure and movement, nitrate, and phytoplankton in the SCCS. While other factors can and do play a factor in the relationships presented in Figure 2, research suggests that the ones featured here are the main contributors (Eppley, Renger, and Harrison 1979; Palacios et al. 2004; Roemmich and McGowan 1995).

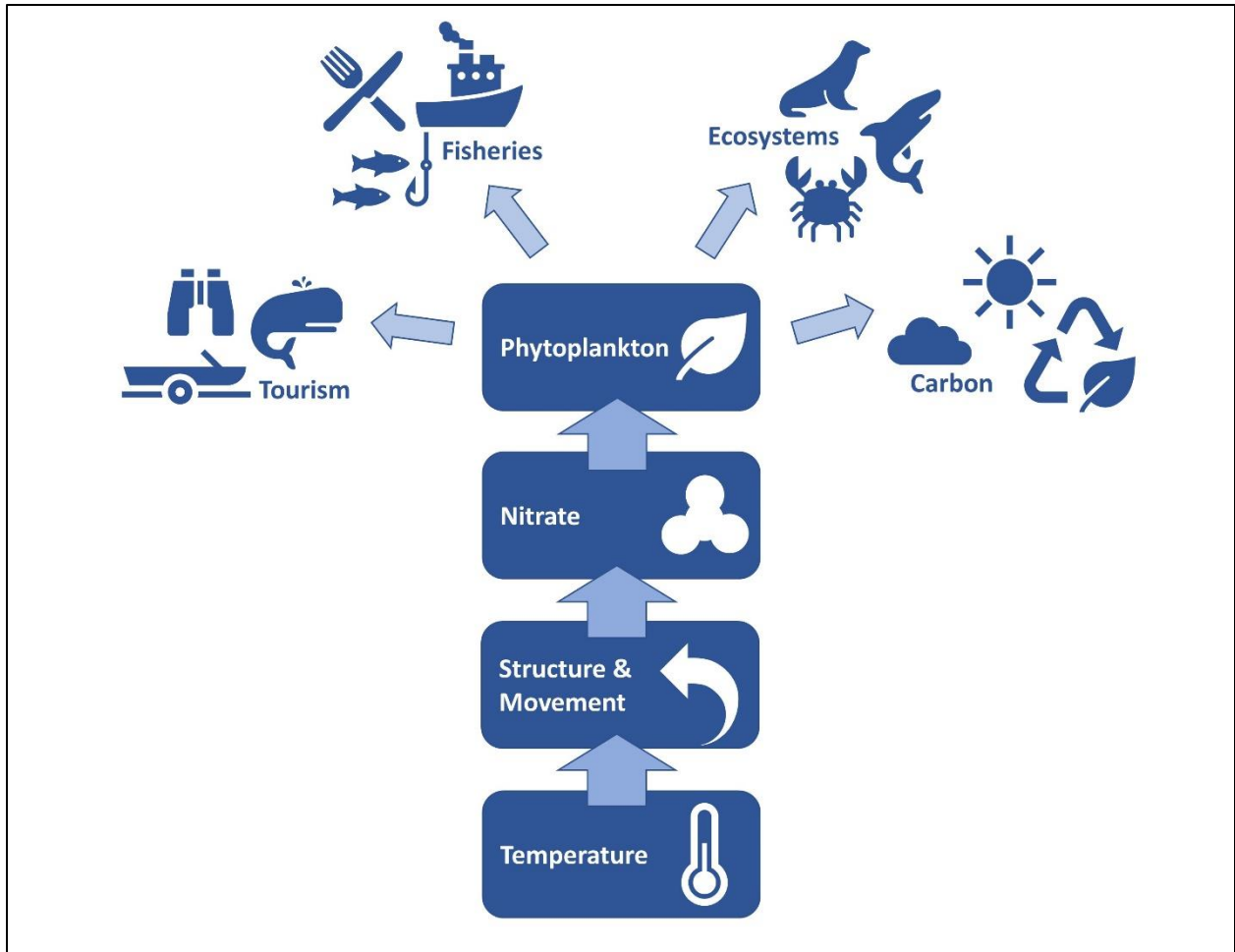


Figure 2 Summary of SCCS dynamics. Temperature plays a major role in determining ocean structure and movement, which determines how much nitrate reaches the surface. Nitrate availability is the limiting factor for phytoplankton, which are the primary producers that sustain the ecosystem, support fisheries, provide a destination for tourism, and even act as a carbon sink
 Source: Eppley, Renger and Harrison 1979; NOAA ENOW 2015; Stukel et al. 2017

Generally speaking, seawater temperature is the main factor that determines the arrangement of layers in the ocean, and how freely water moves and mixes throughout the water column. Specifically, in the CCS, temperature determines the location of the thermocline, a transitional layer sandwiched between the deep layer at the bottom and the mixed layer at the surface (Di Lorenzo et al. 2005; Palacios et al. 2004). The deep layer is nitrate-rich, and the surface is nitrate-poor, so the arrangement of layers and the ability of water and nutrients to move between them determines the availability of nitrate in the upper sunlit regions of the ocean.

The mixed layer above the thermocline is composed of relatively fresh, warm, low density water, while the deep layer below is composed of cold, salty, dense water. The greater the temperature difference between these two layers, the stronger the thermocline, and the less readily nitrate-rich water from the deep layer will move to the surface (Roemmich and McGowan 1995). Separation of the ocean into distinct layers that do not mix easily, by a strengthening thermocline for example, is commonly referred to as stratification.

Movement of nitrate to the surface is important because nitrate is the main nutrient that acts as a “fertilizer” for phytoplankton (microscopic marine algae). Thus, nitrate availability is the limiting factor for phytoplankton growth (Eppley 1979). Phytoplankton are single-celled algae, and like all algae, they derive their energy from photosynthesis, so they can only live in the sunlit euphotic zone at the surface of the ocean. In the California Current Ecosystem (CCE), a name frequently used to refer to the biological aspects to the CCS, phytoplankton are the primary producers that form the base of the marine food chain, nourishing everything from tiny larvae and zooplankton to huge schools of sardines and anchovies. This phytoplankton-fueled food chain is enormously valuable as the support for marine ecosystems, as the basis of commercially valuable fisheries and revenue-generating tourism, and as a carbon sink that might help mitigate climate change.

The amount of nitrate available at the surface controls the productivity of the phytoplankton, the strength of the thermocline controls the movement of nitrate to the surface, and the sea surface temperature (SST) controls the strength of the thermocline (Eppley 1979; Palacios et al. 2004; Roemmich and McGowan 1995). Understanding the relationships between the steps in this process is important, because changes to any step is likely to impact the biologic,

economic, and climatic role played by the SCCS. The past research that supports these connections is discussed in greater depth in Chapter 2.

1.3. Value of the SCCS

The SCCS is a home to a variety of unique marine ecosystems, as well as a hotspot for marine wildlife. This area encompasses open pelagic waters, rocky reefs and kelp forests, sandy and soft bottom habitats, and intertidal shoreline, which all support complex communities of organisms. Just within the Southern California Bight, the nearshore section of the SCCS on the continental shelf, the California Department of Fish and Wildlife has identified 481 species of fish, 195 species of bird, four species of sea turtle, and over 5000 species of invertebrates (Johnson, 2013). In addition, CalCOFI researchers have identified 6 species of pinnipeds, sea otters (1 species), and 18 species of cetacean in the SCCS (Antonelis and Fiscus 1980; Debich, Thayre, and Hildebrand 2017). As a coastal upwelling ecosystem where multiple currents mix, the SCCS hosts impressive biodiversity, in addition to enormous biological productivity.

The SCCS is also home to valuable commercial fisheries. In recent years, market squid and a variety of invertebrates including red urchin and spiny lobster have made up the majority of the fishery, although some fish are also harvested as well. In 2017, the combined value of the commercial fisheries in Santa Barbara area, Los Angeles area, and San Diego area was just under \$105 million (CDFW 2018).

While harvest of living resources is certainly noteworthy, revenue from commercial fisheries in the SCCS is dwarfed by revenue from tourism and recreation. In 2012, ocean-dependent tourism generated over \$8 billion in GDP in Santa Barbara, Ventura, Los Angeles, Orange, and San Diego counties, which comprise the coastline of the SCCS (NOAA ENOW

2015). The ocean ecosystem is a large contributor to ocean-dependent tourism, attracting visitors to the area for recreational diving, boating, fishing, whale/bird watching, and tide pooling.

Finally, recent research has shown that some ocean ecosystems, such as the SCCS can function as carbon sinks, with carbon captured from the atmosphere by phytoplankton eventually exported to the seafloor in the fecal pellets of phytoplankton grazers such as copepods and krill. Specifically, carbon export to the seafloor is higher in ocean systems where seawater fronts with differing temperature and salinity meet, such as the SCCS (Stukel et al. 2017).

1.4. Climate Change and a Productivity Paradox

Researchers forecast that climate change and the warming of the sea surface would cause a stronger thermocline in the CCS, which would prevent the movement of nitrate from the deep water to the surface and bring about a decline in primary productivity and biomass in the ecosystem (Palacios et al. 2004). This was demonstrated by Roemmich and McGowan (1995), who showed that surface temperature increases in the California Current from 1951 until the mid-90's were linked to as much as an 80% decrease in zooplankton in the waters off southern California. Zooplankton feed on the phytoplankton responsible for primary production. They attributed the decrease in zooplankton biomass to an increase in stratification caused by the increase in nutrients, which created a stronger thermocline, preventing nitrate from upwelling from the deep water and decreasing primary production.

Furthermore, researchers found that the thermocline deepened during a change in the Pacific Decadal Oscillation during the late 1970's (McGowan 2003; Di Lorenzo et al. 2005). Both papers describe the Pacific Decadal Oscillation (PDO), as well as El Nino (ENSO) affecting seawater temperatures and anticipated that the deepening of the thermocline would

mean nutrients would be even farther from the phytoplankton in the sunlit surface waters, further limiting primary production.

However, recent research has suggested that the prediction that climate change will bring about decreased primary productivity in the CCE may be incorrect. Satellite and in situ data all show that on average, sea surface temperature has increased, so it is generally accepted that climate change is likely affecting at least the surface layer of the CCE (Di Lorenzo et al. 2005, Roemmich and McGowan 1995). Many studies agree that the thermocline has strengthened (Palacios et al. 2004, Roemmich and McGowan 1995). However, chlorophyll a biomass (a proxy for primary productivity by phytoplankton) has increased (Nezlin et al. 2017). In addition, other researchers tested several methods of estimating total primary productivity from satellite photos and found that the best method matched up with in situ observations and showed an increase in productivity as well (Gnanadesikan et al. 2001, Kahru et al. 2009). This paradoxical result may be explained by an increase in the nitrate concentration in the deep water that supplies it. Research at nearshore and offshore stations showed that, overall, nitrate levels (measured at the pycnocline) have increased.

The cause for an increase in nitrate concentration in the deep water is uncertain, but one model-based research paper suggested a mechanism. A 2010 study suggested that global climate change has had a different effect on the whole system than previous, more regional climate fluctuations (Rykaczewski and Dunne 2010). The deep water in the CCE comes from the California Current, which carries cold, nutrient rich water from the north Pacific along the west coast of North America. The model suggested that as a result of global warming, this current would spend more time traveling along the coast beneath the euphotic zone, causing the water to spend more time picking up nutrients during the journey, which means it would arrive in the

CCE carrying a higher concentration of nitrate. According to the model, elevated nitrate concentration in the deep water circulating down from Alaska would be enough to cause increased primary productivity, despite prevention of vertical nitrate movement due to the strengthening of the thermocline.

1.5. Research Goal

As noted above, recent research has suggested that, counter to expectations based on sea surface warming, primary productivity in the CCE has increased over the past several decades. Some studies suggest that this may be due to an increase in nitrate in the deep layer. Nitrate is essential to primary production, and the quantity of nitrate present limits primary production in the CCE (Nezlin et al. 2017). To further investigate these findings, this project's goal was to determine if the long-term record of CalCOFI's hydrographic data can answer the following questions:

- 1) What are the spatial and temporal changes in temperature in the CCS over the past several decades? Do these indicate that sea surface temperatures are increasing in the CCS?
- 2) What are the spatial and temporal changes in nitrate in the CCS over the past several decades? Do these indicate that nitrate concentration is increasing in the deep water of the CCS?

In addition to creating a greater understanding of the vertical dynamics of the CCE, this project expands the use of GIS in the marine environment.

1.6. Structure of this Thesis

Following this introduction, Chapter 2 provides an in-depth exploration of related research in this field. Also in that chapter, the dynamics of the CCS and recent advances in using GIS to map 3D and 4D ocean datasets are discussed. Next, Chapter 3 Methods provides a detailed description of the steps taken and workflow created to obtain the desired results. The

methods were successful, and Chapter 4 Results describes the outputs of the analysis performed and features several figures for readers to visualize these results. Finally, Chapter 5 Discussion describes conclusions that can be drawn and presents possible causes for the patterns observable in the results.

Chapter 2 Related Research

There is a large body of existing research that supports the ideas presented in Figure 2, that ocean temperatures modulate stratification, stratification controls nitrate flux to the surface, and nitrate availability controls primary productivity by phytoplankton. This ideology leads to the prediction that surface nutrients and primary productivity will decrease in response to sea surface warming. However, more recently, some researchers have suggested that although sea surface temperatures are increasing, this pattern is not playing out as predicted, and primary productivity is actually increasing. These researchers suggest that this may be caused by an unexpected increase in deep layer nitrate. Research is ongoing to understand these discrepancies and reach consensus. While many previous researchers have used some form of spatial statistics to understand these trends, new GIS tools offer an opportunity to analyze spatial and temporal trends in this area with greater clarity and higher resolution.

2.1. Phytoplankton and Nitrate

Primary productivity is extremely important in ocean ecosystems. It is the energy entering at the base of the food chain – the energy that tiny phytoplankton convert from sunlight into organic matter through photosynthesis. This is the basis for all the fish and wildlife that build healthy ecosystems and valuable fisheries. Primary productivity forms the basis for all this. In the CCE, the phytoplankton that are responsible for primary productivity live near the surface, where sunlight can penetrate the seawater. However, there they are limited by the availability of nitrate (Eppley 1979; Rykaczewski and Dunne 2010). Nitrate is scarce in surface waters, because the phytoplankton use up any available supply quickly. However, nitrogen concentrations are much higher in the cold, dark, deep water below. Previous research indicates that most of the primary productivity in the CCE is controlled by the vertical movement of nitrate from the deep

water to the productive surface waters, as opposed to horizontal advection from coastal sources or movement by surface currents (Nezlin et al. 2017).

2.2. Temperature, Ocean Structure, and Movement

Several factors regulate the structure and movement of the ocean, and how nutrients are transported through the water column. In the SCCS, temperature plays the largest role in determining the arrangement of layers in the ocean. Light availability dictates where phytoplankton can photosynthesize. Upwelling and currents move water and nutrients between layers and around ocean basins. While temperature plays a major regulating factor, it is the combination of all these physical factors that determines the productivity of the ecosystem. Since an awareness of these mechanisms is important for understanding the motivation for this project and the conclusions drawn from the results, these are depicted in Figure 3 and discussed in greater depth in the following sections.

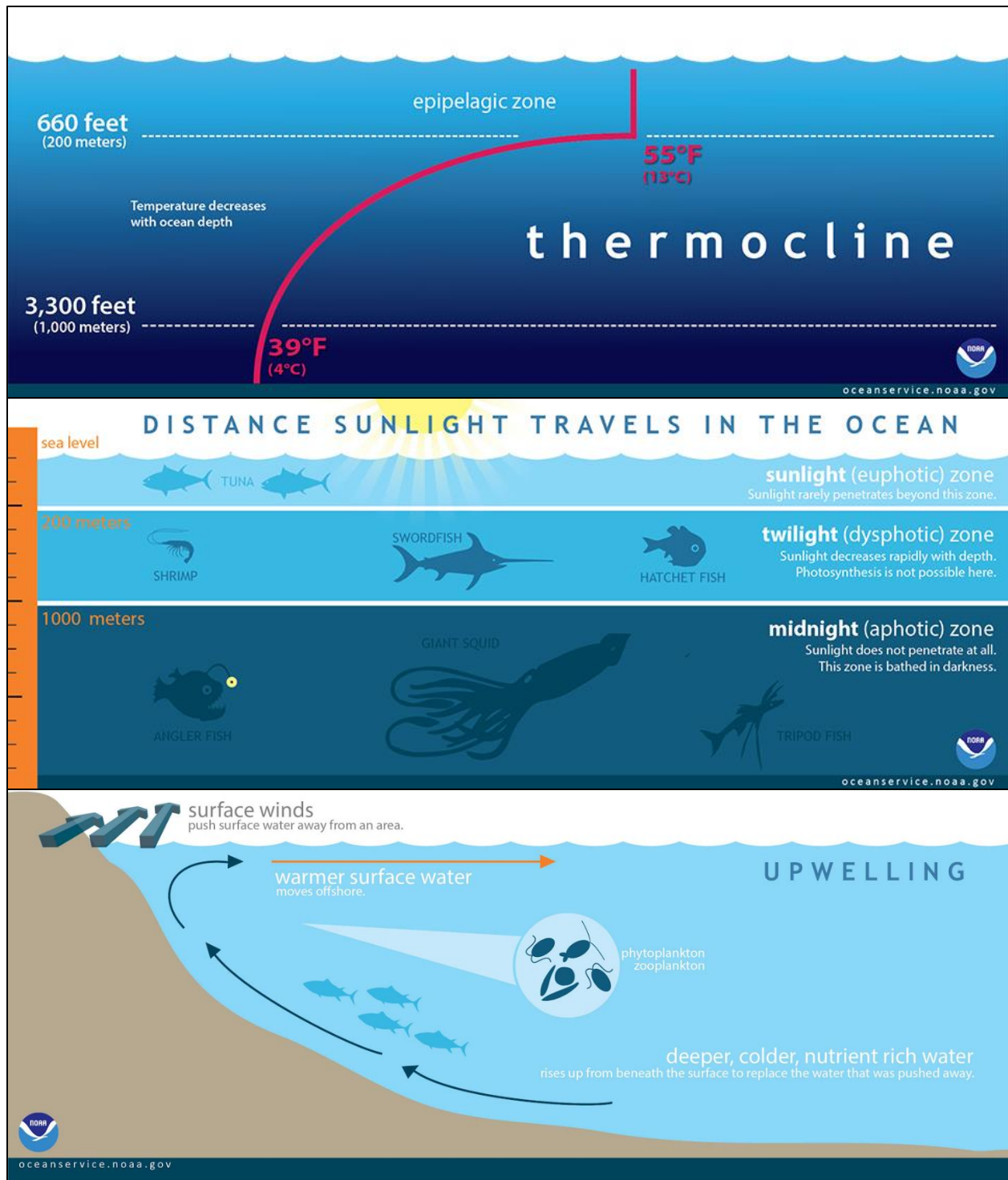


Figure 3 Illustrations of ocean mechanisms and structures (a) thermocline, (b) light-dependent zones, and (c) upwelling. Depths/temperatures are examples, and do not reflect conditions in the SCCS. Source: NOAA 2018a, NOAA 2018b, NOAA 2018c

2.2.1. Stratification and the Thermocline

In the California Current, seawater is stratified into layers of varying density, as illustrated in Figure 3. The surface water is relatively warm and fresh and is often referred to as the “mixed layer” because its temperature, salt, and nutrient concentrations are uniform, due to frequent mixing from movement of the sea surface. This can also be called the epipelagic zone. The deep water is cold, salty and denser than the surface mixed layer. Although it is not mixed much, it moves slowly, and is also homogeneous.

However, between the low-density surface layer and the bottommost layers, there is an area where density changes rapidly with depth, referred to as the pycnocline (Palacios et al. 2004). The pycnocline generally coincides with the thermocline (where temperature changes rapidly), halocline (where salinity changes rapidly), and/or nutricline (where nutrient concentrations change rapidly). This is partly because these factors are responsible for the density of the water, but also because the difference in density means that the surface water does not mix easily with the deep water, but rather floats on top. The pycnocline forms a barrier layer between the two.

In the California Current, temperature difference between the surface water and the deep water is mainly responsible for the pycnocline, so the terms thermocline and pycnocline are often used interchangeably in this region (Palacios et al. 2004). In the CCS, the depth of the thermocline is generally within the range of 30-70 m. The greater the temperature difference, the stronger the pycnocline, and the greater the barrier to mixing between layers. This prevents nutrients, such as nitrate, from reaching surface layers where phytoplankton live.

2.2.2. *Light*

Although temperature plays the largest role in the layering of the ocean, light affects the organisms that live there, and so the ocean can also be divided into layered zones according to how much light they receive, as shown in Figure 3 (NOAA, 2018b). The sunlit top layer of the ocean is called the euphotic zone. Beneath the euphotic zone is the barely-lit twilight or dysphotic zone, and further down is the completely dark midnight or aphotic zone. Macroalgae and phytoplankton live in the euphotic zone, where they can receive sunlight which they use for photosynthesis (NOAA, 2018b).

These light-determined ocean zones occupy and overlap with the temperature-dependent layers of the ocean. Generally, the mixed layer occupies approximately the same space at the surface as the euphotic zone. The thermocline may occupy the same region as the dysphotic zone, and the deep layer will overlap with the aphotic zone, but the precise arrangement depends on the temperature structure and light-permeability of the ocean in that region and season. The arrangement of these zones and layers impacts the organisms that live within them.

Phytoplankton cannot live or grow without nutrients, the nutrients come from either coastal inputs, or the deep layer. The thermocline forms the barrier between the nutrient-rich deep layer and the mixing layer and has a large impact on the amount of nutrients the phytoplankton receive, and thus the productivity of the entire ecosystem (Fielder et al. 2012).

2.2.3. *Currents, Upwelling, and Other Sources of Motion and Mixing*

The CCS is an Eastern Boundary Current, which means it flows along a continent on the eastern side of an ocean basin (and thus the western coast of the continent). Information on the CCS presented here is derived from a summary of research on the location, motion, and dynamics of the CCS and other currents on the North American west coast by Gangopadhyay et

al. (2011). Eastern boundary currents are generally wide, slow-moving currents in comparison to western boundary currents, such as the Gulf Stream. Sources vary, but a compilation of studies estimates the CCS ranges from 100 to 1350 km wide, 0-500 m deep, and has a maximum velocity of 50-70 cm/s. (Gangopadhyay et al. 2011).

Although the CCS is the dominant current in the area, the study area is also affected by the California Undercurrent (CUC). This current flows northward along the continental slope, and its core is beneath the surface layer at 200-275 m deep. It is slower and much smaller than the CCS, but brings relatively warm, high-salinity water up from equatorial regions to mix with the colder, low-salinity water of the CCS.

Like all eastern boundary currents, the CCS is characterized by upwelling, and this process is the main mechanism that brings water and nutrients up from the deep layer to the surface, as illustrated by Figure 2. This mechanism is described by Fewings (2017), and the following description is drawn from her research. Upwelling is driven by a process called Eckman transport, in which a combination of coastal winds and the Coriolis force result in a net movement of water at 90 degrees to the right of the wind direction in the northern hemisphere (90 degrees to the left in the southern hemisphere). On the North American west coast, prevailing coastal winds are from the northwest (moving towards the southeast), generated as air heats up over the continent, rises, and then more air moves in from the ocean to replace it. As a result of Eckman transport, this means the surface water influenced by this wind has a net motion towards the southwest, moving offshore and towards the equator. As the surface water moves offshore, water from beneath upwells (moves upward) to replace it. This brings cold, nutrient rich water to the surface, and supplies nitrate to the phytoplankton of the CCS (Fewings 2017).

While upwelling is the major mechanism of mixing between ocean layers in the CCS, there are a few other possible methods. As ocean currents like the CCS interact with localized upwelling and other currents, such as the CUC, they generate localized temporary eddies (circular currents), jets (narrow high-speed flows), and squirts (fast-moving localized currents moving offshore). These short-lived, small-scale currents contribute to nutrient mixing as well. Friction between two currents, or the motion of the tide can also generate internal waves, which move along the interface of ocean layers of different density - at the thermocline, in the CCS. Because the density difference between layers of seawater is much smaller than the density difference between water and air, internal waves can be much larger (over 100m height) than the surface waves we are more familiar with.

In places where the large, slow waves “break” over seafloor topography, such as in the Santa Cruz and Catalina Basins, this can cause localized nutrient mixing as well (Emery 1956). Finally, it is possible that in some situations a storm or weather event could cause mixing, although it would take a powerful storm and a relatively shallow, weak thermocline for nutrients to be mixed to the surface by wind or wave action. It is important to consider all these mechanisms to understand nutrient mixing in the CCS, and how physical changes to the ocean environment might affect this complex process.

2.3. Predictions of Decreased Surface Nitrate and Productivity as a Result of Surface Warming

Research by Roemmich and McGowan demonstrated that surface temperature increases in the California Current from 1951 until the mid ‘90’s were linked to a decrease in zooplankton in the waters off southern California (Roemmich and McGowan 1995; McGowan 2003). During this time period, there was steady warming coupled with a relatively abrupt change in ocean

temperatures around 1976-1977, likely due to the Pacific Decadal Oscillation (PDO) and or El Nino (ENSO) along with an overall trend of climactic warming. During this time, zooplankton biomass decreased by 80%. Zooplankton feed on the phytoplankton responsible for primary production. These researchers attributed the decrease in zooplankton biomass to an increase in stratification caused by the increase in nutrients, which created a stronger thermocline, preventing nitrate from upwelling from the deep water and decreasing primary production. These papers lay the groundwork for the relationships laid out in Figure 2, where temperature controls stratification, stratification controls nitrate movement, and nitrate availability controls primary production by phytoplankton. Because surface warming during the ocean climate regime change in the mid 1970's was associated with a large decrease in zooplankton biomass, researchers predicted that other surface warming would have similar effects and cause a decrease in productivity.

Research demonstrates that surface waters in the California current are warming, and the thermocline is strengthening. In a 2004 paper, Palacios et al. examined changes in the thermocline along the entire California coast, from 1950 – 1993, using data from the World Ocean Database. They chose eight locations to study and found that mean thermocline depth ranged from 26 to 72 m. Temperature at the thermocline increased in all eight locations, and the depth of the thermocline increased significantly at four of the eight locations (and two showed a non-significant increase in depth) (Palacios et al. 2004). This is clear evidence of a strengthening and deepening of the thermocline over this time period, which would increase the barrier to nutrient movement. Based upon the results of McGowan (2003), Palacios et al. predicted that the strengthening of the thermocline that he and his team observed would cause a decrease in primary productivity.

Results presented in these papers contributed to the expectation that sea surface warming would cause increased stratification, decreased nitrate movement to the surface, and decreased primary productivity in the California Current Ecosystem (CCE). However, more recent papers have shown that productivity has not decreased and indicate that other dynamics may be at play.

2.4. Unexpected Increase in Productivity and Possible Mechanisms

In 2018, Nezlin et al. published an excellent paper investigating increases to productivity and nitrate in the SCCS. Like this project, their goal was to determine what trends were present in nitrate and primary productivity using data from CalCOFI as well as other monitoring stations. However, their main interest was to discern whether changes in nitrate were attributable to anthropogenic sources, so they made a wide comparison between offshore and nearshore trends. They found that productivity (measured with chlorophyll a fluorescence measurements as a proxy) is increasing in this region. They also found that deep layer nitrate is increasing. Their comparison between nearshore and offshore trends did not show a significant difference, indicating that anthropogenic sources of nitrate such as runoff, which would affect only the nearshore measurements, are not the driving cause of this pattern. While their time series analysis was excellent, Nezlin et al.'s results showed averaged trends for the entire offshore and onshore regions and did not find clear spatial patterns that might indicate the source of the increased nitrate. To build upon the findings of Nezlin and his team, this project aims to map the increases in nitrate at a much higher resolution, with the hope that any spatial patterns that emerge may provide a clue pointing to the source of the increasing nitrate.

There is one paper, published by Rykaczewski and Dunne in 2010, which provides a possible explanation for the increase in deep layer nitrate in the SCCS. Rykaczewski and Dunne created an earth system model at NOAA's Geophysical Fluid Dynamics Laboratory to forecast

ocean and climate conditions in the CCS based upon global dynamics. While the papers discussed so far have focused on localized change and trends within the CCS, this one applies a broader perspective based on global effects. Rykaczewski and Dunne's model predicts that nitrate in the upper 200m of the CCE will increase 80% by 2100 and provides an explanatory mechanism.

Their model compares future conditions in the scenario of global warming to pre-industrial era conditions, and predicts that as the global climate changes, a couple of important factors that affect the entire California Current (CC) will change. The source water of the CC is the north Pacific, and from the CC travels southward along the North American west coast, from British Columbia to Baja California, before it turns westward near the equator. A predicted decrease in downwelling of nutrient-poor surface waters in the north Pacific means that the water in the CC would start its journey with a lower percentage of the nutrient-poor water mass, and thus a higher percentage of nitrate-rich water. This effect accounts for about 20% of the observed increase in nitrate in the SCCS.

The larger contributor (about 80%), according to Rykaczewski and Dunne's model, is a difference in the amount of travel time the water in the CC spends beneath the euphotic zone, where phytoplankton will rapidly use any available nitrate. First, the gyres in the north Pacific are predicted to shift further north, so the CC would begin its journey further north and make a longer journey to southern California, picking up more nitrate along the way. Secondly, the depth of the source and trajectory of the CC is predicted to spend more time beneath the euphotic zone, so the water mass will lose less nitrate to phytoplankton in the euphotic zone along its journey. Thus, more nitrate will be delivered by the current to the SCCS.

While the model applied by Rykaczewski and Dunne provides a useful forecast and explanatory mechanisms, their predictions require support from real in situ data. This project aimed to map spatial and temporal trends in nitrate, which may be able to lend support to the idea that nitrate is increasing and that it is supplied by the CC, as suggested by Rykaczewski and Dunne's model.

2.5. GIS for Analysis of 3D Marine Environment

One of the main purposes of this project is to use geographic information systems (GIS) techniques to provide more clarity and map spatial and temporal trends in hydrographic data with higher resolution than previous efforts. Fortunately, the field of marine GIS is currently rapidly expanding. This is due in part to the fact that Esri's current chief scientist (since 2011) is "Deepsea" Dawn Wright, PhD., an experienced oceanographer. She has written two textbooks on ocean GIS and has led the effort to create GIS tools to study the ocean (Wright 2002). She is backed by other leading oceanographers, such as the famous Sylvia Earle, who wrote in a foreword to one of Dr. Wright's books,

Concerns are growing about the collapse of once numerous species of fish and marine mammals, about polluted beaches, toxic algal blooms, "dead zones," and increased occurrence of water-borne diseases. Just as on land, GIS in the sea can facilitate identification of problem areas and help point the way toward solutions. Considering the volume of our oceans and the current rate of change, it is imperative that we make use of GIS as a tool to gain a better understanding of the dynamics of our oceans. -Sylvia Earle (Wright 2002, page ix)

Fortunately, teams at Esri have been hard at work mapping the oceans and developing tools for researchers to map their ocean data as well. One such tool is the Empirical Bayesian Kriging 3D (EBK3D) tool, which was released very recently, on Jan 24, 2019 with ArcGIS Pro 2.3. The EBK3D tool is useful here because it is designed for use specifically with oceanography data, as well as similar three-dimensional datasets, such as atmospheric or geologic data.

Empirical Bayesian Kriging is a useful method because it makes statistical predictions at each point based on the surrounding sample points and also provides an estimate of the error in the predictions. However, the previous two-dimensional version of the tool failed to account for the influence of nearby points in the vertical dimension. In many oceanography data and other three-dimensional datasets, the variables often change most quickly in the vertical direction, so failing to include this in analysis might lead to a significant amount of error. The release of the EBK3D tool opens new methods of data analysis and has not yet been utilized in any published work.

Secondly, the Space Time Cube Analysis toolbox, released within the past four years, contains several tools which allow a user to analyze spatial data over time. While previous studies have condensed nitrate concentration data down to a single time series summarizing average change over the entire region, the Space Time Cube toolbox will allow analysis of several time series at once. The Space Time Cube toolbox also includes an option to analyze the time series within each bin to test for Mann Kendall trends. This will independently indicate increase, decrease, or no significant trend within each bin, and allow a much clearer understanding of how the dataset is changing over time.

Finally, Esri has been developing methods and tools for mapping the world's oceans in 3D. Using NOAA's World Ocean Database, Esri has developed a 3D global map of Ecological Marine Units (EMU). There are 37 EMUs, each representing a different ecosystem in terms of abiotic chemical and physical features of the ocean, and each distinguished using geostatistical clustering to analyze a variety of marine attributes. This is the first global 3D ocean map of its kind, and it was a major inspiration for this project. EMUs surrounding Point Conception and along the California coast are shown in Figure 4. There are many avenues for future work to be

done with this sort of global to regional marine analysis, and this project seeks to explore some of these.

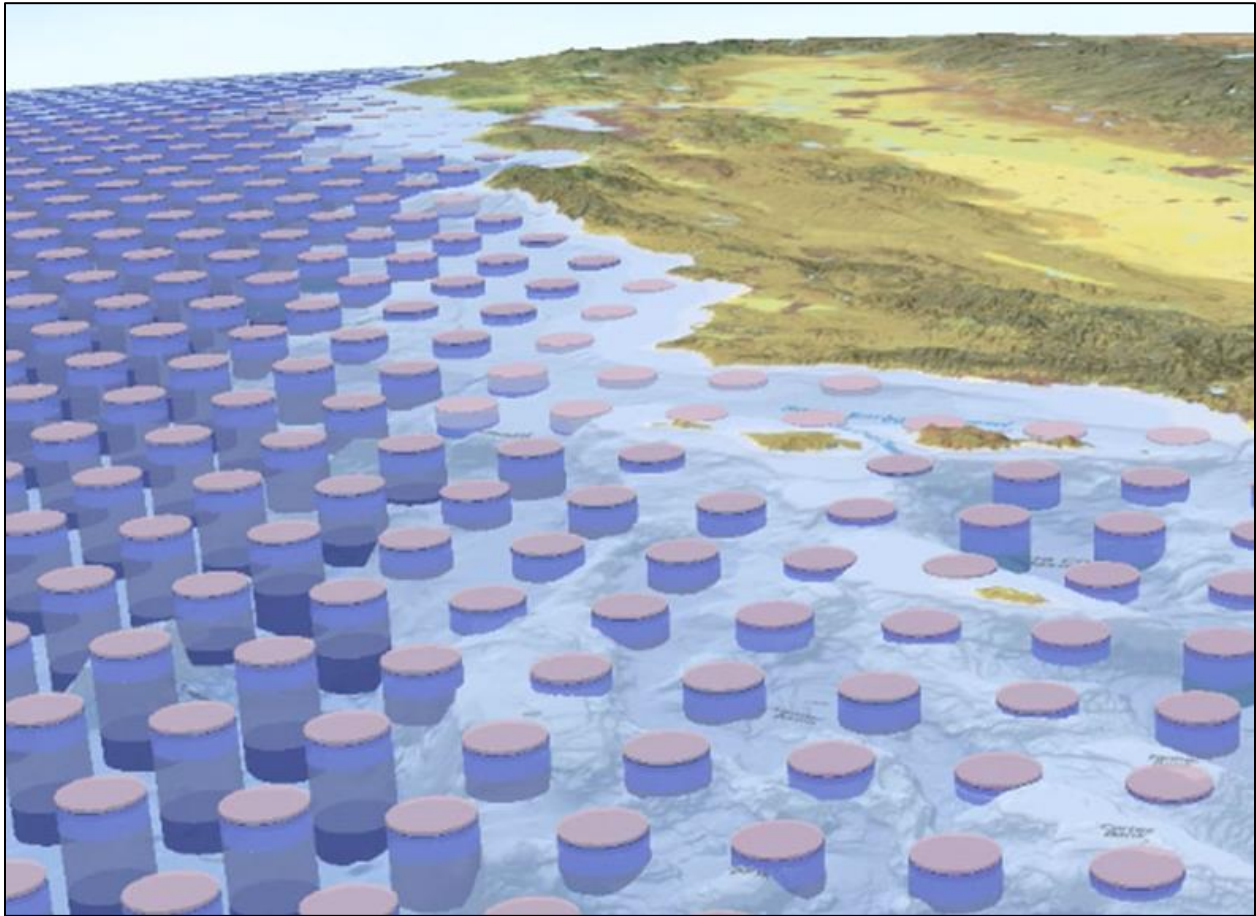


Figure 4 Ecological Marine Units (EMUs) along the California coast. Source: Sayre et al. 2017

First, while it is an impressive global map, Esri's EMU global map is relatively low-resolution. In July 2018, the Esri Oceans group published a workflow for independent researchers to apply their methods to analyze higher-resolution, local datasets using the same clustering geostatistical tools to define EMUs in a manner similar to that used to create Esri's global map (VanGraafeiland, 2018). This workflow was successfully applied to the CalCOFI dataset in the exploratory phase of this project, but it was determined that the raw data did not cluster neatly into groups (pseudo-f statistic did not indicate a greater difference between clusters

than within clusters), so local clusters could not be compared with Esri's global clusters (Sayre et al. 2017). Better comparison might be possible with more sophisticated data preparation.

However, one of the other main future goals of the EMU project is to understand change over time in the ocean, and this is a goal central to this project as well. It is difficult to meaningfully compare unsupervised clusters from one survey event to different unsupervised clusters from a different survey event, since the clusters' "fingerprint" set of parameters is different each time. Instead, the methods presented here, using EBK3D and the STC Toolset were developed to understand change over time within the 3D ocean environment.

The methods utilized in this project were developed partially based upon the research methods described in "The Warming of the California Current System: Dynamics and Ecosystem Implications" (Di Lorenzo et al. 2005). While they do not use tools in ArcGIS, this team of researchers created methods to understand change in temperature and salinity in the CC using "a four-dimensional space time analysis." To do this, they sorted 52-years of CalCOFI data into spatial and temporal bins, which they selected by hand (supervised classification) based upon the spatial and temporal location of the data. They then gridded each binned set of data to an objective map, performed their analysis, and plotted average trends for the whole region. Although they did not use tools in ArcGIS, their workflow was very similar to the objectives of this project.

Following similar logic, in the project reported here the data from each survey was interpolated using EBK3D and exported to gridded target points on several objective maps (representing cross sections). The space time cube toolset was used to sort the resulting cross-sectional maps into spatial and temporal bins. The methods presented here are intended to use tools in ArcGIS to build upon the methods developed by Di Lorenzo et al. While they examined

temperature and salinity, the goal here is to use this workflow to perform analysis on nitrate, an important variable not examined by Di Lorenzo et al., in addition to temperature. Furthermore, this project endeavors to create results showing trends with a high spatial resolution that may shed further light on the dynamics of the SCCS.

Chapter 3 Methods

Based upon a review of the literature, in addition to several conversations with the developers of the tools utilized in these methods, this workflow is novel and unique. This is due in part to the fact that some of the GIS tools used in these methods were released recently. Specifically, the three-dimensional interpolation tool, “Empirical Bayesian Kriging 3D” was released in early 2019, so there are very few examples of the use of this tool. Additionally, most of the Space Time Cube toolset became available in 2015 and 2016, and development is ongoing, so these tools are also relatively new. Published references to either the Space Time Cube toolset or Empirical Bayesian Kriging 3D are rare, and there are no references to any other workflows that use both in conjunction as this workflow does.

Since there are no previous examples of this workflow, care was taken during its development to justify each step and ensure each step is logically sound and statistically valid. Figure 5 shows a generalized version of the workflow used to accomplish the research goals. The following subchapters explain each step of this workflow in greater detail.

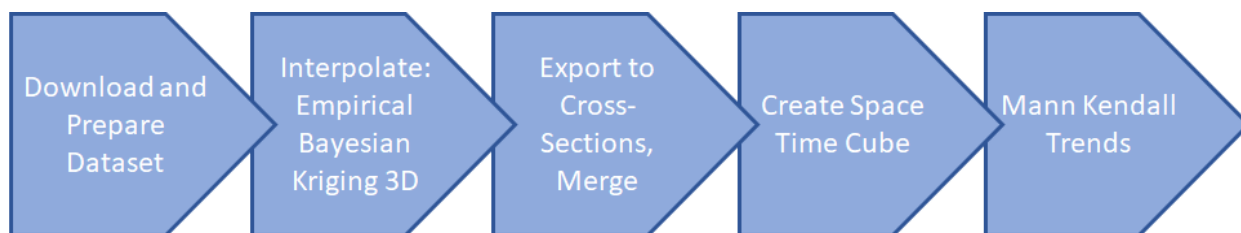


Figure 5 A conceptual summary of the workflow utilized for this project. Apart from the preparation of the data, each step was iterated several times for many surveys and/or cross sections.

3.1. Overview: Challenges and Solutions

Ocean data presents a unique challenge to traditional GIS methods. The ocean is a three-dimensional environment, where each point has a latitude, longitude, and depth. The addition of time creates a fourth dimension in the data. The fluid nature of the ocean dictates that time is an

extremely important element in ocean data - while landscape features like mountains and roads stay relatively fixed over time, features such as ocean currents, upwelling eddies, and algal blooms are subject to significant movement over months, seasons, and years.

It is difficult to accurately represent four-dimensional data on a two-dimensional page or screen. This is especially true if the data represents amorphous characteristics of the environment - in this case, varying concentrations of nutrients over time throughout the water column. In a three-dimensional ArcGIS Scene, this appears as vague colored clouds, where most of the data in the foreground obscures data farther back. With the addition of time, a sequence of muddy clouds is created, and it is extremely difficult for a viewer to visually recognize any clear trends. This is a major obstacle, as visualization of the data is an important tool to reaching a clear understanding of a system as complex and multifaceted as the ocean environment.

Apart from challenges in visualizing the data, it is also important to find an accurate and unbiased method of sorting and summarizing the data in order to gain a clear mathematical understanding of the data. For example, different spatial areas may experience different trends over time, and simply averaging all the data would likely ignore and obscure these trends. However, this dataset contains over 200,000 unique measurements, so is impossible to draw conclusions simply by comparing raw values. It is necessary to find an appropriate level of detail to portray spatial and temporal trends in the data.

Finally, oceanographic data collection is an imperfect science, subject to changes in weather, funding, equipment, crew, and sea state. While an ideal data set would contain only data collected at precisely the same points at precisely the same time and date each year, with the same vessel and equipment, in reality none of these factors are constant. While a multi-decadal dataset such as CalCOFI's is impressive in its reliability and standardization, the numerous

unpredictable factors present in oceanography work are nonetheless present. Samples were generally collected at the same locations each year, but there were exceptions. Similarly, survey dates were approximately seasonal, but varied depending on funding and vessel availability. Over several decades, the instruments used to measure attributes such as nutrients improved. While all data available on the calcofi.org website has been quality controlled, older instruments are liable to have greater error than newer ones (CalCOFI 2019b). Even measured perfectly, the ocean data itself does not perfectly follow mathematical curves but exhibits lots of noise and fluctuations due to the somewhat random interactions between weather in the atmosphere above and currents moving through the entire surrounding ocean basin.

To solve the issues of visualization, mathematical summary, and interpretation of imperfect samples and random noise, a few key strategies have been employed. First, 3D interpolation of the dataset from each survey creates a standardized pointfield of data in which locations are the same for each survey event, so data collected at the same locations can be compared across time. Secondly, division of the 3D data into 2D cross sections makes it much easier to visualize and allows the use of ArcGIS toolsets to mathematically analyze the data across both space and time. Specifically, the Space Time Cube pattern mining toolbox makes it possible to “stack” several “time slices” of data into a 3D grid of bins spread across the survey area (like pixels), then visualize and analyze temporal patterns in the bins. Finally, the Mann Kendall statistic can be used to summarize the trend in each vertical stack of bins (visualized as a column), indicating in a reliable and unbiased manner whether the temporal trend in the attribute represented across time in each bin-location is positive, negative, or not significant. Ultimately, this supplies the information necessary to show which attributes are increasing, decreasing, or

unchanging at each point in a series of cross sections depicting the entire three-dimensional spatial extent of the dataset.

3.2. Four-Dimensional Ocean Data

CalCOFI's dataset is four-dimensional (three spatial and one time dimension), and that makes it difficult to collect, and difficult to analyze with traditional 2D and 3D analysis methods. However, years of surveys has allowed CalCOFI to continually improve and perfect their field sampling methods. Similarly, the tools and technology for modeling and analyzing the CalCOFI data has also come a long way since the era of hand-drawn contour maps when the project began (CalCOFI 2019b). Here, methods of data collection and analysis are summarized.

3.2.1. Data Collection Methods

CalCOFI surveys the study area four times each year, or once per season. Samples are collected by repeatedly casting a collection device (named a CTD) overboard from a research vessel, as shown in Figure 6 (CalCOFI 2019a). CalCOFI conducts surveys from a variety of research vessels, based upon logistical requirements and availability. A full list of vessels is available at calcofi.org, but recent surveys have been conducted on the Scripps research vessel *Sally Ride*, or the NOAA research vessel *Reuben Lasker* (CalCOFI 2019a). The vessel collects approximately 20 seawater samples using the CTD at each of 75 standard sampling stations, located along six transects off the California coast (Figure 1). The transects are referred to as Line 77, 80, 83, 87, 90, and 93 moving from north to south. These transects were designed to be perpendicular to the California coastline, and while the coastline is not a straight line, this is true in general. The transect lines are roughly 100 km apart and offshore the collection points are separated by approximately 100 km. Inshore, the distance between points on a transect line varies. Transects are usually traversed by the research vessel heading offshore from San Diego

along Line 93 until the vessel reaches the end, then briefly north, then inshore along Line 90, then north to Line 87, and so on, zig zagging along the transects from south to north. In the event of weather constraints or other logistical issues, this pattern is sometimes interrupted or adapted to fit the situation. Along each transect, the vessel stops at several stations (coordinate locations visited each survey) to collect samples. At each station, the vessel uses a crane and winch to lift the CTD into the water and lower it to the desired depth (typically about 500m, bottom depth permitting).

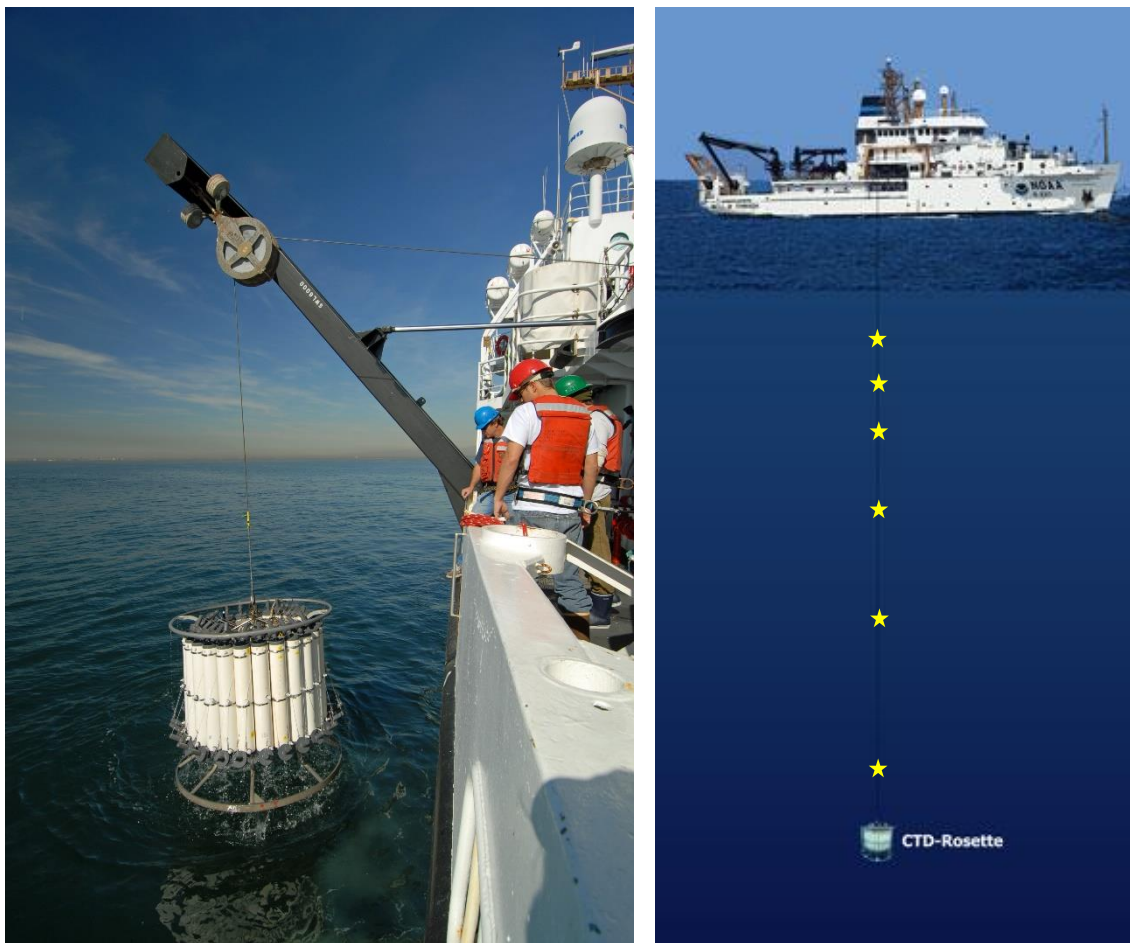


Figure 6 CTD sampling. (Left) The CTD is lowered from the research vessel. The white cylinders are the Niskin “bottles” that collect seawater samples. (Right) Schematic showing the CTD beneath the research vessel. Stars indicate points where the CTD will take a water sample.

The CTD is named for its sensors, which detect conductivity, temperature, and depth of the seawater and relay these measurements to the vessel via a communications cable as it is lifted back into the ship. The standard CalCOFI CTD is composed of 24 Niskin bottles mounted on a “carousel,” which is equipped with mechanisms that allow researchers to trigger each bottle to snap closed from the ship, trapping a water sample from the desired depth inside (CalCOFI 2019b). Decades ago, bottles were triggered mechanically, and CTDs used reversing thermometers, which were triggered to flip upside-down, thereby recording the temperature at the depth where the thermometer was triggered to flip. Early CalCOFI data was collected in this manner. Today, however, the CTD is equipped with sensors including a digital thermometer that continuously relays temperature readings to the ship via the communications cable, and researchers can trigger bottles to collect a water sample from a computer. Bottles are triggered, sensor measurements are logged at these depths, and samples are collected “from the bottom up” as the CTD is winched up towards the surface from its maximum depth. When the CTD is brought back onboard the research vessel, water samples are taken from each bottle and analyzed for nutrients, oxygen, and other variables of interest.

The variables of interest for this project are temperature and nitrate. In early CalCOFI surveys, temperature was measured using an (analog) reversing thermometer, but since 1993, they have been measured digitally by the CTD sensors (CalCOFI 2019a). CalCOFI started measuring nitrate in 1961, but nitrate samples were not collected consistently across the whole sample area until 1969. Nitrate concentration is measured onboard using colorimetric assays performed on a QuAatro continuous segmented flow autoanalyzer (SEAL Analytical), although prior to 2003 an AutoAnalyzer 3 (AA3) was used for nutrient analysis. (CalCOFI 2019c). Nitrate

is measured in micromoles per liter. Further details concerning sampling methods are available on the CalCOFI website at calcofi.org.

3.2.2. Data Preparation

Five datasets were used in this workflow, as shown in Table 1. The main files utilized were the CalCOFI *Casts* and *Bottles* datasets, which together contained all the hydrographic data necessary for the project. However, a couple more datasets were necessary for clipping the 3D study area to the correct extent and defining cross sections. The polygon defining the study area in the “CalCOFI 75 Station Area” was used to clip data to the correct extent in the horizontal direction, and the point shapefile “CalCOFI 75 Stations” was used to define transect lines where vertical cross sections were “sliced.” The bathymetry DEM SRTM30Plus was used to trim vertical cross sections where seafloor features intruded into the 0-500 m depth range survey.

Table 1 Datasets used in the completion of this project, with sources and a brief description of contents.

Name	Source	File Type	Description
CalCOFI <i>Casts</i>	calcofi.org	CSV	contains Cst_Cnt (Cast Count), cast ID, coordinates, station, date, survey, vessel, and weather information
CalCOFI <i>Bottles</i>	calcofi.org	CSV	contains Cst_Cnt (Cast Count), cast ID, and attribute information for each depth sampled on each cast, incl. temperature, salinity, density, nutrients, oxygen, chlorophyll, etc.
CalCOFI 75 Station Area	calcofi.org	KML	polygon depicting the study area encompassed by the routinely-sampled 75 stations
CalCOFI 75 Station	calcofi.org	KML	point locations of each of the 75 stations
SRTM30Plus	topex.ucsd.edu	KMZ	global bathymetry DEM with 30 arc-second resolution

To prepare the data for analysis, the two CalCOFI datasets, *Casts* and *Bottles* were downloaded as CSV files from the CalCOFI website, then opened in MS Excel. Here, all

columns concerning measurement values other than nitrate and temperature were removed, as well as any extraneous columns, such as weather and comments. This is summarized in Table 2. Both files were then imported into ArcGIS Pro, and converted using the “Excel to Table” script. The two tables were then joined on the field “Cst_Cnt,” (“Cast Count” abbreviated), the ID for each sampling event. This ensured that each sample had a spatial location and date, as well as a value for the attributes collected.

Table 2 Summary of fields kept in *Casts* and *Bottles* tables of CalCOFI data after trimming.

<i>Casts</i>	
Field Name	Description
Cst_Cnt	An ID number unique to each cast
Latitude	Latitude of the location where data was collected (not always exactly on the standard sampling station) in decimal degrees
Longitude	Longitude of the location where data was collected (not always exactly on the standard sampling station) in decimal degrees
Cruise	An ID number unique to each cruise, composed of the year and month when the cruise began (for example, an August 2019 cruise would be 201908). This field was later used for file names and to append dates to point shapefiles.
<i>Bottles</i>	
Field Name	Description
BottleID	An ID number unique to each bottle, or distinct sample in the 4D dataset.
Cst_Cnt	An ID number unique to each cast, used to join to <i>Casts</i> table
Depth	Depth in meters where the bottle sample was collected
Temp_DegC	Temperature in degrees Celsius
NO3	Nitrate concentration, in micromols per liter

Because nitrate was not sampled consistently until 1969, data from before this time was discarded. In addition, there were some points far outside the standard CalCOFI 75 Station Survey area, and these were also removed because these extra areas were only surveyed occasionally and cannot be used to represent trends across the entire time span. To accomplish this, the entire dataset was clipped to the CalCOFI 75 Station Survey Area, which is the most reliably surveyed station pattern over the decades. This is available on the CalCOFI website at calcofi.org as a KML file. To ensure no samples were lost at the edges of the survey area, a 50-

km buffer was applied, and all samples within this area were kept for analysis. After removing surveys that didn't measure nitrate, 181 surveys remained representing data collected for 50 years, from 1969 to 2018.

Once the combined table had been trimmed to the data of interest, it was plotted as a 3D point layer using "XY Table to Point." The points were plotted in a Local Scene in ArcGIS Pro using WGS 1984 UTM Zone 10N. This is displayed in Figure 7, where all points (within the visible extent) from 1969-2018 are shown. The whole study area is not shown in Figure 7 because displaying all the points in 3D was too much for the graphics card (AMD Radeon HD 7900) in the computer used for data analysis. To accurately compare surveys over time, it is necessary to compare values in the same locations. Since the data as they were collected are not in the same exact locations on each survey, it was necessary to interpolate the data into comparable 3D volumes and export the interpolated values to standardized sets of target points that can be fairly compared across surveys.

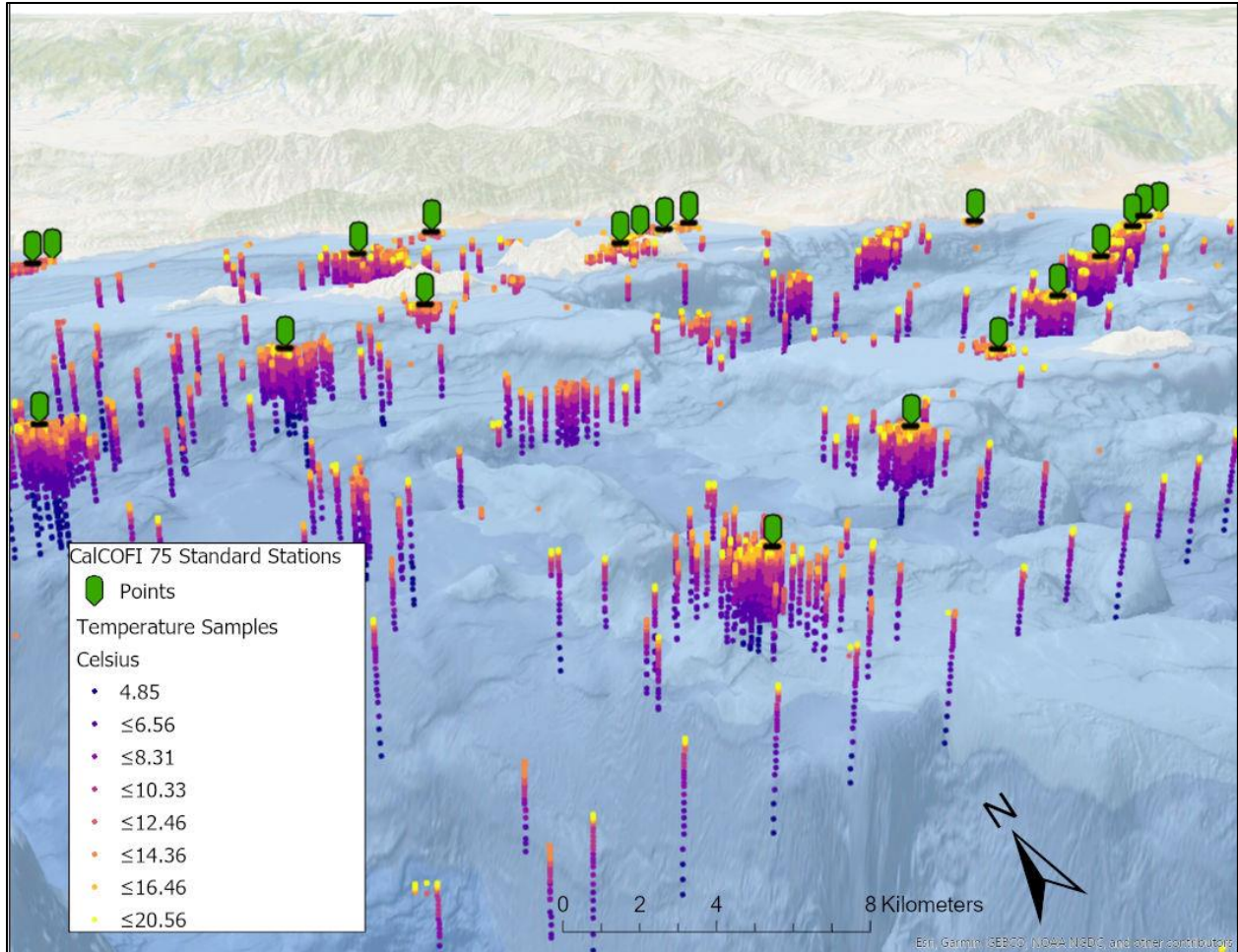


Figure 7 3D Scene with Raw Data Points and CalCOFI Standard Stations. Sample points are symbolized in a yellow-to-purple gradient to represent warm to cold temperature. CalCOFI stations are green bars at the top of the stacks of points. Note that sample points mostly cluster around CalCOFI stations but are not precisely located at the target coordinates.

While it is clear that most of the points in Figure 7 cluster around the CalCOFI stations, there is some clear variation. Some differences in sample collection location are caused by wind, weather, or other conditions inhibiting precise positioning of the research vessel. However, a portion of this variation is due to inaccuracy in the positioning system of the research vessels. CalCOFI began collecting data before GPS was invented. According to Dr. Sam McClatchie, early CalCOFI surveys used celestial navigation techniques, supplemented with Loran-A in the early 70's. Precise descriptions were not provided, but positional accuracy was described as

“within miles.” Next Loran-C was introduced (accuracy within 1 nautical mile), followed briefly by Omega navigation (accuracy unknown). GPS was adopted sometime in the late 70’s or 80’s, depending on the research vessel used, and today all of the research vessels used by CalCOFI are equipped with differential GPS (dGPS). (McClatchie, 2013) Units vary between vessels, but a typical dGPS unit would be similar to the Simrad MX512 unit used on the NOAA research vessel *Reuben Lasker*. This unit is accurate to under 3 meters if signal from a dGPS beacon is available, or within 5 meters if no beacon is available and the unit is only receiving satellite signal (NOAA OMAO 2017, Simrad 2010).

3.2.3. Development of Custom Iterative Workflows

To complete the analysis of this large multi-dimensional dataset, it was necessary to build several custom iterative workflows to automate the analytical processes. Namely, the data from each of 181 surveys was interpolated individually using EBK3D into two three-dimensional x,y,z cubes representing the relevant attribute (temperature or nitrate) throughout the volume of sea water in the study area. The results of each interpolation were “sliced” into six horizontal cross sections and six vertical cross sections, resulting in 12 output files (one for each slice) from each of the 181 survey events, for a total of 2,172 output files. It would have been prohibitively time-consuming to do all this by hand, so automation using iterators to repeat the same process for many subsets of data and files proved essential to the success of this project. Workflows were created as models using ModelBuilder in ArcGIS Pro. These are shown in Appendix A.

3.3. Empirical Bayesian Kriging 3D

The first step of data analysis was to use Esri’s new tool, Empirical Bayesian Kriging 3D, to interpolate the sample points into a three-dimensional prediction volume representing the

attribute of interest (temperature or nitrate). The following description is extracted from Esri's help pages about the tool (Esri 2019a). While the 2D Empirical Bayesian kriging tool is well-known and well-loved in the research community as a probabilistic tool for interpolating data into prediction surfaces with associated measures of error, this tool is only capable of handling two-dimensional data, where each point has an attribute value along with x- and y-coordinates. In many instances, the attribute value is treated as the third dimension, and the prediction surface is displayed as a three-dimensional elevation surface, where peaks represent high attribute values and valleys represent low attribute values. While this tool is extremely useful in many disciplines, it failed to accurately represent data that vary along x-, y-, and z-axes, as well as having an attribute value at each point in space.

The three-dimensional version of Empirical Bayesian Kriging works similarly to the well-known two-dimensional version, with a few key differences. Both two-dimensional and three-dimensional versions of EBK build semivariogram models based on subsets of the data and make predictions from the local models in the neighborhood of the prediction location, using the principle of spatial autocorrelation. Whereas traditional EBK uses distances on a 2D plane to build subsets and determine neighborhoods, EBK3D uses 3D Euclidean distances to determine these parameters.

A second important difference is that EBK3D includes an Elevation Inflation Factor. The elevation inflation factor corrects for the fact that in the ocean (or atmosphere, or geologic strata, or other earth environments), attribute values change faster in the vertical direction than the horizontal. Multiplying distances in the vertical direction by an elevation inflation factor is done to ensure that the data changes at approximately the same rate regardless of direction, which allows the creation of more accurate semivariograms and ensures the search neighborhood used

to make the prediction includes the most influential contributors and weights them appropriately. For analysis of this dataset, EBK3D was allowed to optimize the elevation inflation factor for each survey to obtain the best semivariograms, and in general the optimal elevation inflation factor fell in the range of 700 - 1000. After making the statistical calculation, the elevation inflation factor is removed. However, in this study, the data were later displayed after further analysis using an inflated vertical z-axis (by a factor of 1000) to allow better construction of a space time cube in later steps, and better visualization of the results.

The results of EBK3D occupy a cube of 3D space, but they can be more easily viewed in horizontal slices (cross sections), by using an elevation slider present in the EBK3D output display to select the z-value at which to display the values along a particular horizontal plane, as shown in Figure 8. While this is useful when visualizing and understanding values from a single survey at a single point in time, it is still difficult to compare the results of two different surveys - to do this, the data must be sliced into analogous cross sections that can be viewed side by side. Fortunately, the results of the EBK3D tool can be exported to either horizontal raster slices or 3D target points.

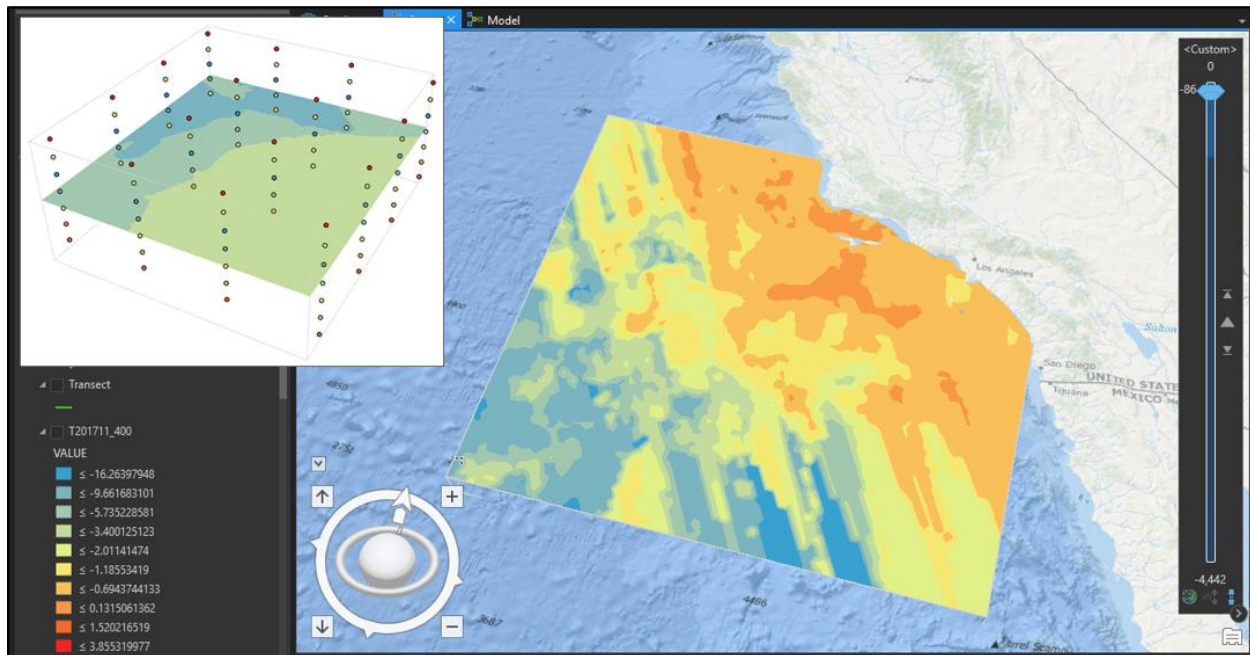


Figure 8 (Inset) Conceptual representation of EBK3D and target points. (Large Frame) Results of EBK3D with CalCOFI nitrate data, with depth slider on the right side. This image shows one horizontal plane of the 3D results.

The EBK3D tool has several parameters that can either be left as default for the tool to optimize, or manually specified by the user. As mentioned above, a custom workflow was developed for this project to iterate the process of interpolating the data from each of the surveys with EBK3D. Because there were 181 surveys, and both temperature and nitrate were analyzed from each one, this came to a total of 362 iterations of EBK3D. Adjusting the parameters of EBK3D manually for each of the 362 iterations surveys would have been prohibitively time-consuming. For this study, at the suggestion of Dr. Kevin Butler, parameters of EBK3D were left as defaults so that the EBK3D tool could adjust the values such as elevation inflation factor to best model each of the 181 surveys. Similarly, no transformations were applied to the data prior to use of EBK3D because this often caused errors due to zero values in the data (for Log Empirical Transformation), or no significant improvement (Empirical Transformation) and no

single transformation was effective for all 181 different surveys. No first order trend was removed, because there was not a first order trend present in all surveys.

The best way to ensure that EBK3D predictions are reliable is to view the results of cross validation. An example, showing nitrate measured on the survey of November 1987, is shown in Figure 9. Although it would have been prohibitively time consuming to examine the cross validation results of all 362 surveys, a subset of cross validation results from ten surveys were examined. For each attribute (temperature and nitrate), the cross validation results from one random survey from each decade were examined. In 9/10 cases, the cross validation results showed that EBK3D had produced very reliable results. Mean and mean standardized statistics were close to zero, indicating that the model had very little bias (Esri 2019a). In addition, root mean square values indicated that temperature predictions were all on average within a degree of the measured values, and 4/5 nitrate predictions were all within 1 micromol/liter of the measured value. The 10th survey was examined showed nitrate predictions from data collected in the 70's, and cross validation showed that the predictions were not accurate. Mean and Mean Standardized statistics were still fairly low, but the chart showed a wild scatter of points, and the root mean squared statistic indicated that on average predictions were over 9 micromol/liter different from measured values.

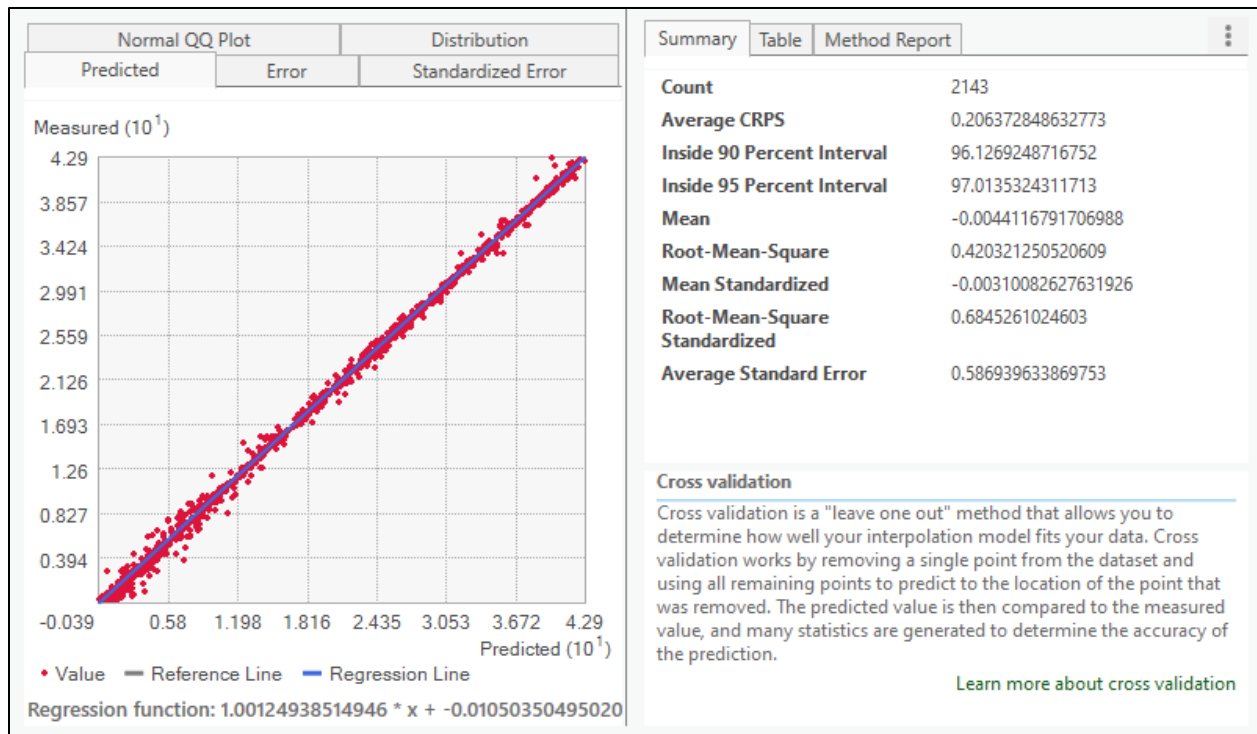


Figure 9 Example of cross validation results of EBK3D. This specific set of results came from the EBK3D output predictions of nitrate for the November 1987 survey.

3.4. Export to Cross Sections and Data Merging Across Time: Preparation for Space Time Cubes

Once the data had been interpolated into homologous 3D prediction surfaces, it was necessary to “slice” the 3D prediction volume into 2D cross sections to effectively visualize the data and analyze trends using the Space Time Cube toolset in the next step. In order to best represent the data, each 3D prediction volume was sliced into six horizontal cross sections at different depths below the sea surface, and six vertical cross sections along the six transects where the original data were collected. This is depicted in Figure 10, and the entire model is shown in Appendix A. The horizontal cross sections were created at 0 m, 100 m, 200 m, 300 m, 400 m, and 500 m below the sea surface. Vertical cross sections were created along the six transects in the standard CalCOFI 75 station survey, referred to (from north to south) as Line 77, Line 80, Line 83, Line 87, Line 90, and Line 93.

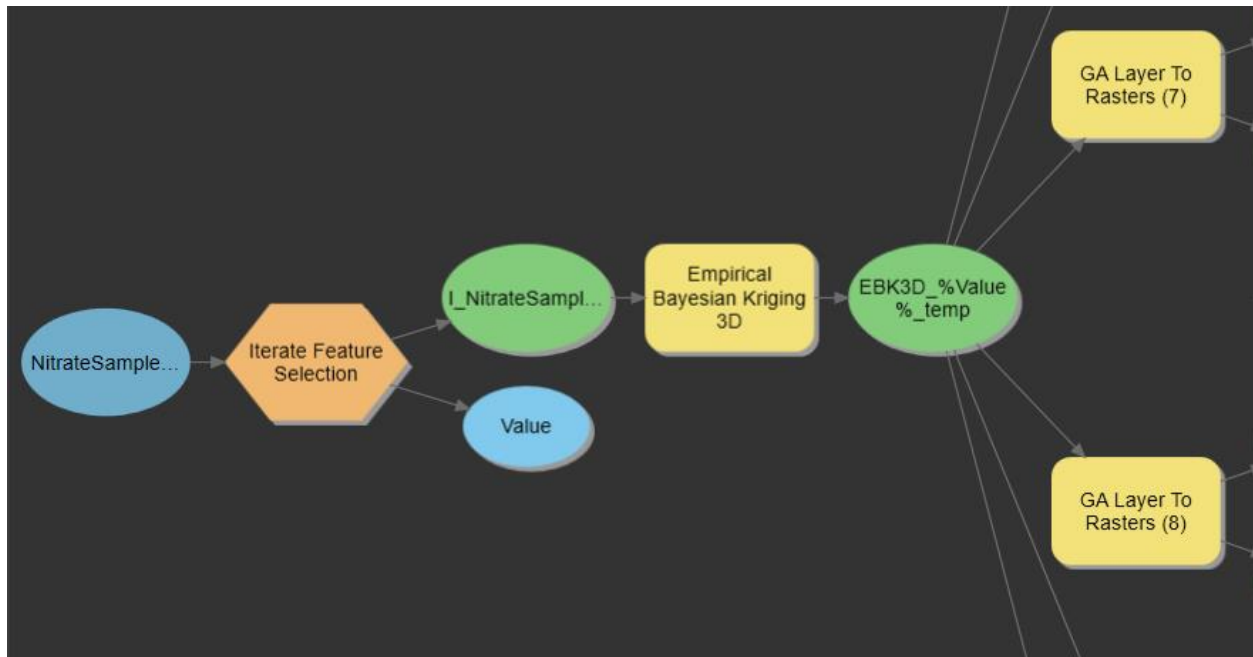


Figure 10 First portion of the model to create horizontal cross sections with temperature data.

The iterator selects all the data from each survey, inputs it into EBK3D, and the interpolated results are sliced into six cross sections (only two fit in the frame of this figure) and exported as rasters.

3.4.1. Horizontal Cross Sections

To create the horizontal cross sections, each 3D prediction volume generated for a single survey by EBK3D was exported as six rasters at elevations specified as 0, -100, -200, -300, -400, and -500. Then, each elevation raster was converted to points using the Raster to Point tool and the resulting six point shapefiles were clipped to the CalCOFI 75 Station Area layer. A new column with the date of the survey repeated in every cell was appended to the attribute tables for each set of cross section point shapefiles for a single survey, as well as being included in the filename of each cross section. Figure 11 shows an example of this process, for the 300m horizontal cross section of temperature data. The steps shown in Figure 11 happened six times in parallel, once for each depth.

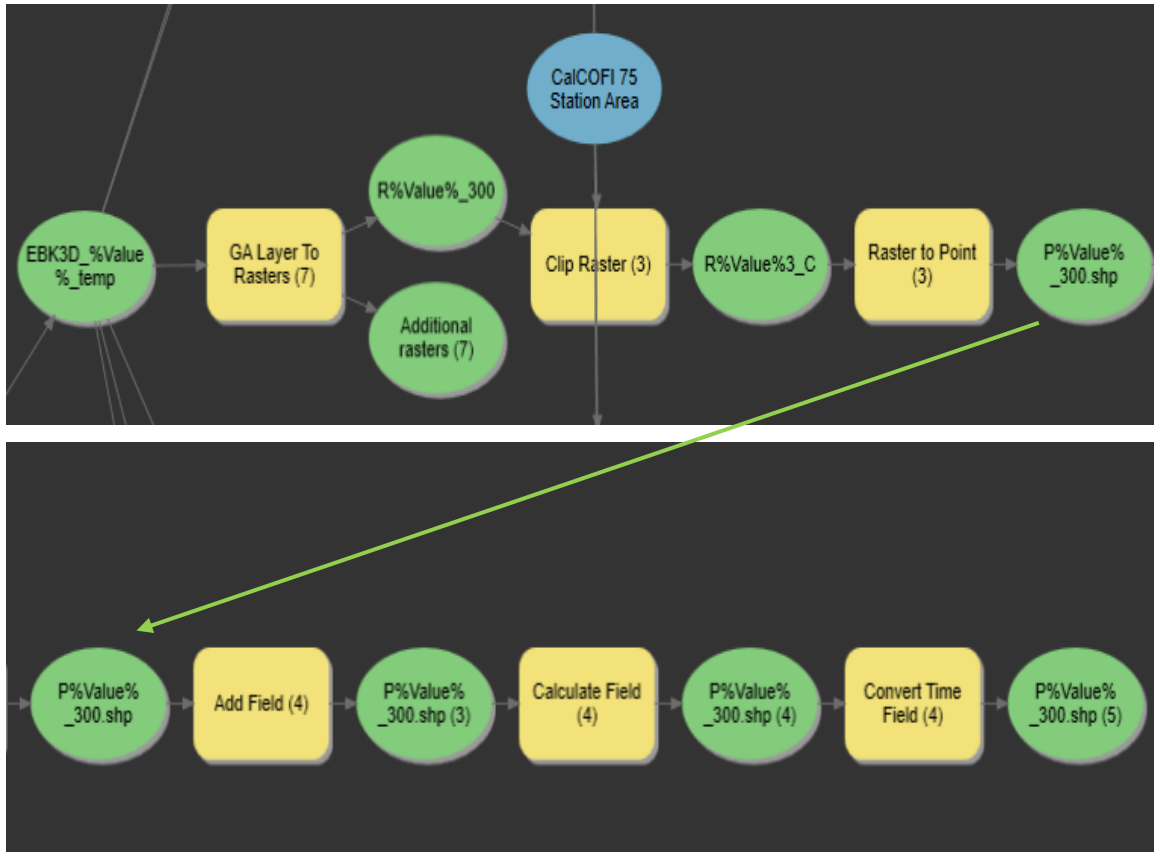


Figure 11 Steps to convert a raster slice of the prediction volume of EBK3D to a point shapefile, with date appended to the attribute table, in the correct folder according to depth. This example shows this process for the horizontal cross sections of temperature data at 300m deep.

After all cross section point shapefiles had been created, these shapefiles were sorted into folders according to the depth they were sliced at: 0, 100, 200, 300, 400, and 500. Finally, all the shapefiles in each depth folder were merged to create a single point shapefile containing all the points measured at the given depth with their associated values (temperature or nitrate) associated with the date each value was collected. This merge resulted in point shapefiles with multiple points in the same locations across five decades of surveys. In this form, the data was ready to be converted to a NetCDF space time cube file.

3.4.2. Vertical Cross Sections

Creating vertical cross sections of the data proved to be challenging, but ultimately feasible. While horizontal cross sections could simply be exported as rasters from the results of EBK3D, vertical rasters are not an option in ArcGIS Pro. Instead, the results of EBK3D were exported to vertical planes of target points. These vertical planes of gridded points were arranged such that each of the six transects defined a vertical plane, stretching the length of the transect and from 0 to 500 m of depth. In places where the seafloor was less than 500m deep, the vertical cross section was clipped to represent this. Vertical slices were taken along the transect lines because they are evenly spaced, and the interpolated results are most accurate close to the points where the samples were originally taken.

Creation of target points to export the results of EBK3D into ultimately required a custom workflow. First, transect lines were traced in ArcGIS Pro using the KML point shapefile of CalCOFI stations available at calcofi.org as a guide. This created a two-dimensional line shapefile containing the six transect lines. Second, the SRTM30plus bathymetry layer was added as an elevation layer (Becker et al. 2009). Next, the 2D lines representing the transects on the surface were “projected” onto the 3D elevation surface of the seafloor to create 3D polylines representing the CalCOFI transects along the seafloor.

Each polyline was converted to many evenly-spaced points using the “Create point features along a line” tool, and the coordinate data for each point in these polylines was added to an attribute table. This table was then edited by hand in MS Excel such that, for each individual XY point location, additional points were added with the same XY coordinates, but Z values ranging from 0 to 500 m of depth at 5 m intervals. XY locations where the 3D polyline indicated that the seafloor depth was less than 500 m had additional points with Z values added only to the depth of the seafloor, rounded down to the nearest 5m interval. Finally, the polyline points that

extended below 500m were deleted. This resulted in a flat 3D shapefile of points arranged in vertical slices taken along each of the six transect lines, with point elevations ranging from 0 to 500 m of depth, but clipped to bathymetric features in areas where the seafloor was less than 500 m deep, as shown in Figure 12.

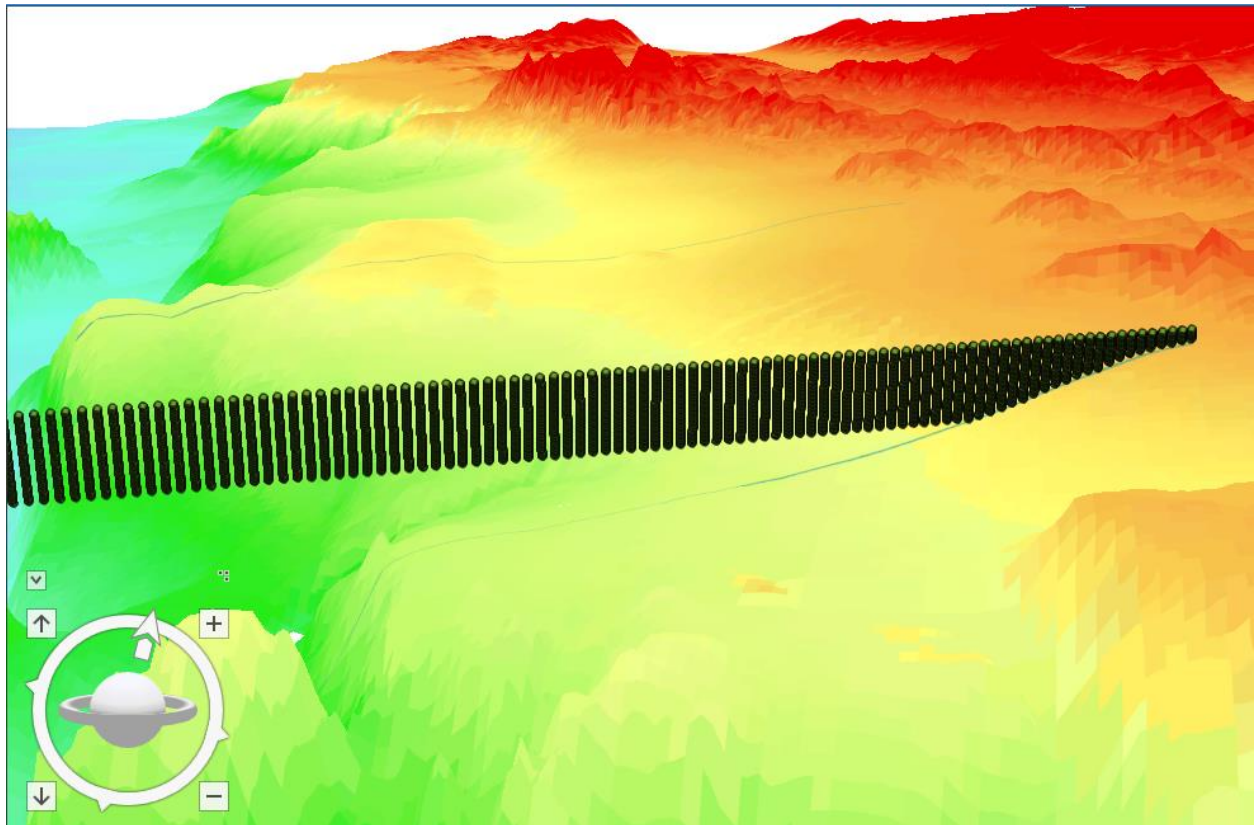


Figure 12 Point shapefile of a vertical cross section, with SRTM30Plus as the elevation surface.

Using the EBK3D tool, predicted values were exported from the predication volumes to these vertical planes of target points. Each survey yielded six shapefiles of target points (one from each transect), and columns were appended to the attribute tables of these files with the survey date. Shapefiles were saved in folders organized by transect line: 77, 80, 83, 87, 90, and 93. Once they were sorted into the folders, files within each folder were merged in the same manner as the horizontal cross section files to prepare for the creation of space time cubes.

After vertical cross section files had been created and merged, the points were mapped in a new horizontal coordinate system, because the Space Time Cube toolset requires input data in a horizontal plane. To do this, two columns were added to the attribute table for each slice, for “Inflated Depth” and “Distance From Shore.” The “Inflated Depth” column was calculated using the formula $\text{Inflated Depth} = 1000(\text{depth})$. The depth was inflated because the length of the transects is over 500 km, while the depth is 0.5 km (500m). Inflating the depth by a factor of 1000 to make a footprint for the space time cube with similar length and width. It was statistically valid to inflate the vertical depth axis because the Mann Kendall test used to evaluate trends in each column of the subsequent space time cube is spatially independent, so each bin is evaluated without influence of any others in its spatial neighborhood. Therefore, the visual arrangement and spacing of the bins does not affect the analysis of the trends. The depth was inflated by a factor of 1000 partly because this was a convenient round value, but also because 3D interpolation determined that the optimal elevation inflation factor for each survey was around 1000 (ranged from approximately 600 - 1000). This indicates that the data varies spatially in the inflated vertical direction at about the same rate as in a horizontal plane, so inflating the vertical axis to this factor best facilitates visualization and analysis of trends.

The “Distance From Shore” was slightly more complicated to calculate. A line was drawn from the surface to 500m depth along the eastern edge of the point shapefile for each slice, and the “Near” tool was used to calculate the distance from each point to this eastern edge and populate the table with the values. These values were all multiplied by (-1) so that they would map to the west/left of the shoreline in the next map. Finally, the attribute tables for these vertical cross sections were added to a brand new Local Scene (coordinate system WGS 1984 UTM 10N) and mapped using “XY Table to Point.” Instead of using their original XY

coordinates, each point was mapped using “Distance from Shore” as the X-coordinate, and “Depth Inflated” as the Y-coordinate. With these steps, vertical cross sections were “laid down” into a horizontal plane, so that they could be input into a space time cube in the next step. This process is illustrated in Figure 13.

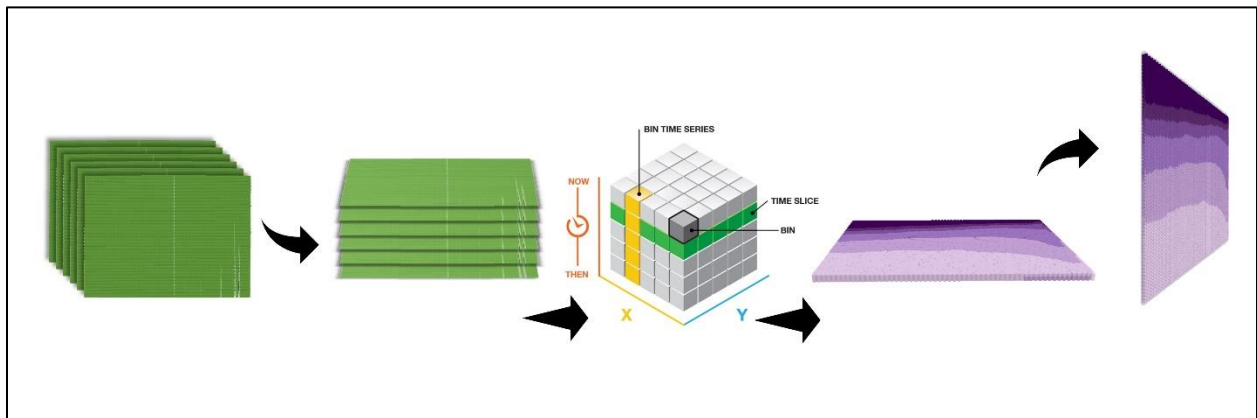


Figure 13 Schematic representing the process of creating vertical cross sections, “laying them down” in a new coordinate system, creating a Space Time Cube, and then re-visualizing the results of the cube as a vertical slice.

3.5. Space Time Cubes

A space time cube is a netCDF file generated by ArcGIS where the x- and y-coordinates represent a spatial location, and the z-coordinate is used to represent time. This description of Space Time Cubes and associated tools comes from the help pages provided by Esri (Esri 2019b). Source data points are summarized into “bins” defined horizontally by a grid of squares or hexagons and vertically by time steps, with more recent samples stacked on top of older ones. This is a powerful tool for visualizing data that varies across both space and time. This method of sorting and grouping data into bins is also an extremely effective method to prepare the data for further analysis of time series trends within each column of bins, so temporal trends can be modeled across the entire spatial extent of the dataset in reasonably high resolution.

It is noteworthy that the space time cube and associated toolsets so far only accept datasets that have two spatial dimensions in addition to time - a time series on a plane. Within ArcGIS, there is no method of modeling temporal trends in a 3D dataset, so this was why it was necessary to slice the 3D data into 2D cross sections at depths and along transects.

3.5.1. Constructing Horizontal Cross Section Space Time Cubes

To create space time cubes for changes over time at each depth (horizontal cross sections), each merged shapefile of all points over time for a particular depth was simply input into the “Create Space Time Cube by Aggregating Points” tool without any modification. Temperature and nitrate data from 1969-2018 were aggregated into 5-year bins and summarized with a mean of the values falling in each bin. There were less than 5% empty bins for each cube, but empty bins were filled with space-time neighbors. Because nitrate data from the 1970’s proved unreliable, the nitrate data was also analyzed from 1985-2017 with the same settings but using 3-year bins to group the data.

The results of analysis of a space time cube are dependent on the horizontal and temporal spacing of the bins. When choosing the temporal duration (time step) for each bin, it is important to consider that the time series should divide evenly amongst a minimum of ten temporal bins in order to reliably analyze Mann Kendall trends. If the duration of the entire time series does not divide evenly into the bins, one or both bins on the ends of the time span bin will have an incomplete set of data. For example, if a 51-year time series is divided into 5-year bins, there will be 11 bins. Ten of the bins will each contain 5-years’ worth of data, but the 11th will only contain one year’s data, which will likely skew the results. To deal with this, the temperature and nitrate data were initially analyzed using 5-year time steps to represent the dataset from 1969 to 2018 (50 years). However, results showed that some of the nitrate data and the survey schedule

in the 1970's was very erratic, so the space time cubes for nitrate were reconstructed using 3-year bins over the time series from 1985-2017 (33 years) because surveys were much more consistent during this time period. Space time cubes were also created to analyze temperature data from 1985-2017, but most of the trends observed in the longer time series were not significant in this shorter time series. The observation of poor nitrate data quality in the 1970's was consistent with the results of EBK3D cross validation, discussed earlier. The anomalous nitrate data is shown in Appendix B.

3.5.2. Constructing Vertical Cross Section Space Time Cubes

Vertical cross sections required slightly more preparation. The “Create Space Time Cube by Aggregating Points” tool requires data with an x-coordinate, a y-coordinate, and a time field, so the data had to be prepared as discussed previously and shown in Figure 13. Once the data had been re-mapped into a new Local Scene, it was input into “Create Space Time Cube by Aggregating Points,” and the same parameters as in the horizontal cross section procedure were used. Temperature and nitrate data from 1969-2018 were analyzed with 5-year bins, and nitrate was analyzed from 1985 to 2017 with 3-year bins. Bin data was summarized with means, and rare empty bins were filled with space time neighbors.

3.6. Mann Kendall Trends

Mann Kendall tests are described in the Esri help pages for “Visualize a Space Time Cube in 2D,” and the following information is derived from that source (Esri 2019b). The Mann Kendall test is a nonparametric test used to determine whether data exhibits a monotonic trend. In other words, the Mann Kendall test shows whether a time series of data steadily increases, decreases, or has no significant trend over time. The Mann Kendall test was used to identify trends in nitrate and temperature data. To view the Mann Kendall trends for each Space Time

Cube, the cube was input into the “Visualize Space Time Cube in 2D” tool, and the “trends” option was selected. This tool analyzed each column of bins in the Space Time Cube individually (and independently of other columns). The Mann Kendall test produces results indicating whether the trend is increasing, decreasing, or not statistically significant. The confidence level of a Mann Kendall trend is the probability that the trend detected is a “real” trend and not a result of random fluctuation. For this analysis, only trends with a 95% confidence level or higher were recognized and symbolized as increasing or decreasing. Any trends with lower confidence levels were symbolized as not statistically significant.

The Mann Kendall trend test registers monotonic trends and is less likely to report a significant trend in very noisy data, or data with any sort of seasonal variation. Taking the mean of temperatures in 5-year bins smooths the time series somewhat, and effectively controls for variation due to differences in annual seasons (spring, summer, fall, winter), but would not smooth out multi-annual cyclic signals in the data due to effects such as El Nino (ENSO) or the Pacific Decadal Oscillation (PDO). These effects would cause the Mann Kendall statistic to under-report trends in areas with a lot of variations from these signals. Similarly, reducing the time bins for nitrate to 3-year steps would likely result in a noisier time series of nitrate data, and possible under-reporting of trends by the Mann Kendall test.

3.7. Visualization of Results

The dataset was analyzed using the methods described in the previous sections. This was successful and yielded cross sections of the 3D study area with some clear temporal and spatial trends. This turned out to be a computationally intensive process, with multiple custom ModelBuilder tools that ran for up to 5 days continuously, and the final project taking over 130 GB of hard drive space.

Once the analysis was complete, developing a method to understand, visualize and compare these complex four-dimensional results sliced on two different axes was needed. A number of graphical techniques were tested with the best visualizations becoming the ones used in the next chapter to show the results. However, due to the four-dimensional nature of the dataset, some initial explanation of the presentation of results may be helpful. Some points to keep in mind:

- In the 2D maps, each hexagonal “pixel” represents an independent time series. Each time series is a sequence of values, where each value is the mean of points falling within the bin at each location over a 5-year (or 3-year) time period.
- The Mann Kendall trends are symbolized with red indicating statistically significant increase and blue indicating statistically significant decrease in the time series at each hexagonally-shaped bin location.
- In some figures, the time series is depicted as a “film strip” at the bottom, with darker purples depicting higher mean values. Each “frame” of the “film strip” shows a 3- or 5-year time period

Vertical cross sections also require some explanation. While taking vertical slices of a 3D study area is conceptually straightforward, this is not a common frame of reference in ArcGIS. Furthermore, users familiar with the Space Time Cube toolset will realize that this group of analysis tools is only used for data that occupies a horizontal plane, and then symbolizes the progression of time as a stack of bins in the z-direction. As described in the Methods section, vertical cross sections of data were transferred to horizontal plane coordinate systems to use the Space Time Cube toolset for analysis, but here they are visualized as vertical slices once again. This is illustrated in Figure 14, where each transect line has a vertical cross section showing the

(time series Mann Kendall) nitrate data on that slice. Note that the vertical axis is inflated by 1000, so while the X and Y axis are in kilometers, the vertical axis is in meters. While the view presented in Figure 14 is conceptually explanatory, the 3D perspective and overlay of multiple cross sections makes it difficult for the viewer to see the slices in full detail. Subsequent figures are presented with each cross-sectional slice shown separately.

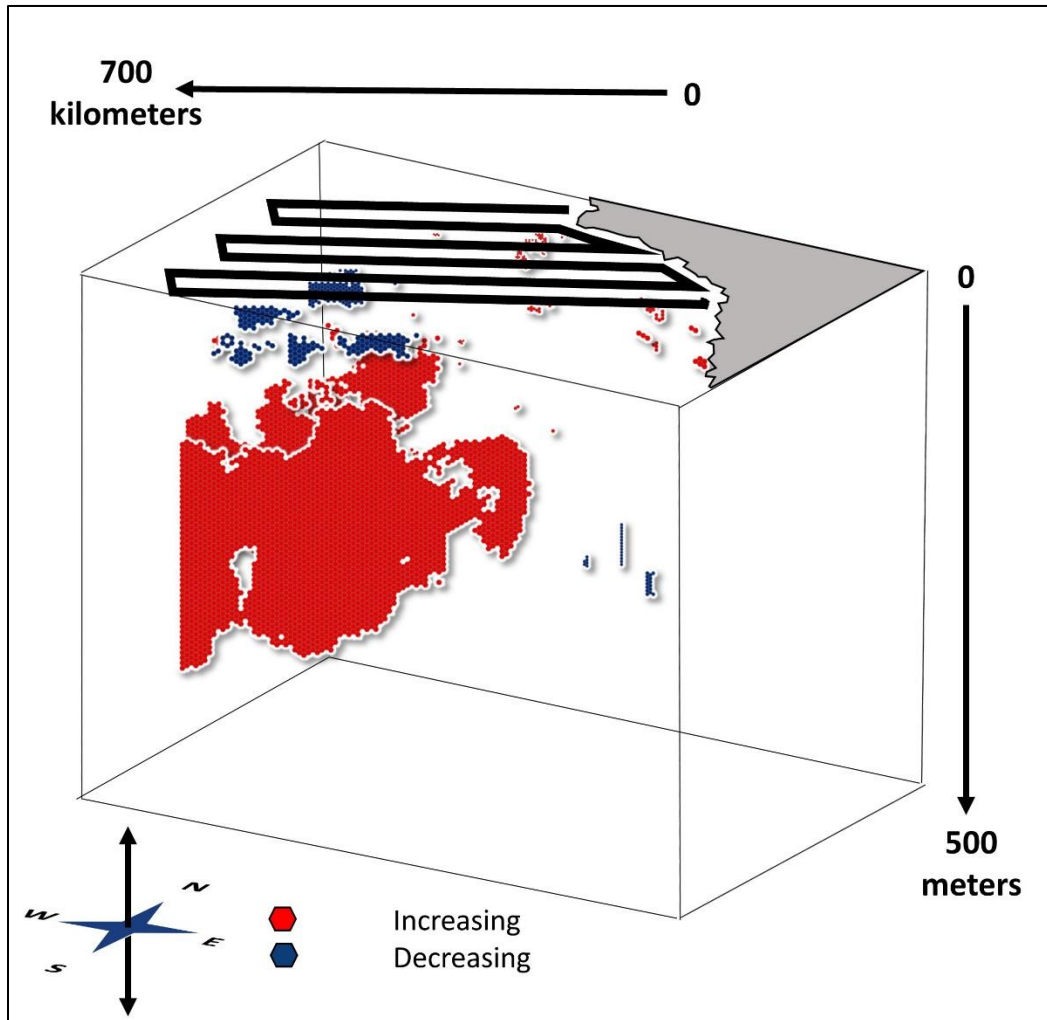


Figure 14 A conceptual view of vertical cross sections of Mann Kendall trends in nitrate data in relation to the surveyed transects on the surface (bottom). CalCOFI's 75 station pattern is shown in the top right for reference. This figure shows nitrate data from 1985-2018, analyzed in 3-year bins.

Chapter 4 Results

The complex methodology of this project generated large quantities of output data at each step. Intermediate steps and final results created over 130 GB of data, comprised of thousands of shapefiles, two dozen space time cubes, and two dozen cross sections showing Mann Kendall trends resulting from analysis of these cubes. The sheer quantity of data is too large to show here in its entirety. Instead, a sampling of results from each step is shown, in addition to all of the Mann Kendall trends for all cross sections. In addition, efforts were made to ensure that the results presented here are statistically sound. A subsample of EBK3D results were cross validated to show that these predictions were reliable, and Mann Kendall trends were only shown if the confidence level that the trend was statistically significant was greater than 95% ($p < 0.05$).

4.1. EBK3D

Use of EBK3D to interpolate the data into comparable prediction volumes is one of the main ways this research expands upon past work. There were 362 separate instances of the EBK3D tool (temperature and nitrate from each of the 181 surveys). Figure 15 shows an example set of results from the survey that took place in March of 2012, where temperature values are interpolated. As shown in the figure, temperatures are warm at the surface (0m), decline through 100 and 200 m, and are fairly uniformly cold at 300 – 500m depth. The results of EBK3D give an elegant and intuitive overview of the temperature patterns present in the water column during the March 2012 cruise. As shown in Figure 16, results of cross validation show that for this survey, predictions from the EBK3D model are very close to the measured values. Mean and Mean Standardized statistics are close to zero, indicating that there is very little bias in the model. The Root Mean Square value is 0.181, meaning that predictions by the model are on average within 0.181 degrees Celsius of the measured values. This shows that the prediction

surface generated by EBK3D for this survey is reliable, and that it is statistically valid to use this output for comparisons over time in later steps. While it was not feasible to cross validate each one of 362 iterations of EBK3D, an inspection of a randomized group of ten indicated found that nine of the ten had good cross validation results. The tenth, which showed poor cross validation, was nitrate data from the 1970s, which was later removed.

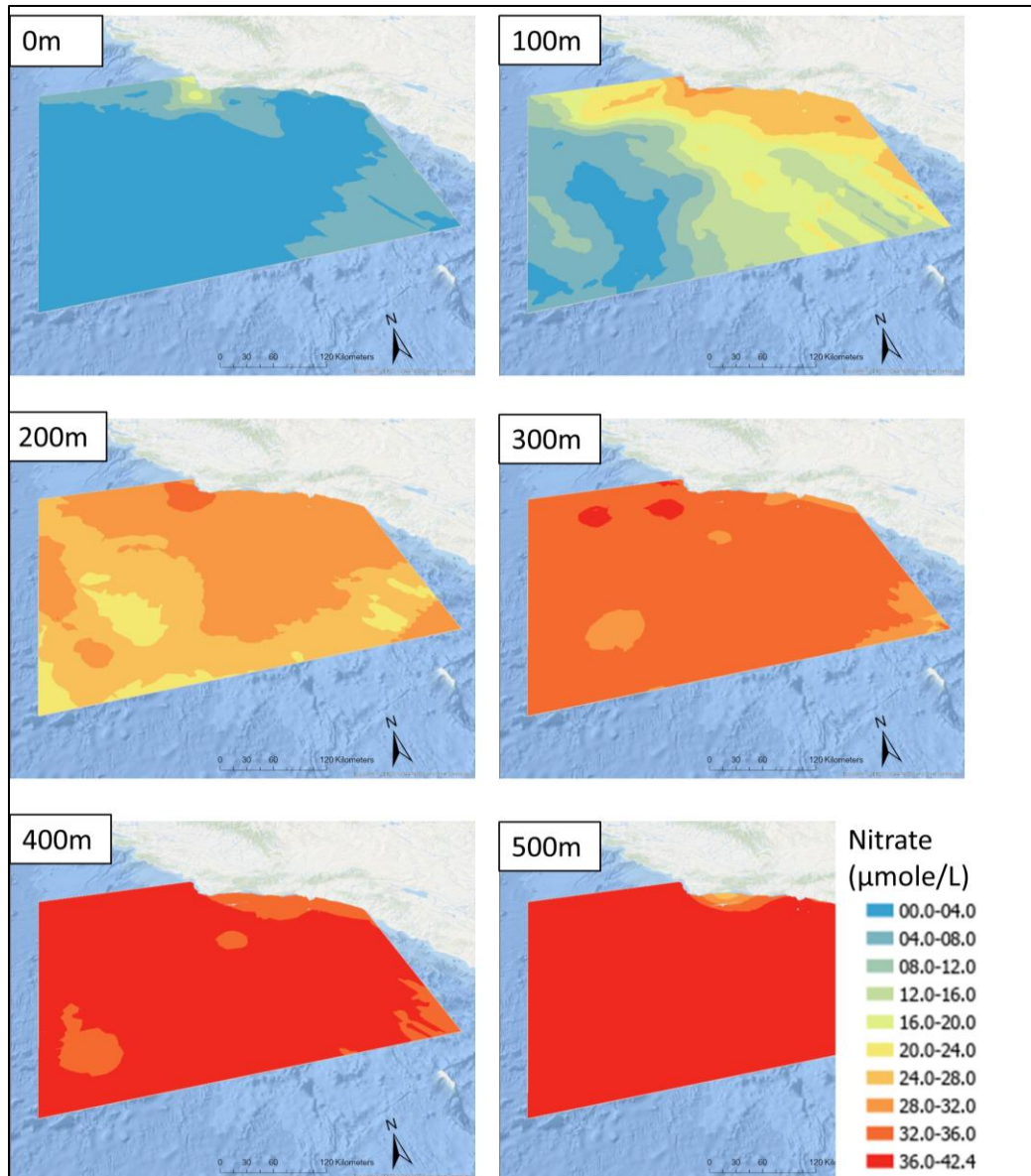


Figure 15 EBK3D results of interpolation of nitrate data from survey 201203, or March 2012. The output of EBK3D is a 3D prediction volume, but this is viewed as a series of horizontal cross sections, which can be viewed at any depth in the range. Here, cross sections are viewed at

0, 100, 200, 300, 400, and 500 m – the cross sections that were exported for analysis with the Space Time Cube. Cross validation results (shown in Figure 16, below) demonstrate that the EBK3D predictions generated by this interpolation model are accurate.

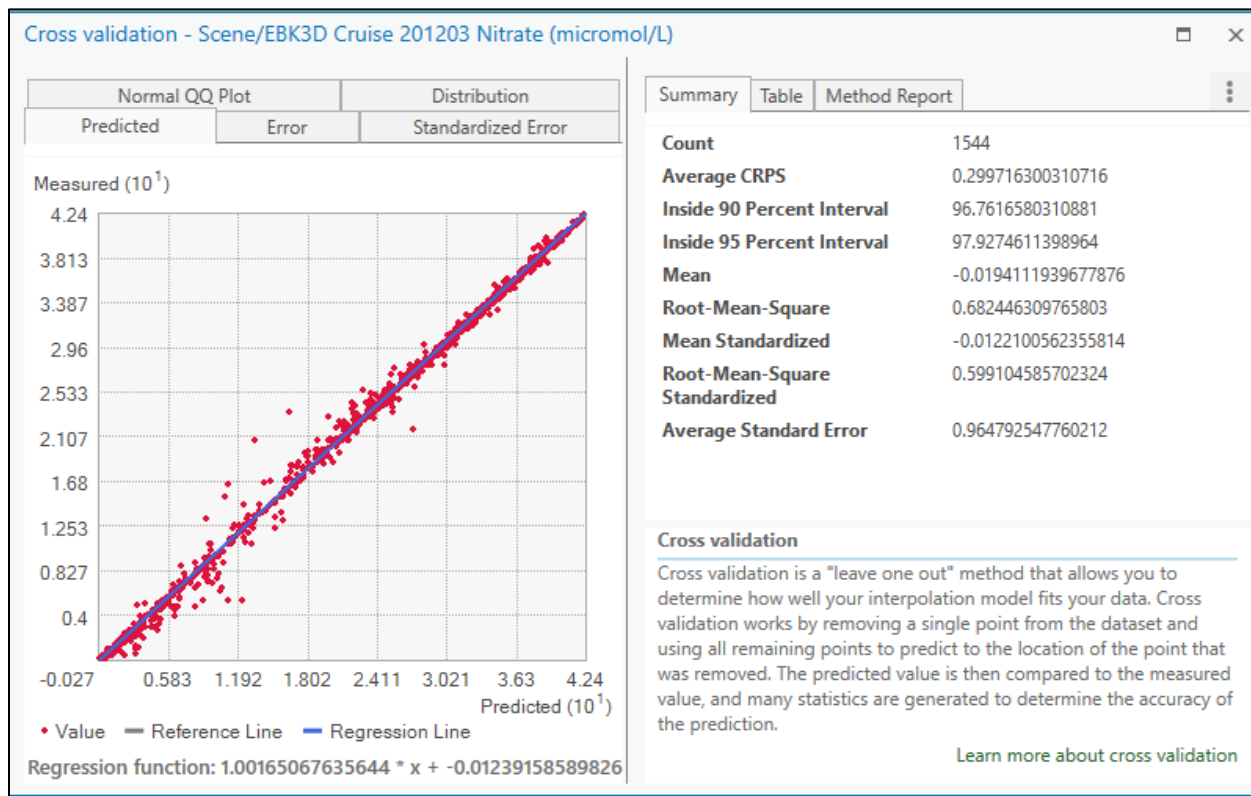


Figure 16 Cross validation results for EBK3D predictions for nitrate from cruise 201203 shown in Figure 15.

4.2. Space Time Cubes

The Space Time Cube toolset proved to be an effective method of modeling change over time across the spatial extent of each cross section. Six space time cubes were created to represent change in temperature from 1969 to 2018 and change in nitrate from 1985 to 2017, one at each horizontal cross section representing depths at 0, 100, 200, 300, 400, and 500m. A Space Time Cube created from the 0m horizontal cross section temperature data is shown in Figure 16.

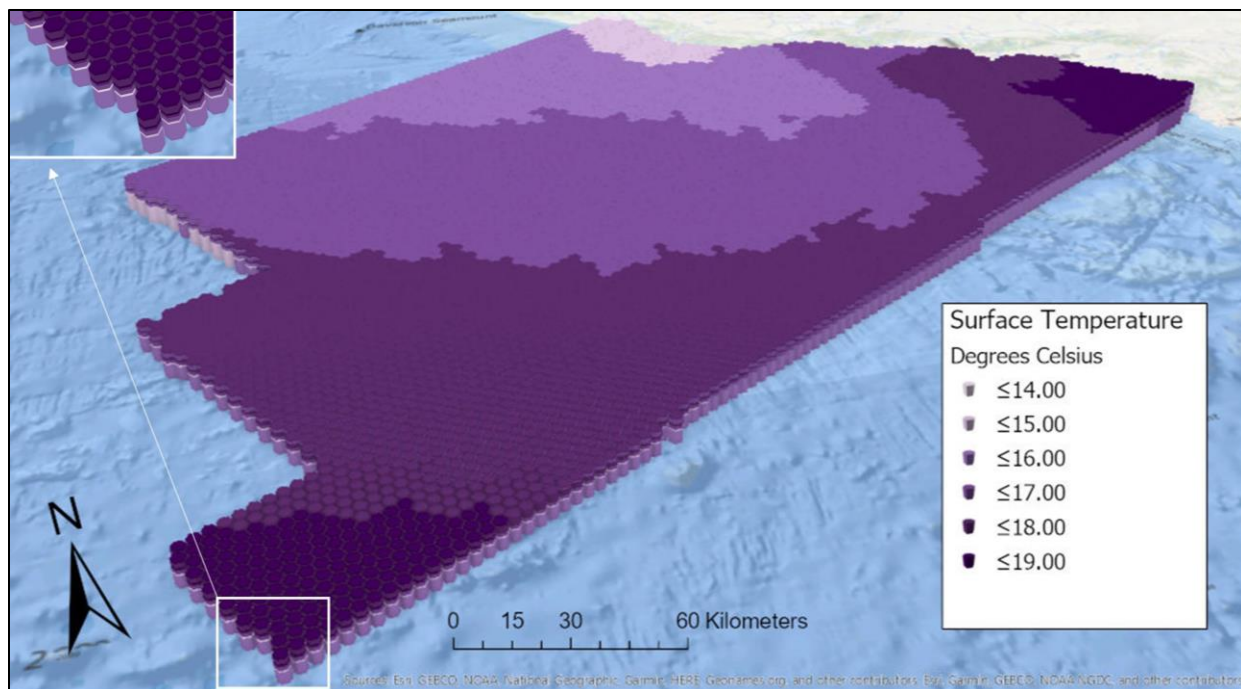


Figure 17 Space Time Cube at 0m cross section showing temperature values from 1969 to 2018. The vertical bin columns stack up 10 hexagons showing temperature averaged over each 5-year time step, stacked to represent the duration of the full time period.

Similarly, six space time cubes represent vertical cross sections at Line 77, 80, 83, 87, 90 and 93, depicting change in temperature from 1968 to 2018 and change in nitrate from 1985 to 2017 along these cross-sections. The Space Time Cube depicting change in temperature along the vertical cross section of Line 93 is shown in Figure 18. Although this Space Time Cube was created by re-mapping the vertical cross section in a horizontal plane, the results have been rotated into a vertical plane once more to show their location in the water column. In this orientation, the time steps stack from the left to the right of the image, as is visible in the inset. The remaining representations of the vertical cross section cubes and data in this chapter are shown with a view angle from approximately where the compass rose is located, so that the entire slice is viewed head on with no distortion due to perspective.

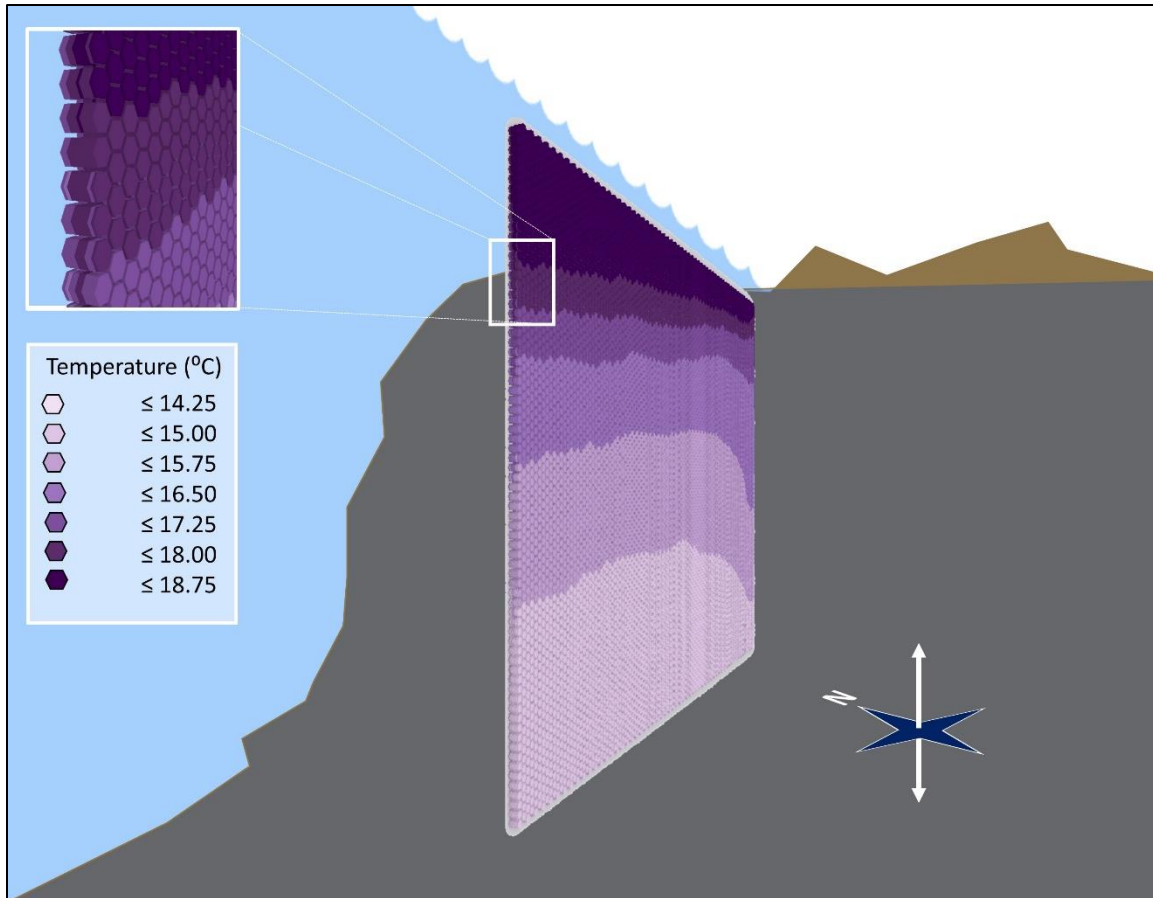


Figure 18 Space Time Cube results at Line 93, representing temperature data from 1969 to 2018. Although the Space Time Cube toolset is used on horizontal planes, in this schematic the output data has been rotated back to its original vertical position to show the location of the data in the water column.

4.3. Mann Kendall Trends

Mann Kendall trends were analyzed for each space time cube. The Mann Kendall trend test determines whether values in a series of time steps show a statistically significant (95% confidence) increase or decrease. The Mann Kendall trend for each hexagonal bin in each Space Time Cube was analyzed separately. While the Space Time Cube is a 3D volume that shows the values at each time step stacked, Mann Kendall trends are displayed as a 2D layer summarizing the trends. Each time step in the Space Time Cube can be displayed as a frame in a film strip, with the Mann Kendall trends shown as a summary of the trend that took place over the duration

of the “film strip,” as depicted in Figure 19 and Figure 20 and described below. The full set of 6 horizontal and 6 vertical cross-section results for the Mann Kendall statistic for both temperature and nitrate, for a full set of 24, are included in Appendix D.

Figure 19 shows the progression of temperatures at the sea surface (0m) and the summarizing Mann Kendall trends. From the film strip along the bottom, it appears the study area underwent warming in the 3rd through 6th time steps, then some cooling in the 7th and 8th time steps, and then warming in the 9th and 10th steps. Despite this fluctuation, Mann Kendall trends, displayed in the larger frame top left, show that the offshore region experienced a statistically significant increase in temperature overall.

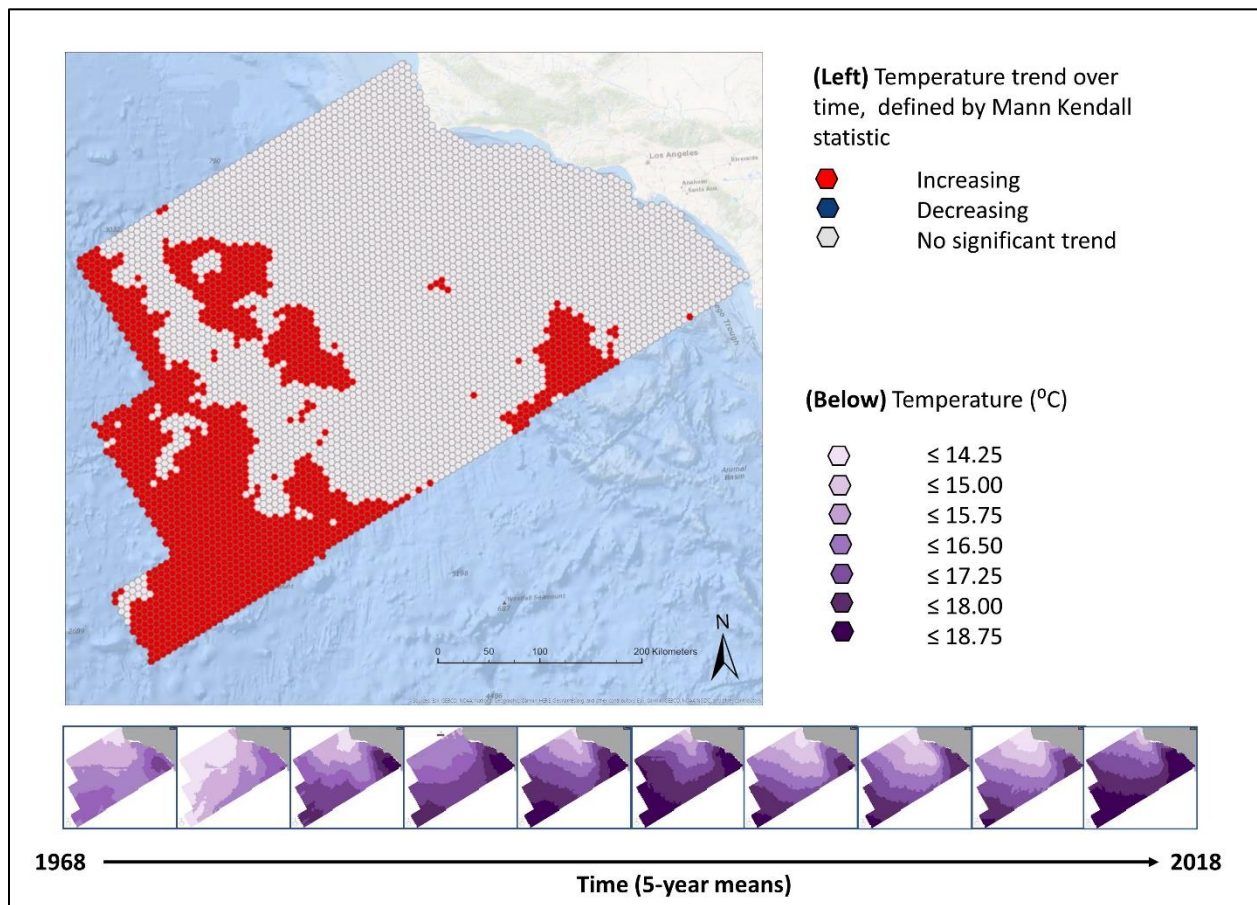


Figure 19 Temperature trends at the sea surface (0m), with data from 1968-2018 in 5-year bins. The purple data in the "filmstrip" at the bottom of the figure shows the values for each time-step

in the space time cube, and the larger figure (top left) shows the Mann Kendall trends that resulted from analyzing these values.

Figure 20 shows the progression of nitrate values on the vertical cross section of Line 93 and the summarizing Mann Kendall trends. While the Mann Kendall trend indicates statistically significant increases in nitrate in the middle of the water column offshore, examination of the film strip reveals that the changes in nitrate values are much more subtle than the changes in temperature shown in the previous figure. While the change in values is hard to detect by visual examination of the film strip, it is clearly detected by the Mann Kendall trend test because when the Mann Kendall trend is analyzed, only the direction and not the magnitude of change between time steps is registered. Therefore, many small changes in the positive direction result in a statistically significant increasing Mann Kendall trend, and that is what is shown in the central region of Line 93 in Figure 20.

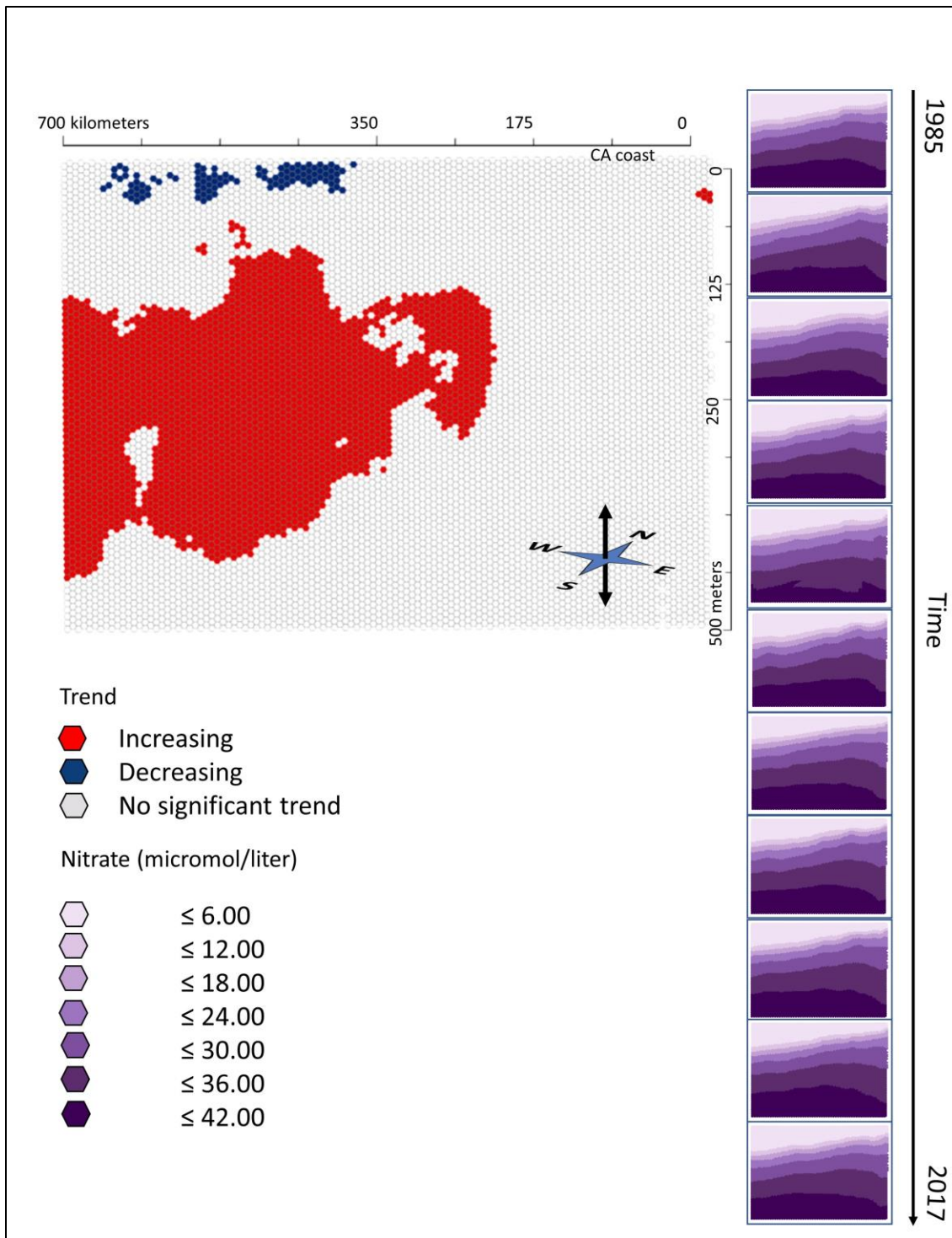


Figure 20 Nitrate trends on Line 93, with data from 1985-2017 in 3-year bins. The purple data in the "filmstrip" at the bottom of the figure shows the values for each time-step in the space time cube, and the larger figure (top left) shows the Mann Kendall trends that resulted from analyzing these values.

4.3.1. Temperature Trends

Temperature data analysis, using data from 1968 to 2018, went smoothly. The results are included in Appendix D and the trends are summarized in Table 3 and **Error! Reference source not found.** The temperature data did not show any obvious outliers or strange data. Nitrate data showed some anomalous values in the 1970s (shown in Appendix C), so nitrate data was analyzed from 1985 – 2017, representing a shorter but more consistent series of surveys. For consistency, temperature was also analyzed across this shorter time span, but the temperature trends observed in the longer time-series were not significant over a shorter time span. These results are shown in Appendix B.

Examination of both horizontal cross sections (Figure 21) and vertical cross sections (Figure 22) show that a warming trend occurs only on the surface, at less than 100 m of depth. Although surface temperatures fluctuated during this time period, overall Mann Kendall trend analysis of the temperature data of the SCCS showed a clear increase (at 95% confidence, $p < 0.05$) at the surface (0m) from 1968 to 2018, as shown in Figure 21. This temporal trend at the surface also shows a horizontal spatial pattern. Areas with statistically significant positive trend occupy the southwest corner of the study area and are generally at least 100 km offshore. Figure 21 and Figure 22 show that at depths of 100m and greater, there are small patches of cooling trends. These deep areas of cooling are generally located approximate 300 km offshore and in the northern portion of the study area.

Table 3 Summary of observed Mann Kendall trends in temperature in horizontal cross sections from 1969-2018

Horizontal Cross Sections	
Depth	Trends Observed
<i>Overall</i>	Warming at the surface in the offshore region, scattered cooling at all other depths
0 m	Increase in temperature in the offshore region, starting at around 300 km from the coast. No significant trend nearshore. No cooling
100 m	No warming. Cooling trend 0-200 km offshore. Cooling is most apparent near Point Conception, where cooling trend is adjacent to the land, and less pronounced in the south, where the cooling trend is 100-200 km off the coast. No trend farther offshore.
200 m	Scattered patches of cooling 100-400 km offshore, one patch of warming nearshore in the east corner.
300 m	Mostly no trend. A couple patches of cooling in the north
400 m	Mostly no trend. An oblong patch of cooling in the north
500 m	Mostly no trend. An oblong patch of cooling in the north

Table 4 Summary of observed Mann Kendall trends in temperature in vertical cross sections from 1969-2018

Vertical Cross Sections	
Line	Trends Observed
<i>Overall</i>	Warming at the surface, particularly offshore in the south. Some cooling mid-water column, most pronounce in the north
Line 77	Small patch of warming offshore at the surface, large patches of cooling 100-500 m depth
Line 80	Small patch of warming offshore at the surface, patches of cooling 100-300 m depth closer to shore
Line 83	Warming patch offshore at surface. Small cooling patches 100-200m, west of island bathymetry
Line 87	Warming patch offshore at surface. Small cooling patches 100-200m, west of island bathymetry
Line 90	Warming patches at the surface, scattered cooling patches 200-300 m depth
Line 93	Large warming patch extending across the surface, and small warming patch nearshore at about 300 m deep. Scattered small cooling patches 200-400 m deep.

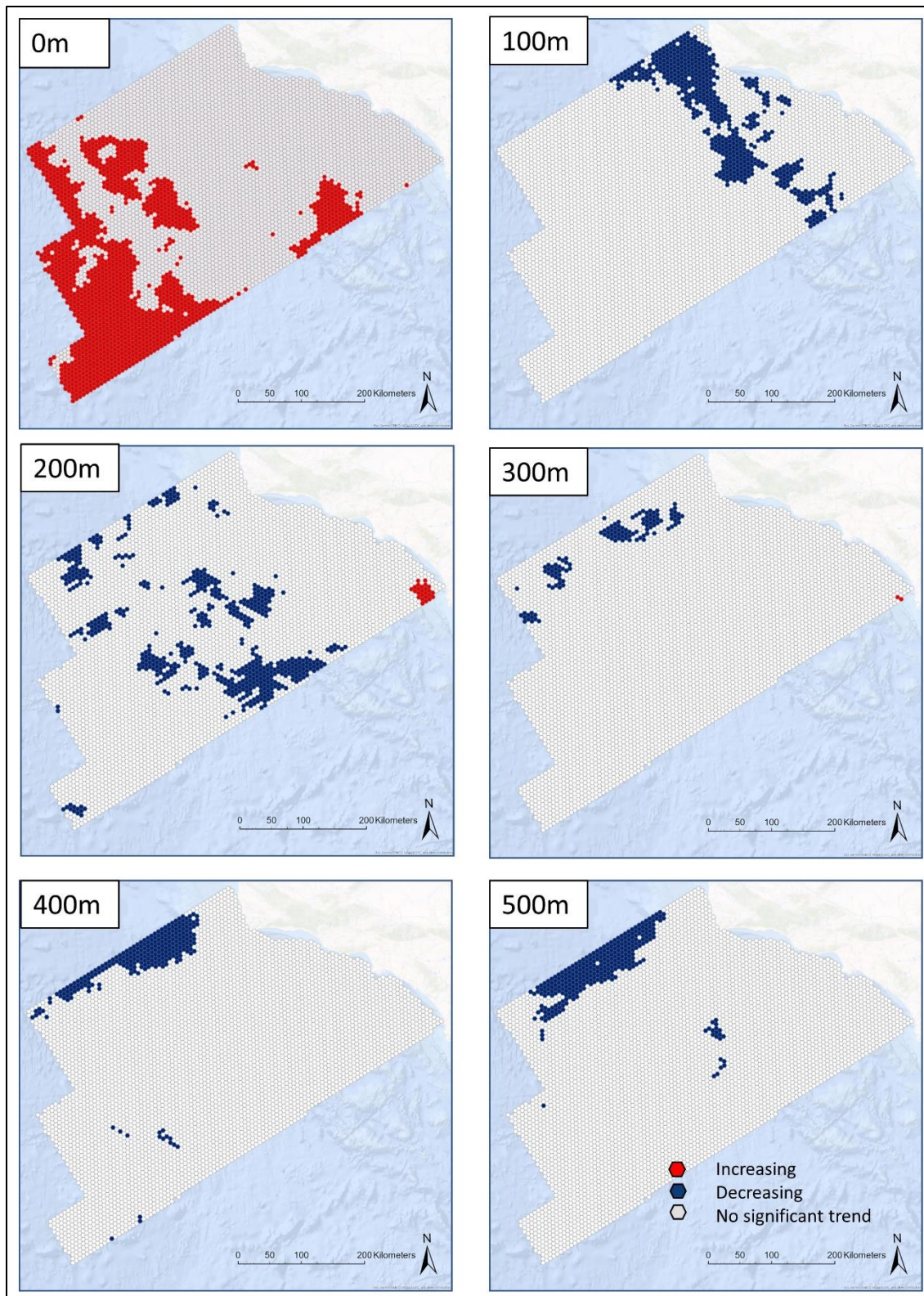


Figure 21 Horizontal cross sections showing temperature trends at 0, 100, 200, 300, 400, and 500 m of depth from 1969-2018

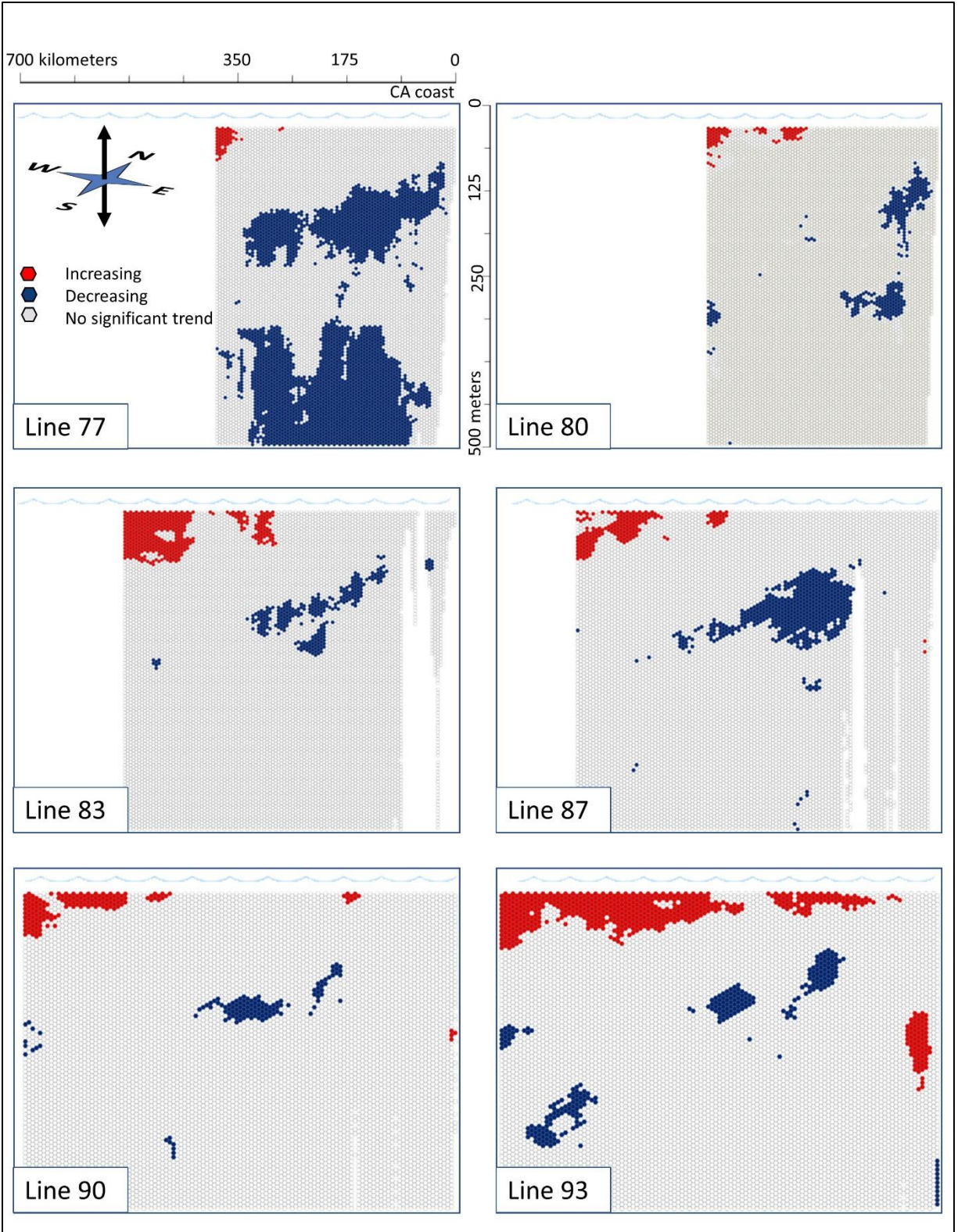


Figure 22 Vertical cross sections showing temperature trends on transect Line 77, 80, 83, 87, 90, and 93 from 1969-2018

4.3.2. Nitrate Trends

As noted in Section 3.5, data exploration revealed that nitrate data prior to 1980 were problematic and it was thus eliminated for the final analysis. Only the nitrate data from 1985-2018 were analyzed, because this period was characterized by very consistent surveys. The results are shown in Figure 23 and Figure 24. Similar trends, without the anomalies, were apparent in the data.

Even analyzed over a shorter time span, the data showed a couple of significant patterns of change in nitrate concentration in the SCCS. Nitrate trends are summarized in Table 5 and Table 6. Nitrate decreased at the surface (0 m) offshore, in the southwest corner of the study area, as shown in Figure 23. However, nitrate is increasing in a large area in the middle of the water column, most notably offshore in the southwest corner. This is evident in Figure 23, where there are large areas of increasing nitrate in the 200m and 300m cross sections, with small areas of increase bounding this area at 100 and 400m. Interestingly, nitrate is not increasing at the 500m level, and shows a small area of decrease nearshore close to Point Conception. The vertical cross sections in Figure 24 also clearly show that the area of nitrate increase occupies the water column from about 100 to 400 m of depth and is most prevalent in the more southern transects (Line 87, 90, and 93).

Table 5 Summary of observed Mann Kendall trends in nitrate in horizontal cross sections from 1985-2017

Horizontal Cross Sections	
Depth	Trends Observed
<i>Overall</i>	Region of increase offshore in the southwest region from 100-400 m depth. Small regions of decrease offshore at 0 m and inshore at 500 m.
0 m	Decrease offshore in southwest corner. Tiny patch of increase near Pt. Conception
100 m	Patch of increase about 400-600 km offshore in southern region, other small scattered patches of increase. No decrease, large areas of no significant trend.
200 m	Region of increase offshore in southwest corner. Otherwise, no significant trend.
300 m	Slightly larger region of increase than at 200m, offshore in southwest corner. Otherwise, no significant trend.
400 m	Patchy area of increase, offshore in southwest corner. Tiny patches of decrease nearshore in the north. Otherwise, no significant trend.
500 m	Small patch of decrease near Pt. Conception. Otherwise, no significant trend.

Table 6 Summary of observed Mann Kendall trends in nitrate in vertical cross sections from 1985-2017

Vertical Cross Sections	
Line	Trends Observed
<i>Overall</i>	Increases in oblong area, most prominent in southern cross sections (Line 87, 90, and 93) between 100-400 m depths. Small patches of decrease at the surface.
Line 77	No significant trends.
Line 80	No significant trends, except for small parch of increase nearshore at the surface.
Line 83	Small scattered patches of increase offshore at 200 and 400 m depth, tiny patch of decrease offshore at the surface.
Line 87	Large patch of increase from about 200 - 400 m depth, on offshore edge of cross section. Small patch of decrease above, at the surface on the offshore edge.
Line 90	Large, but somewhat scattered patch of increase offshore from about 100-400m depth and 400-600 km from the coast. Small patch of decrease offshore at the surface.
Line 93	Huge solid patch of increase, stretching from 100-400 m depth and 300-700 km offshore. Small patches of decrease offshore at the surface.

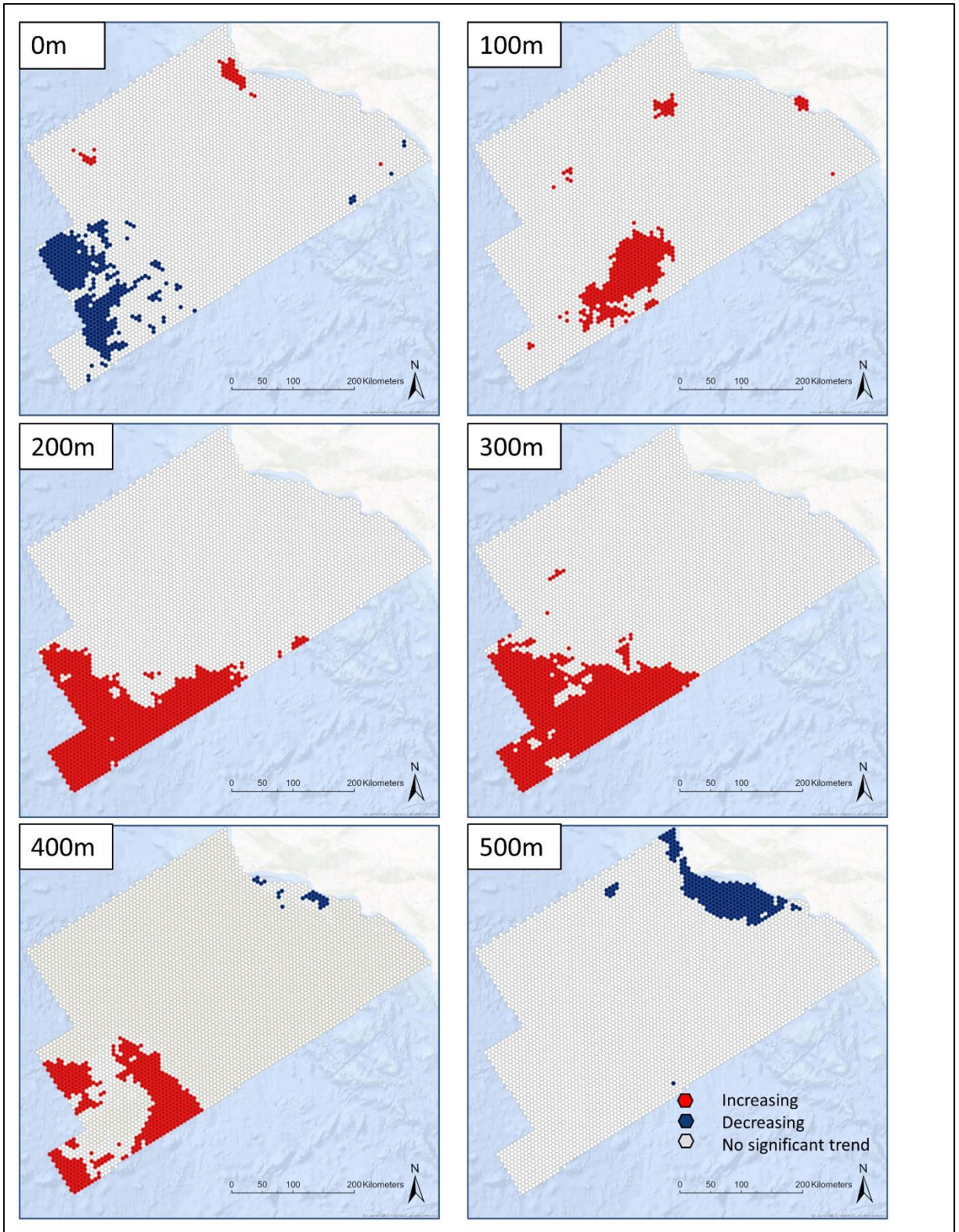


Figure 23 Horizontal cross sections showing nitrate trends at 100, 200, 300, 400, and 500m from 1985-2017

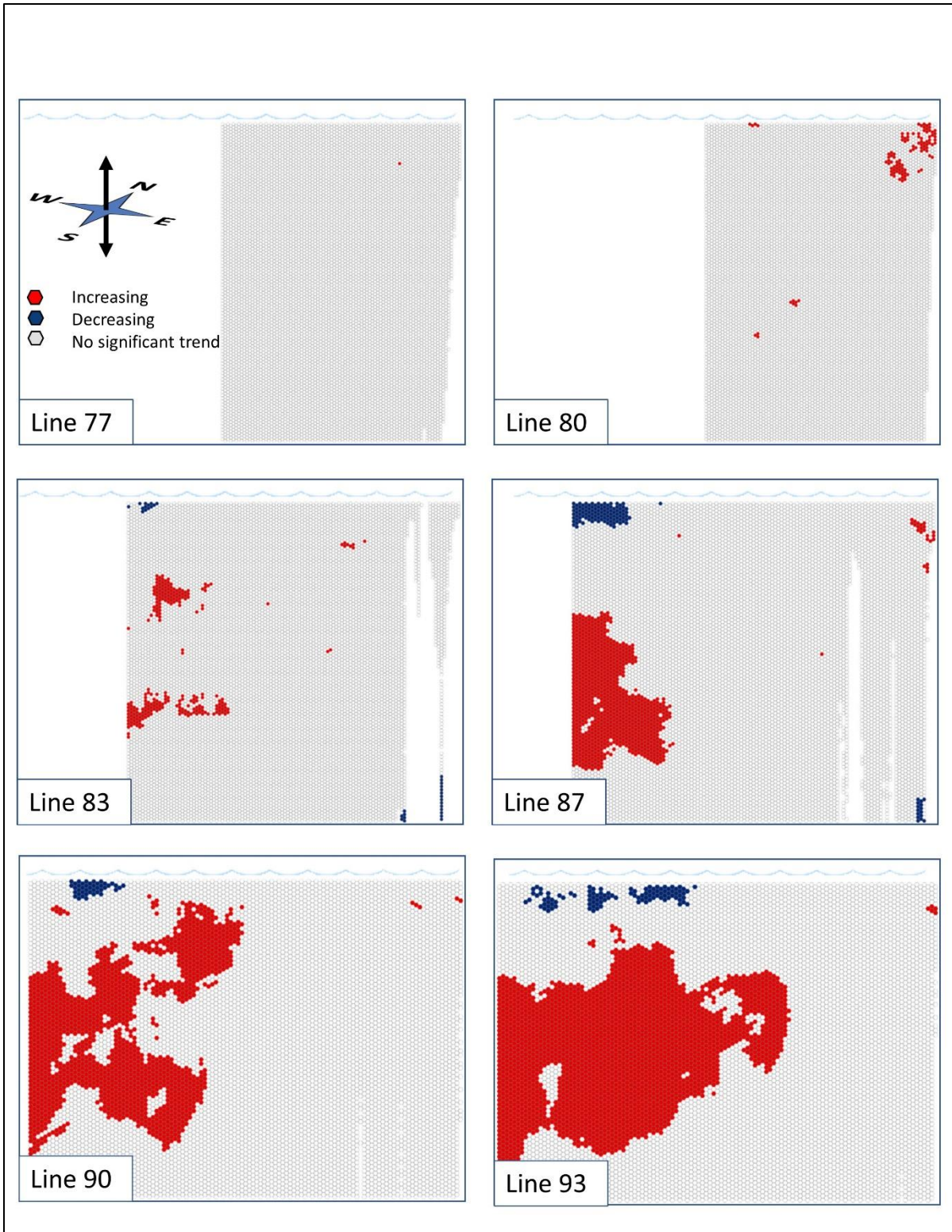


Figure 24 Vertical cross sections showing nitrate trends on Line 77, 80, 83, 87, 90, and 93 from 1985-2017

The vertical cross sections viewed individually give a reasonable impression of the shape of the area of increasing nitrate in the water column, but it is useful to see the combination of these cross sections to get an idea of the three-dimensional shape of the area of nitrate increase. This is depicted in Figure 25. To create this figure, it was assumed that the coast of California is a straight line, and the right edges (the northeast ends) of the cross sections were aligned. The “no significant trend” areas of the six cross sections were symbolized as transparent, and the cross sections were overlaid, with Line 77 in the back and Line 93 in the front. The increasing and decreasing trend areas are symbolized as 50% transparent, so that areas of more intense color indicate where several cross sections had the same trend in the same area. This creates a view as if from underwater in the middle of the water column southeast of the study area, looking north. As shown, the resulting area of nitrate increase is an oblong shape, mid-water column, reaching from about 300 to 700 km offshore. The vertical inflation of the data makes the oblong area of increase appear deeper than it truly is; in reality this area is actually much wider in the horizontal plane than it is deep in the horizontal plane. However, this shape is typical of cross-sectional ocean data in this region and provides an example of the principle that gradients in the ocean change much more rapidly in the vertical direction than the horizontal direction, as discussed in Section 3.3 (Gnanadesikan et al. 2001).

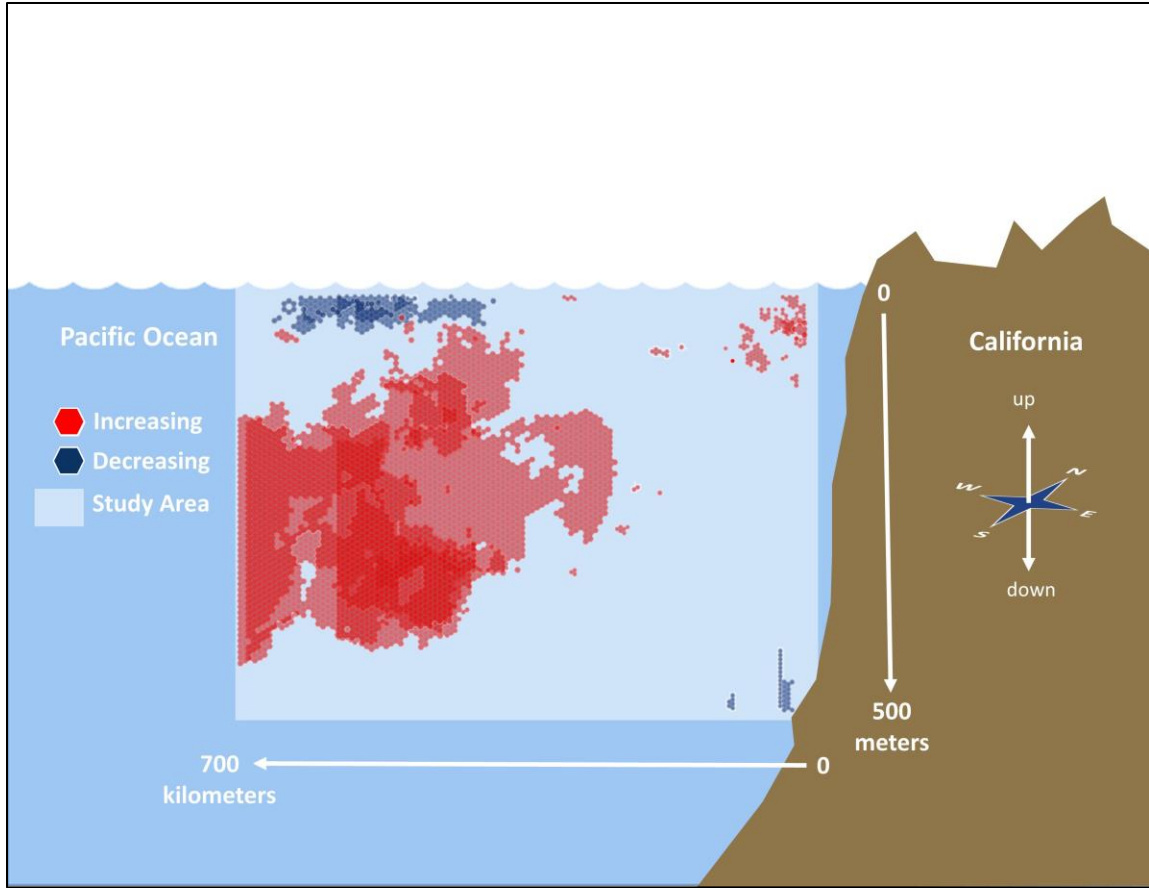


Figure 25 Vertical cross sections of nitrate trends, overlaid to depict overall combined layout of areas of increase and decrease

Chapter 5 Discussion and Conclusions

This project was designed to answer a two main research questions, concerning temperature and nitrate in the SCCS.

- 1) What are the spatial and temporal changes in temperature in the CCS over the past several decades? Do these indicate that sea surface temperatures are increasing in the CCS?
- 2) What are the spatial and temporal changes in nitrate in the CCS over the past several decades? Do these indicate that nitrate concentration is increasing in the deep water of the CCS?

The results have provided answers to these questions, and they are discussed in the following sections. In summary, sea surface temperature (SST) is increasing in the offshore region of the SCCS, and deep layer nitrate is also increasing in the offshore region between 100 and 400 m of depth. Other spatial patterns are also present, such as a decrease in nitrate at the surface in the offshore region.

5.1. Temperature

Results showed that sea *surface* temperatures (SST) are increasing in the SCCS, in a large offshore area in the southwest corner of the study area. No significant trend was detected near shore, either because no change has occurred or because the temperature data in this area is too noisy for a Mann Kendall test to detect a trend. The temperature trend of surface warming revealed by this project is consistent with other reports of surface warming in the SCCS (e.g. Palacios et al. 2004). This confirmation suggests that the methods used here are sound, and that trends revealed in less-reported areas beneath the surface are reliable.

The sea surface temperature (SST) is affected by atmospheric conditions and warming of the atmosphere can cause warming of the sea surface. An increase in sea surface temperature with no matching increase in deeper waters results in a greater difference in temperature between

the surface layer and the deep layer, resulting in a stronger thermocline. The clearest increases in SST were in the southwest corner of the study area, so it follows that the thermocline has strengthened the most in this area as well.

Patches of cooling trends near the continental shelf at 100m of depth and around Point Conception may be indicators an increase in upwelling over the period 1968-2018 in these areas. A search of the related literature reveals that there is no consensus whether upwelling has increased over this period. Upwelling is driven by coastal winds. In a review of related literature, Rykaczewski, and Dunne found that while some previous researchers have found an increase in coastal winds, others have found that the change is not significant (Rykaczewski, and Dunne 2018). If upwelling near the continental shelf has increased, it might offset the effects of increased stratification in those areas.

5.2. Nitrate

The results show that nitrate concentrations in the deep layer have increased from 1985 to 2017 in a region that ranges approximately 300-700 km offshore and from 100-400 m below the surface, as shown in **Error! Reference source not found.** The thermocline in this region is generally estimated around 30-70 m below the surface, so the region where nitrate is increasing is below the thermocline, in the deep layer. (Palacios et al. 2004). Figure 25 also shows there is also a region of nitrate decrease at the surface, ranging approximately 400-600 km offshore. This area of nitrate decrease is situated directly above the larger area of nitrate increase, with the thermocline in between. This is the same area where surface temperature was shown to increase. This implies that a strengthening thermocline is preventing nitrate from reaching the surface, despite increasing nitrate concentration in the deep layer below. While the results obtained here

cannot prove a connection or causality between these processes, the patterns found here warrant further research.

Closer to shore, there is some evidence that dynamics of the system may be different. It appears that in a small nearshore region, nitrate near the surface is increasing. There are a couple of possible explanations for this trend. First, it is possible that the increased levels of nitrate are coming from sources on land, and that rivers or runoff are carrying increased amounts of nitrate to the sea, but Nezlin et al. (2017) did not find significant evidence that anthropogenic sources caused an increase in nearshore nitrate.

The other possibility is that upwelling is bringing increased nitrate to the surface near shore from the offshore deep layer area of increase. The temperature data showed some evidence of decreasing water temperatures above the continental shelf and near shore at 100 m, and this may be evidence of increasing amounts of cold water upwelling from below. An increase in nearshore upwelling in combination with an increased supply of nitrate in the deep layer could supply increased amounts of nitrate to the surface in areas where upwelling is strong, despite increased stratification overall. This is a possible explanation to the paradoxical pattern observed by Nezlin et al. (2017), Gnanadesikan et al. (2001), and others, where primary productivity in the SCCS appears to be increasing despite increasing SST. An increasing source of nitrate in the deep water combined with increased upwelling to deliver it to the surface could spark increasing amounts of productivity at the surface in these areas. This balance between stratification and upwelling would regulate the amount of nitrate reaching the surface, and thus the primary productivity of the ecosystem, as shown in Figure 26.

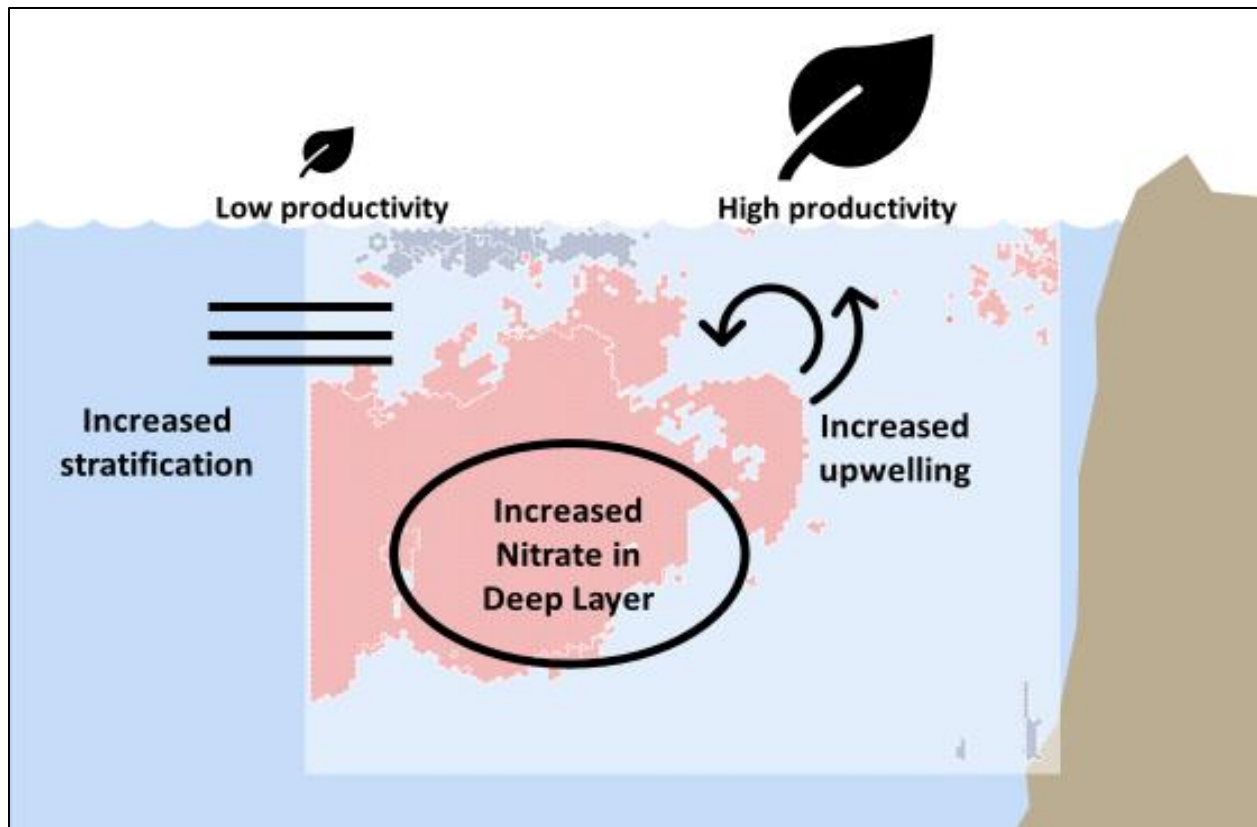


Figure 26 Schematic representing mechanisms controlling nitrate transport to the mixed layer at the surface, and the resulting effects on primary productivity

5.3. Source of the Nitrate Increase

The results clearly show that nitrate is increasing offshore below the thermocline, but where is it coming from? Based upon the shape and position of the area of increase, it is likely that the California Current is transporting nitrate into the area from further north. Summarizing the work of past researchers, Gangopahyay et al. (2011) describe the California Current as a current 100-1350 km wide, ranging from 0-500 m deep, with a nearshore edge that averages (along the whole US west coast) 100-150 km off the coast. A more detailed description indicates that in southern California it is further offshore than the average 100-150 km. Although this is a rather broad description, it fits the pattern of nitrate increase shown in Figure 25.

However, in addition to a description, visualizing the current is helpful in comparing it to the areas of nitrate increase. Past researchers have made many attempts to map the California current, and their results are shown in Figure 27.

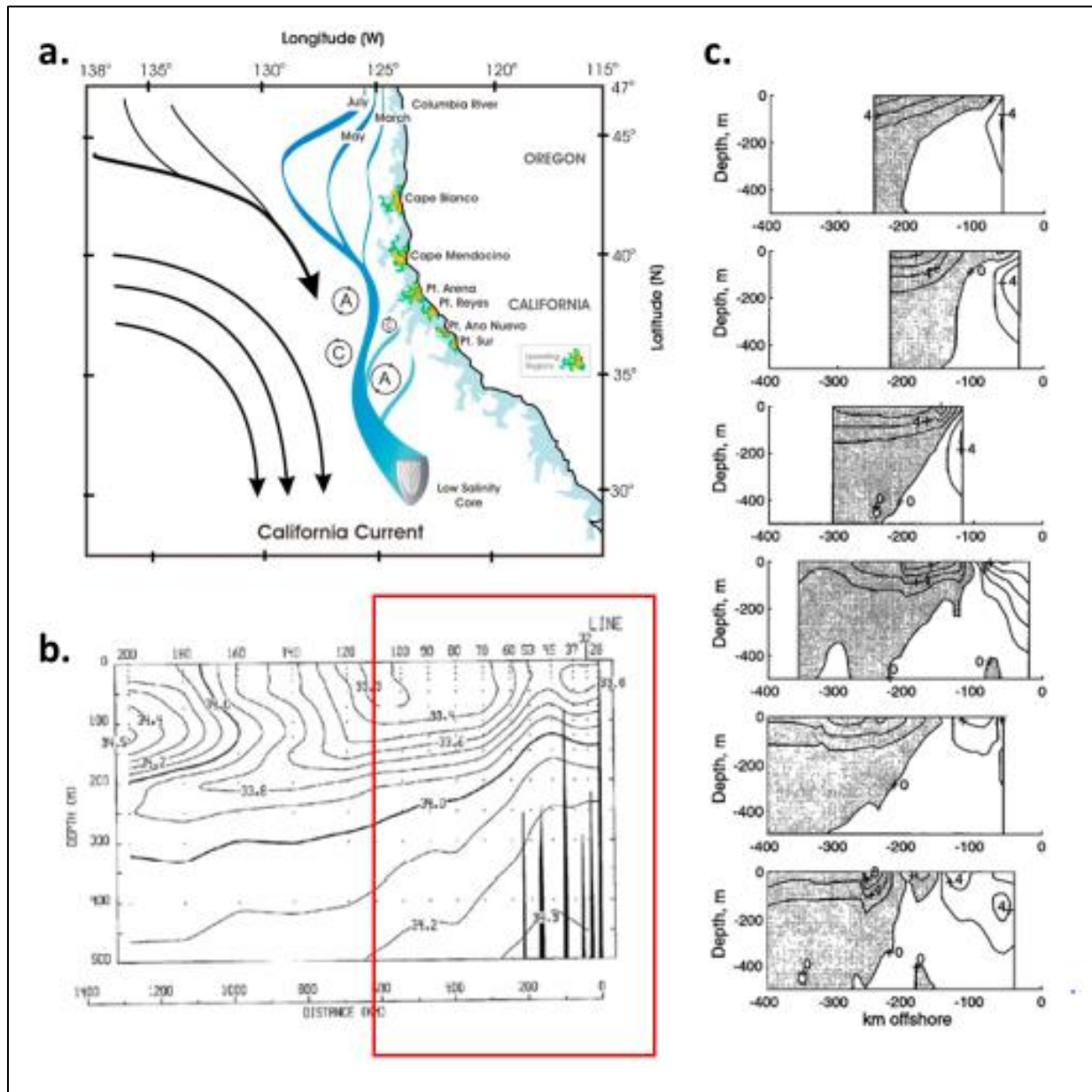


Figure 27 Research indicating the location and extent of the California Current system. (a) shows a schematic of the CCS and the meander-eddy-upwelling system off the coast of CA in spring/summer (Mooers and Robinson, 1984). (b) shows salinity contours along CalCOFI line

90. (Lynn, Bliss and Eber 1982). (c) shows vertical cross sections of CalCOFI transects, Line 77, 80, 83, 87, 90, and 93, from top to bottom. Contours indicate current velocity (gray is southbound, white is northbound) (Bray, Keyes and Morawitz 1999).

Figure 27 Part (a) shows an overall schematic of the path of the CCS from Washington down to southern California and indicates how it changes throughout the seasons as proposed by Moores and Robinson (1984). In this view, the main core of the CC is symbolized in darker blue, and areas of coastal upwelling are symbolized in lighter blues and greens.

Figure 27 Part (b), from Lynn, Bliss and Eber (1982), shows salinity contours along CalCOFI Line 90 in vertical cross sections. The authors of this figure surveyed twice the usual length of transect line 90, so the portion normally surveyed and comparable to data presented here is outlined by the red box. The CCS is defined by fresher, less-salty water than the surrounding seas, so the low-salinity parabolic bowl-shaped contours ranging from about 200-700 km offshore indicate the core of the CCS.

Finally, Figure 27 Part (c) shows cross sections from all six of the CalCOFI transects (Bray, Keyes and Morawitz. 1999). The grey areas symbolize areas of southward flow, showing that the CCS is in the offshore portions of these transects, and reaches from 0-500 m depth. Visual comparison of these previous researchers' results to the increases in nitrate detected in this project suggest that the California Current is a likely source for the increases in nitrate.

One possible reason for the delivery of increased amounts of nitrate by the California Current was suggested by Rykaczewski and Dunne (2010). As discussed in Chapter 2, Rykaczewski and Dunne created an earth system model which they used to forecast the effects of global climate change on the CCS. Their model predicted "increases in nitrate supply and productivity in the 21st century despite increases in stratification and limited change in wind-driven upwelling." This is exactly the pattern seen in the results of this project. Their model suggested that, in comparison to past conditions, water in the California Current will start its

journey farther north, and spend more time beneath the euphotic zone, so it will have time to accumulate more nitrate on its journey to southern California, and less of this nitrate will get used up by organisms in the euphotic zone. As a result, increased amounts of nitrate will arrive in the SCCS as a result of global change in the currents in the North Pacific.

The trends in temperature and nitrate suggest that the SCCS is changing, and if current trends continue, it appears it is moving towards greater extremes of nutrient scarcity and abundance. Nitrate is increasing in the deep water but increasing surface temperatures and stratification may make it impossible for nitrate in the deep water to reach the surface, creating a low-productivity nutrient desert in highly stratified areas offshore. However, closer to shore, upwelling will bring the increased amount of nitrate to the surface, potentially fueling a highly productive ecosystem in this area. While other factors, such as oxygen, will affect ecosystem outcomes as well, it would be wise to consider these trends in nitrate when making policy decisions and constructing marine protected areas (MPAs) to preserve the ecosystems and fisheries in these productive areas.

5.4. Conclusion

Further research is necessary to inform plans for the future of this area. While this research has shown trends in past data, it cannot make any mathematical projections about the future. Improvements to the statistical methods would be beneficial. Specifically, future work on this topic would benefit from more sophisticated statistical methods for smoothing the time series data used to build the space time cubes and calculate trends.

Additionally, while the Mann Kendall test is a useful indicator of increase or decrease in a time series, it does not result in any slope or magnitude of increase or decrease. Space time cube results might be more useful if linear regression or Sen's slope statistics could be applied to

each bin column. The “time series clustering” tool for space time cube analysis may also prove useful in future research, although comparing clusters built from different data is somewhat problematic.

Presenters at the 2019 Esri User Conference announced that three-dimensional voxels are an upcoming feature in ArcGIS, and this new format may revolutionize analysis of datasets such as this one in the future. While this and other opportunities to improve data analysis techniques for this and other multidimensional spatio-temporal datasets may soon become more accessible, It is hoped that the results obtained here may prove useful as they stand. Many researchers are building models to forecast future change, and these models require a clear understanding of the mechanisms that affect the system, and accurate data to validate the model. Perhaps the results of this project will be useful in constructing better and more accurate models for forecasting changes in this complex ocean environment.

The methods presented in this thesis have plenty of opportunities for improvement. More exploration of the dataset prior to analysis might have shown that nitrate measurements in the 1970’s were inconsistent, and this would have saved time and effort in discovering this and then trimming the nitrate data to a shorter time span later. Also, hindsight shows that some unnecessary columns (such as attributes like oxygen concentration) that were never used were left in data tables during the original trimming of the data. Removing the superfluous data earlier on in the process would improve processing speed when analyzing large tables and save memory for large point shapefiles. Finally, improvements could be made to custom ModelBuilder tools and the methods for creation of vertical cross sections.

The custom iterative workflows that were developed for this thesis accomplished their goals but were computationally intensive and took a very long time to run. With a better

understanding of which tasks take the longest times and greatest processing power, better models could be created to minimize processing time.

In future development of these methods, it would be beneficial to build some sort of quality control for EBK3D into the ModelBuilder workflow. The goal would be to ensure that each iteration of EBK3D meets a certain standard of cross validation. Ideally, a user would be notified if cross validation results of EBK3D indicated that the interpolated predictions were not reliable, and the user could then investigate the cause of the inaccuracy of the predictions (for example, small input sample size, error in measured value, or bias in the data). Data could be edited or discarded to remedy the errors, and any resulting gaps in data could be filled with the option to fill empty bins with space time neighbors during the creation of the Space Time Cube. It may be possible to write a custom Python script to ensure that important summary statistics of EBK3D, such as Root Mean Squares, are below a certain threshold of error.

In addition, the workflow for creating target points in vertical cross sections was time-intensive and inelegant. If this workflow were to be repeated, it might be worth writing scripts in Python or SQL to automate the construction of a grid of target points for each vertical cross section, as this was a very monotonous and time-consuming task to do by hand. Because there were no prior examples of the workflow utilized in this thesis available in related literature, this novel workflow was created through a process of trial and error. Undoubtedly, future versions of this workflow could be much more efficient.

While there are many opportunities for improvement of the methods developed in this research, they may prove useful in analyzing other datasets. Although CalCOFI's dataset has the distinction of being the oldest of its kind, there are many other hydrographic datasets worldwide that could be analyzed using similar methods. Organizations across the globe are seeking new

methods to understand three-dimensional ocean data. For example, one of the future goals of Esri's Ecological Marine Units project is to map change over time in their 3D ocean data worldwide.

New exploration is continuously taking place in the deep sea and the polar oceans, and in some areas the oceans are changing faster than we can measure them. It is necessary for researchers to develop new methods for collecting and analyzing ocean data to understand these changes quickly. Hopefully the methods and results presented here will contribute to this global effort.

References

- Antonelis, George A, and Clifford H Fiscus. 1980. "The Pinnipeds of the California Current." CalCOFI Rep., Vol. XXI, 1980.
- Becker, J. J., D. T. Sandwell, W. H. F. Smith, J. Braud, B. Binder, J. Depner, D. Fabre, et al. 2009. "Global Bathymetry and Elevation Data at 30 Arc Seconds Resolution: SRTM30_PLUS." *Marine Geodesy* 32 (4): 355–71. <https://doi.org/10.1080/01490410903297766>.
- Bograd, Steven J, David A Checkley, and Warren S Wooster. 2003. "CalCOFI: A Half Century of Physical, Chemical, and Biological Research in the California Current System." *Deep Sea Research Part II: Topical Studies in Oceanography* 50 (14–16): 2349–53. [https://doi.org/10.1016/S0967-0645\(03\)00122-X](https://doi.org/10.1016/S0967-0645(03)00122-X).
- Bray, N. A., A. Keyes, and W. M. L. Morawitz. 1999. "The California Current System in the Southern California Bight and the Santa Barbara Channel." *Journal of Geophysical Research: Oceans* 104 (C4): 7695–7714. <https://doi.org/10.1029/1998JC900038>.
- CalCOFI 2019a. "CalCOFI Research Plan Final.Pdf." n.d. Accessed January 15, 2019. <https://swfsc.noaa.gov/uploadedFiles/Divisions/FRD/CalCOFI/CalCOFI%20research%20plan%20final.pdf>.
- CalCOFI 2019b. "Methods Timeline." n.d. Accessed August 12, 2019. <https://calcofi.org/about-calcofi/methods/5-methods-timeline.html>.
- CalCOFI 2019c. "Nutrient Methods." n.d. Accessed August 12, 2019. <https://calcofi.org/cruises/2011-cruises/calcofi-1101nh/422-1101nh-preliminary-plots.html>.
- California Sea Grant. 2019. "Santa Barbara Channel | California Sea Grant." n.d. Accessed August 4, 2019. <https://caseagrant.ucsd.edu/project/discover-california-commercial-fisheries/regions/santa-barbara-channel>.
- CDFW 2018. "Table 15 – Poundage And Value Of Landings Of Commercial Fish Into California By Area." System: CFIS Table 15. Accessed August 8, 2019. <https://nrm.dfg.ca.gov/FileHandler.ashx?DocumentID=159560&inline>
- Chao, Yi, John D. Farrara, Hongchun Zhang, Kevin J. Armenta, Luca Centurioni, Francisco Chavez, James B. Girton, Dan Rudnick, and Ryan K. Walter. 2018. "Development, Implementation, and Validation of a California Coastal Ocean Modeling, Data Assimilation, and Forecasting System." *Deep Sea Research Part II: Topical Studies in Oceanography* 151 (May): 49–63. <https://doi.org/10.1016/j.dsr2.2017.04.013>.
- Debich, Amanda J, Bruce Thayre, and John A Hildebrand. 2017. "Marine Mammal Monitoring on California Cooperative Oceanic Fisheries Investigation (CALCOFI) Cruises: Summary of Results 2012-2016." MPL Technical Memorandum 609.

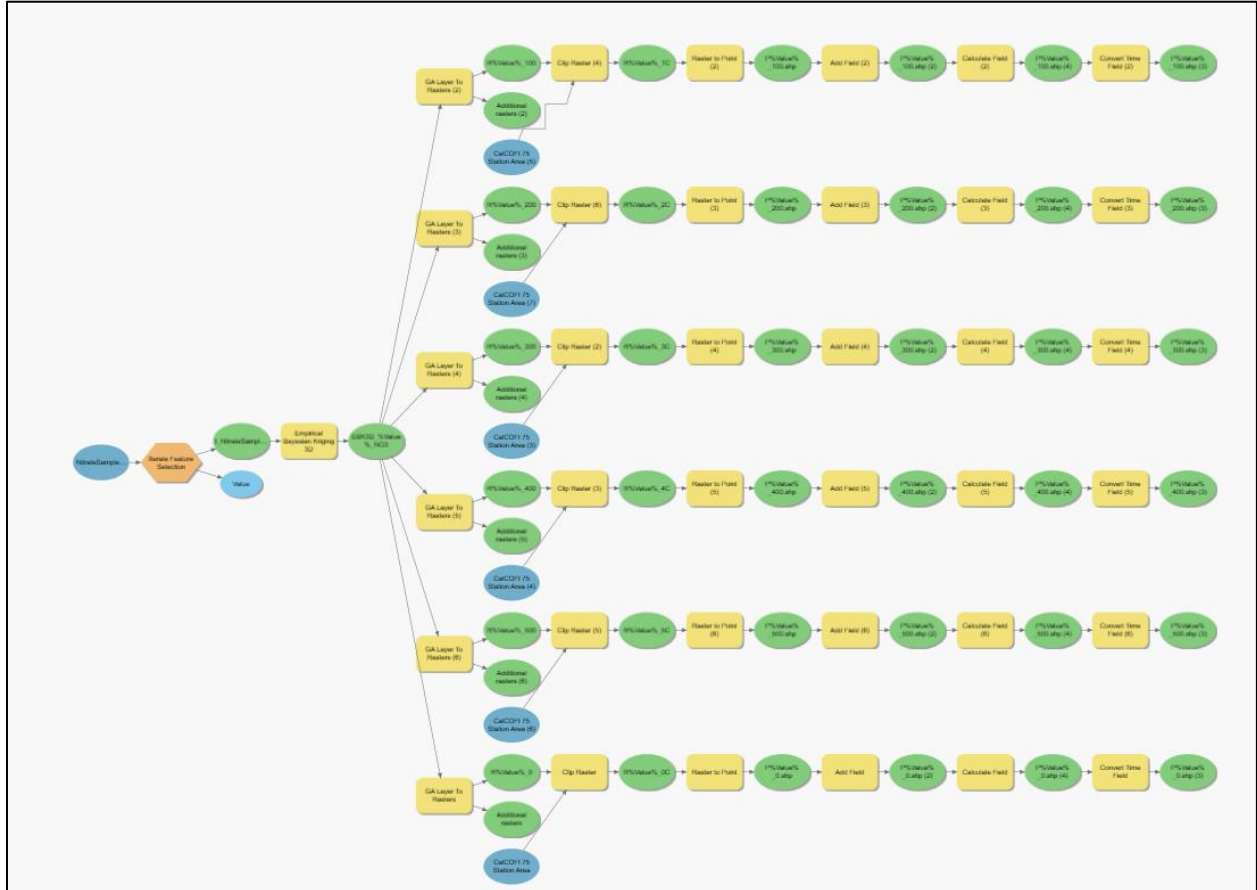
- Di Lorenzo, Emanuele, Arthur J. Miller, Niklas Schneider, and James C. McWilliams. 2005. “The Warming of the California Current System: Dynamics and Ecosystem Implications.” *Journal of Physical Oceanography* 35 (3): 336–62. <https://doi.org/10.1175/JPO-2690.1>.
- Emery, K. O. 1956. “Deep Standing Internal Waves in California Basins1.” *Limnology and Oceanography* 1 (1): 35–41. <https://doi.org/10.4319/lo.1956.1.1.0035>.
- Eppley, RW, Renger, EH, Harrison, WG. 1979. “Nitrate and Phytoplankton in southern California coastal waters.” Accessed August 19, 2019. http://terascan.smast.umassd.edu/nasdata/archive/Bisagni_Data/students/abrunner/My%20Documents/Classes/ECOS630/papers/Eppley__1979.pdf.
- Esri 2019a. “What Is Empirical Bayesian Kriging 3D?—ArcGIS Pro | ArcGIS Desktop.” n.d. Accessed August 20, 2019. <https://pro.arcgis.com/en/pro-app/help/analysis/geostatistical-analyst/what-is-empirical-bayesian-kriging-3d-.htm>.
- Esri 2019b. “How Creating a Space Time Cube Works—ArcGIS Help | ArcGIS Desktop.” n.d. Accessed August 20, 2019. <https://pro.arcgis.com/en/pro-app/tool-reference/space-time-pattern-mining/learnmorecreatecube.htm>.
- Fewings, Melanie R. 2017. “Large-Scale Structure in Wind Forcing over the California Current System in Summer.” *Monthly Weather Review* 145 (10): 4227–47. <https://doi.org/10.1175/MWR-D-17-0106.1>.
- Fielder, Paul C., Roy Mendelssohn, Daniel M. Palacios, and Steven J. Bograd. 2012. “Pycnocline Variations in the Eastern Tropical and North Pacific, 1958–2008.” *Journal of Climate* 26 (2): 583–99. <https://doi.org/10.1175/JCLI-D-11-00728.1>.
- Gangopadhyay, Avijit, Pierre F.J. Lermusiaux, Leslie Rosenfeld, Allan R. Robinson, Leandro Calado, Hyun Sook Kim, Wayne G. Leslie, and Patrick J. Haley. 2011. “The California Current System: A Multiscale Overview and the Development of a Feature-Oriented Regional Modeling System (FORMS).” *Dynamics of Atmospheres and Oceans* 52 (1–2): 131–69. <https://doi.org/10.1016/j.dynatmoce.2011.04.003>.
- Gnanadesikan, Anand, Richard D. Slater, Nicolas Gruber, and Jorge L. Sarmiento. 2001. “Oceanic Vertical Exchange and New Production: A Comparison between Models and Observations.” *Deep Sea Research Part II: Topical Studies in Oceanography* 49 (1–3): 363–401. [https://doi.org/10.1016/S0967-0645\(01\)00107-2](https://doi.org/10.1016/S0967-0645(01)00107-2).
- Johnson, Alexa. 2013. “Catalina Island Conservancy.” Accessed August 4, 2019. https://www.catalinaconservancy.org/index.php?s=news&p=article_311.
- Kahru, Mati, Raphael Kudela, Marlenne Manzano-Sarabia, and B. Greg Mitchell. 2009. “Trends in Primary Production in the California Current Detected with Satellite Data.” *Journal of Geophysical Research: Oceans* 114 (C2). <https://doi.org/10.1029/2008JC004979>.

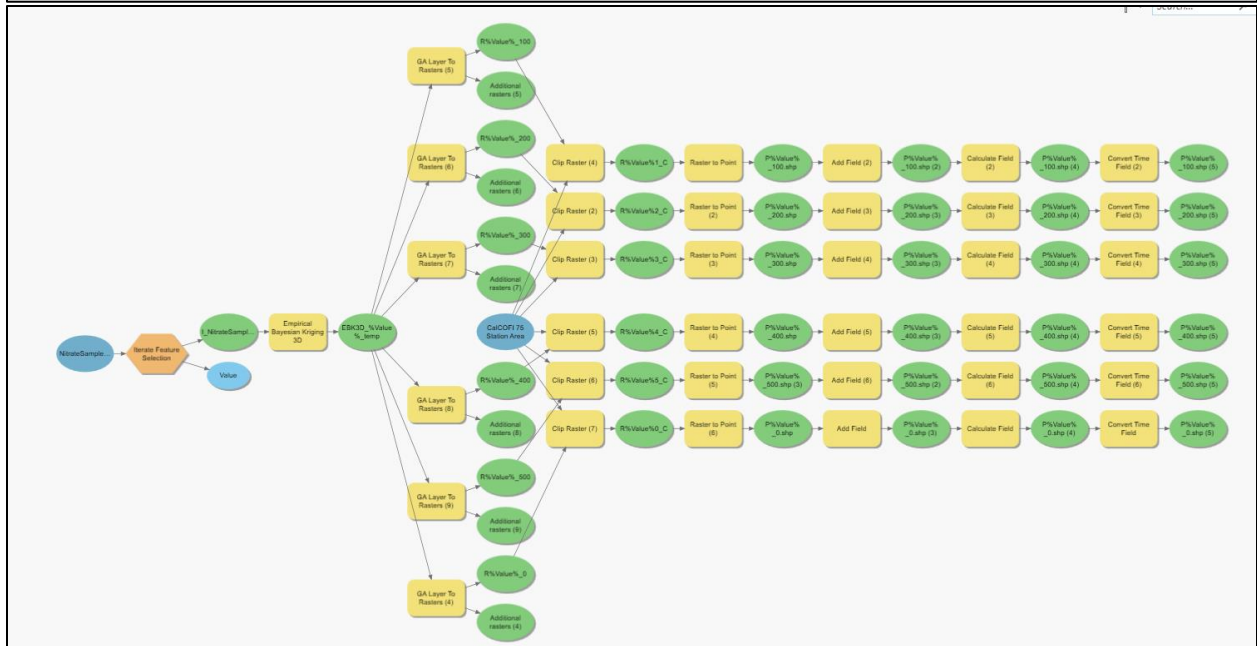
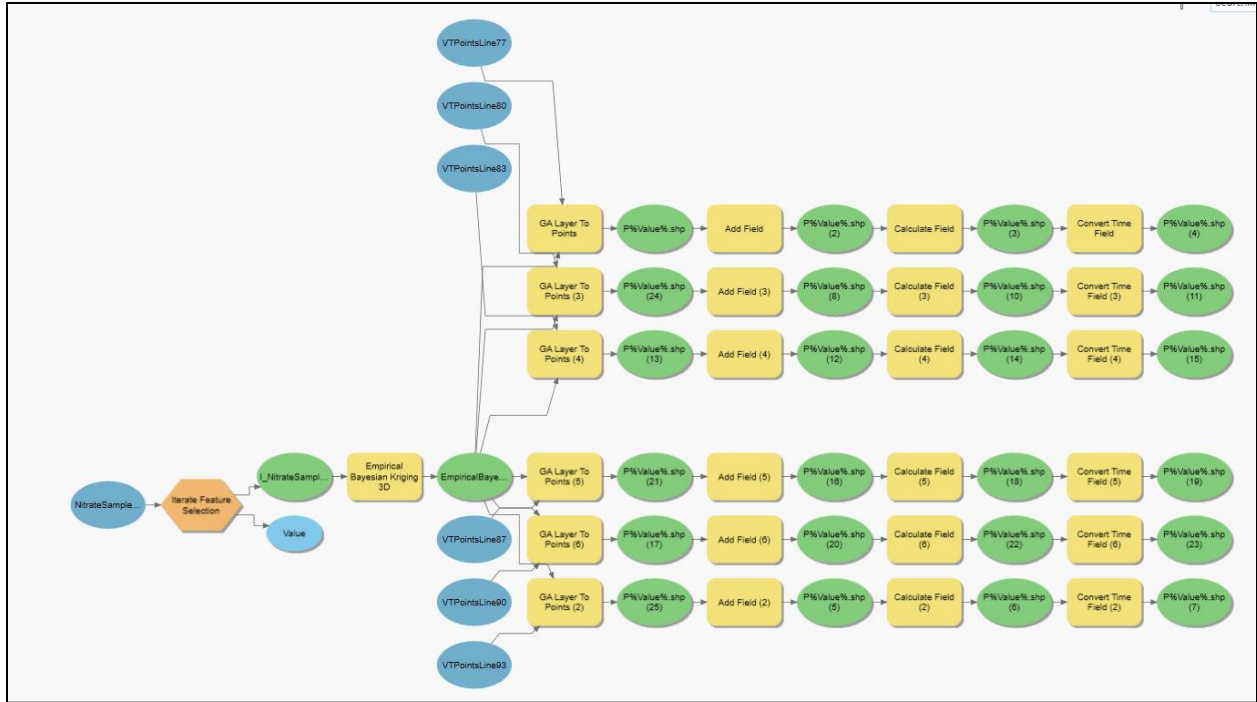
- Kudela, R. M., and R. C. Dugdale. 2000. "Nutrient Regulation of Phytoplankton Productivity in Monterey Bay, California." *Deep Sea Research Part II: Topical Studies in Oceanography* 47 (5): 1023–53. [https://doi.org/10.1016/S0967-0645\(99\)00135-6](https://doi.org/10.1016/S0967-0645(99)00135-6).
- Lynn, K. J., K. A. Bliss, and L. E. Eber. 1982. "Vertical and horizontal distributions of seasonal mean temperature, salinity, sigma-t, stability, dynamic height, oxygen and oxygen saturation in the California Current, 1950-1978," *Calif. Coop. Oceanic Fish. Invest. Atlas* 30. La Jolla, Calif.: Scripps Institution of Oceanography, 513 pp.
- McClatchie, Sam. 2013. *Regional Fisheries Oceanography of the California Current System: The CalCOFI Program*. Springer Science & Business Media.
- McGowan, John A, Steven J Bograd, Ronald J Lynn, and Arthur J Miller. 2003. "The Biological Response to the 1977 Regime Shift in the California Current." *Deep Sea Research Part II: Topical Studies in Oceanography, CalCOFI: A Half Century of Physical, Chemical and Biological Research in the California Current System*, 50 (14): 2567–82. [https://doi.org/10.1016/S0967-0645\(03\)00135-8](https://doi.org/10.1016/S0967-0645(03)00135-8).
- Miller, Arthur J, Alber J Gabric, John R. Moisan, Fei Chai, Douglas J. Neilson, David W. Pierce, Emmanuele Di Lorenzo. "Global Change and Oceanic Primary Productivity: Effects of Ocean-Atmosphere-Biological Feedbacks. Miller_et_al_2006_ocean_prim_prod_and_clim_change_ocean_atmo_feedbacks.Pdf." n.d. Accessed March 10, 2019. http://meteora.ucsd.edu/~pierce/papers/Miller_et_al_2006_ocean_prim_prod_and_clim_change_ocean_atmo_feedbacks.PDF.
- Mooers, C. N., and A. R. Robinson. 1984. "Turbulent Jets and Eddies in the California Current and Inferred Cross-Shore Transports." *Science (New York, N.Y.)* 223 (4631): 51–53. <https://doi.org/10.1126/science.223.4631.51>.
- Nezlin, Nikolay P., Karen McLaughlin, J. Ashley T. Booth, Curtis L. Cash, Dario W. Diehl, Kristen A. Davis, Adriano Feit, et al. 2018. "Spatial and Temporal Patterns of Chlorophyll Concentration in the Southern California Bight." *Journal of Geophysical Research: Oceans* 123 (1): 231–45. <https://doi.org/10.1002/2017JC013324>.
- NOAA. n.d. "Research in the California Current - SWFSC." Accessed January 18, 2019. <https://swfsc.noaa.gov/textblock.aspx?id=1051> <https://swfsc.noaa.gov/textblock.aspx?id=1051>.
- NOAA 2018a. "What Is a Thermocline?" Accessed August 16, 2019b. <https://oceanservice.noaa.gov/facts/thermocline.html>.
- NOAA 2018b. US Department of Commerce, National Oceanic and Atmospheric Administration. n.d. "How Far Does Light Travel in the Ocean?" Accessed August 16, 2019a. https://oceanservice.noaa.gov/facts/light_travel.html.
- NOAA 2018c. "What Is Upwelling?" Accessed August 16, 2019. <https://oceanservice.noaa.gov/facts/upwelling.html>.

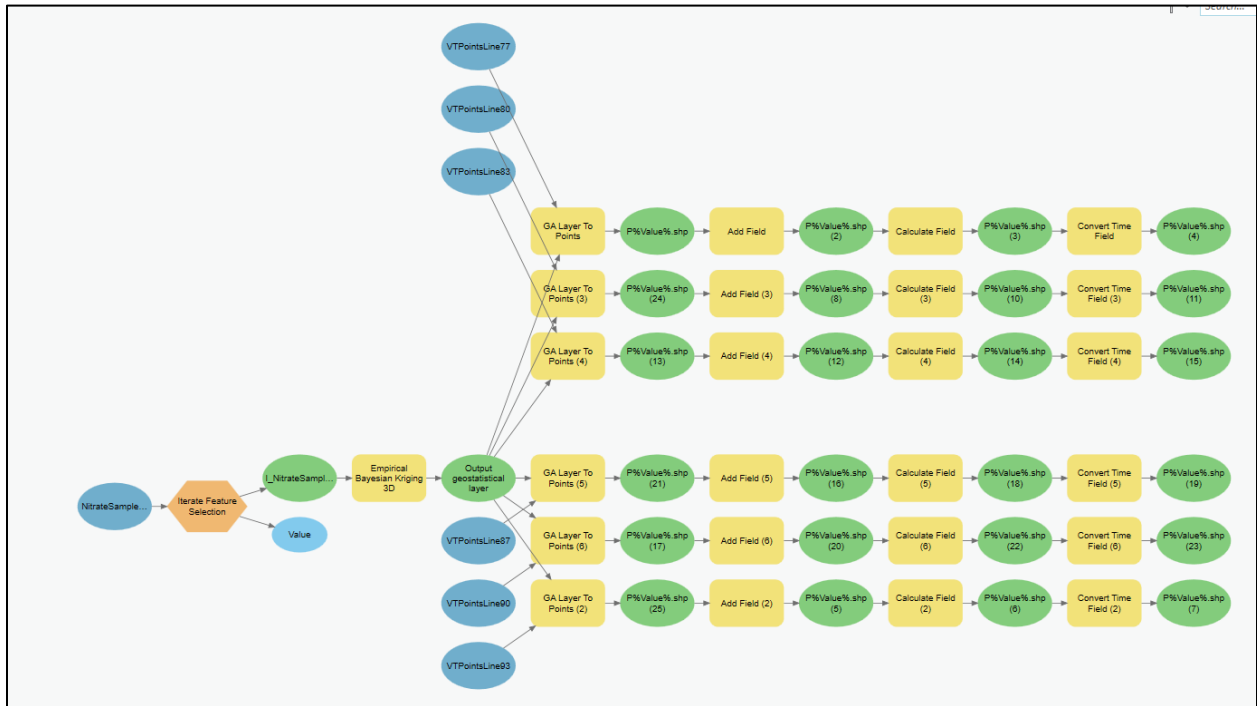
- NOAA ENOW 2015. ENOW Explorer. Accessed August 2, 2019.
<https://coast.noaa.gov/enowexplorer/#/gdp/tourism/2015/06037>
- NOAA OMAO. 2017. "Specifications | Office of Marine and Aviation Operations." Accessed August 21, 2019. <https://www.oma.noaa.gov/learn/marine-operations/ships/reuben-lasker/about/specifications>.
- Ohman, Mark, and Elizabeth Venrick. 2003. "CalCOFI in a Changing Ocean." *Oceanography* 16 (3): 76–85. <https://doi.org/10.5670/oceanog.2003.34>.
- Palacios, Daniel M., Elliott L. Hazen, Isaac D. Schroeder, and Steven J. Bograd. 2013. "Modeling the Temperature-Nitrate Relationship in the Coastal Upwelling Domain of the California Current." *Journal of Geophysical Research: Oceans* 118 (7): 3223–39. <https://doi.org/10.1002/jgrc.20216>.
- Palacios, Daniel M., Steven J. Bograd, Roy Mendelssohn, and Franklin B. Schwing. 2004. "Long-Term and Seasonal Trends in Stratification in the California Current, 1950–1993." *Journal of Geophysical Research: Oceans* 109 (C10). <https://doi.org/10.1029/2004JC002380>.
- Roemmich, Dean, and John McGowan. 1995. "Climatic Warming and the Decline of Zooplankton in the California Current." *Science* 267 (5202): 1324–26. <https://doi.org/10.1126/science.267.5202.1324>.
- Rykaczewski, Ryan R., and John P. Dunne. 2010. "Enhanced Nutrient Supply to the California Current Ecosystem with Global Warming and Increased Stratification in an Earth System Model." *Geophysical Research Letters* 37 (21). <https://doi.org/10.1029/2010GL045019>.
- Sayre, Roger G., Dawn J. Wright, Sean P. Breyer, Kevin A. Butler, Keith Van Graafeiland, Mark J. Costello, Peter T. Harris, et al. 2017. "A Three-Dimensional Mapping of the Ocean Based on Environmental Data." *Oceanography* 30 (1): 90–103.
- Simrad. 2010. "MX510-MX512_OM_EN_510-100-2002_B_w.Pdf." n.d. Accessed August 21, 2019. https://www.navico-commercial.com/Root/SimradProSeries_docs/MX510-MX512_OM_%20EN_510-100-2002_B_w.pdf.
- Stukel, Michael R., Lihini I. Aluwihare, Katherine A. Barbeau, Alexander M. Chekalyuk, Ralf Goericke, Arthur J. Miller, Mark D. Ohman, et al. 2017. "Mesoscale Ocean Fronts Enhance Carbon Export Due to Gravitational Sinking and Subduction." *Proceedings of the National Academy of Sciences*, January, 2016. <https://doi.org/10.1073/pnas.1609435114>.
- Sydeman, William J., Sarah Ann Thompson, Jarrod A. Santora, J. Anthony Koslow, Ralf Goericke, and Mark D. Ohman. 2015. "Climate–Ecosystem Change off Southern California: Time-Dependent Seabird Predator–Prey Numerical Responses." *Deep Sea Research Part II: Topical Studies in Oceanography* 112 (February): 158–70. <https://doi.org/10.1016/j.dsr2.2014.03.008>.

- Thompson, Andrew R, Sam McClatchie, Robert M Suryan, Jane Dolliver, and Stephanie Loreda. 2018. "State of the California Current 2017–18: Still Not Quite Normal In The North And Getting Interesting In The South" 59: 66.
- VanGraafeiland, Keith 2018. "Local EMU Pro Project with Tasks." Accessed March 15, 2019. <https://www.arcgis.com/home/item.html?id=fb50e08dda3a46ab815ad871ee8c7840>
- Wright, Dawn J., ed. 2002. *Undersea with GIS*. Redlands, Calif: ESRI Press.
- Xiu, Peng, Fei Chai, Enrique N. Curchitser, and Frederic S. Castruccio. 2018. "Future Changes in Coastal Upwelling Ecosystems with Global Warming: The Case of the California Current System." *Scientific Reports* 8 (1): 2866. <https://doi.org/10.1038/s41598-018-21247-7>.

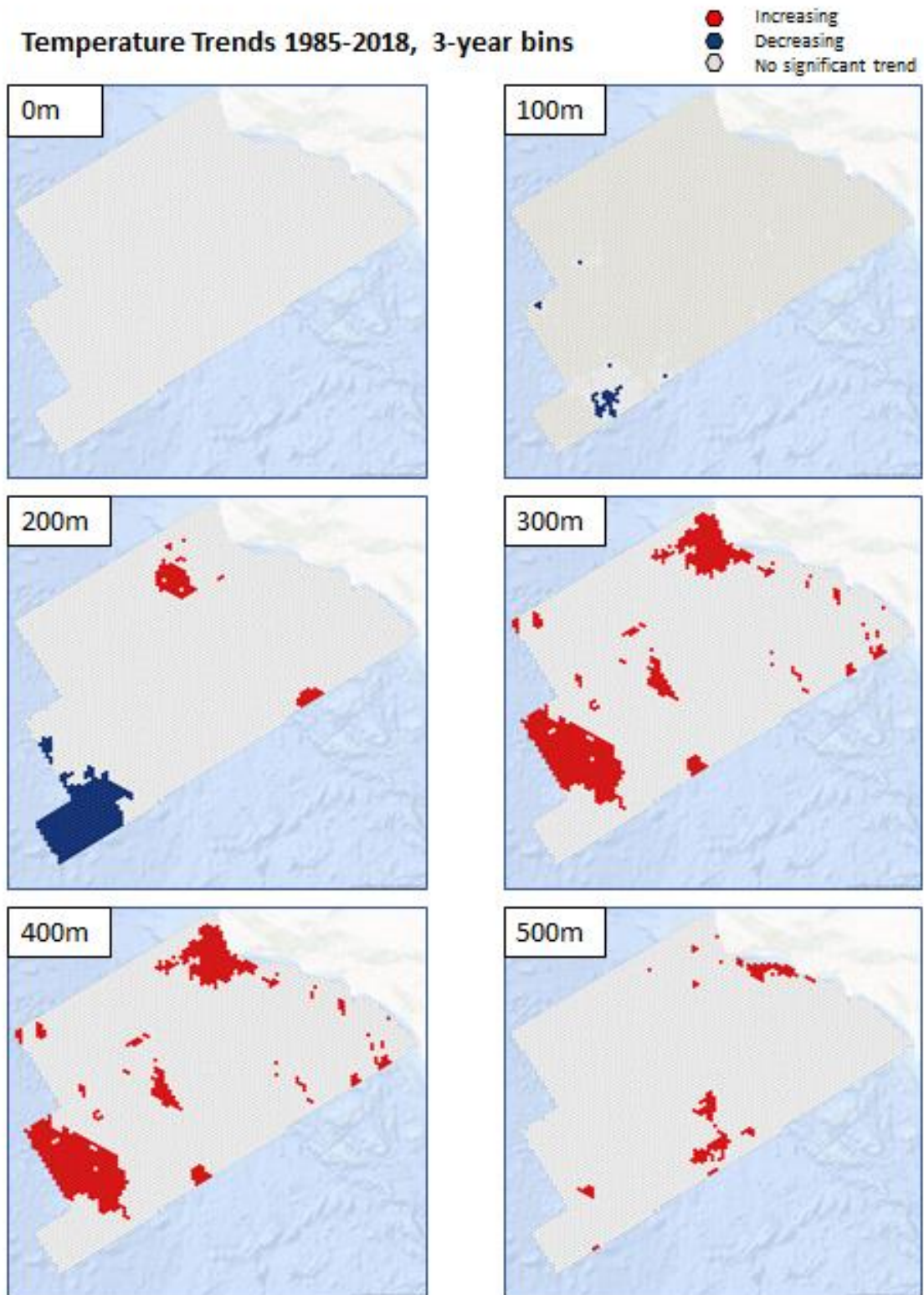
Appendix A Iterative Workflows in ModelBuilder



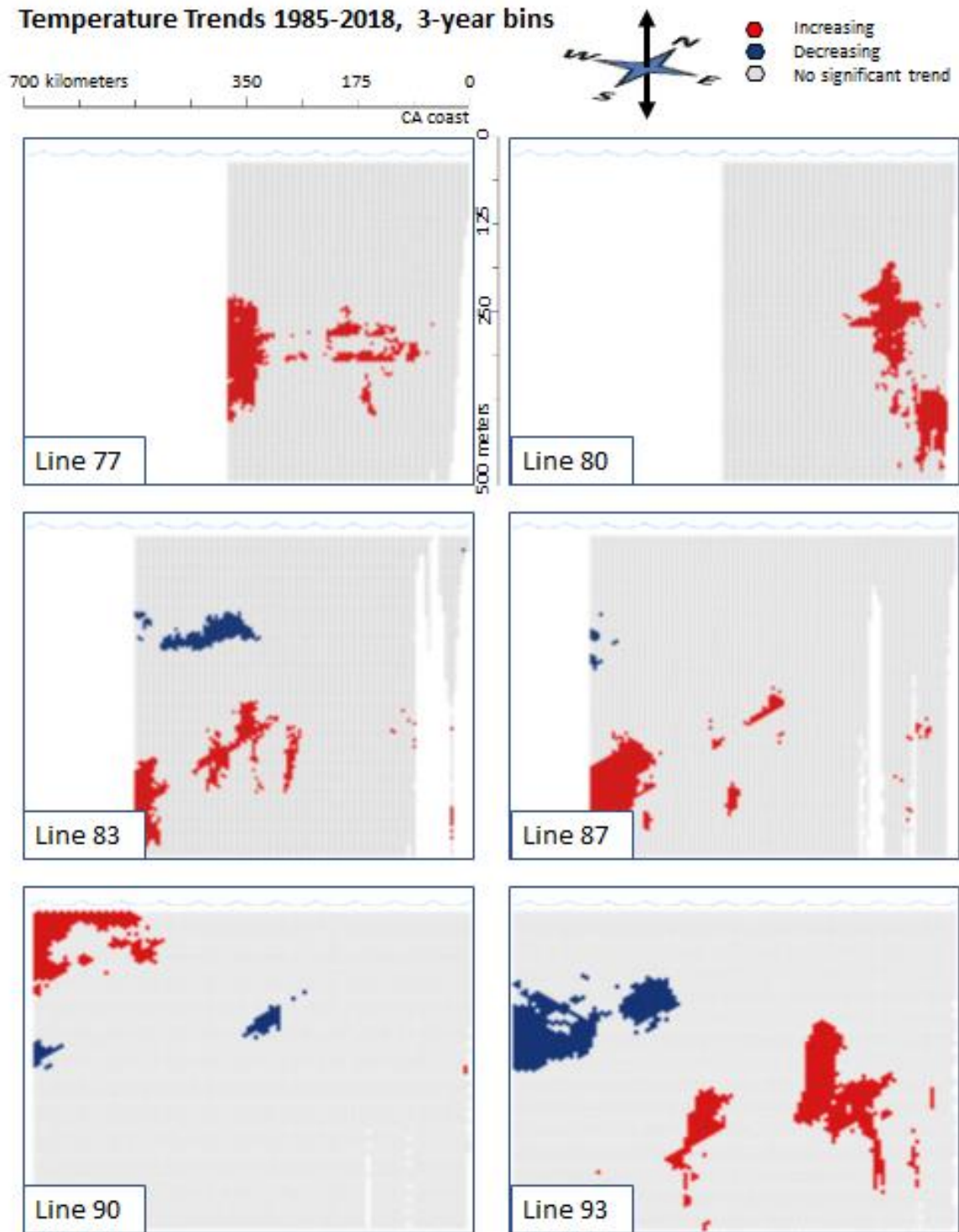




Appendix B Trends Not Used in Main Body of Thesis

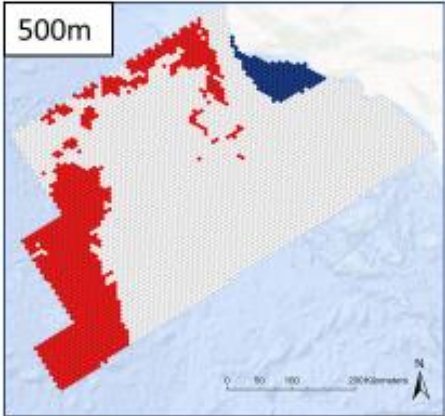
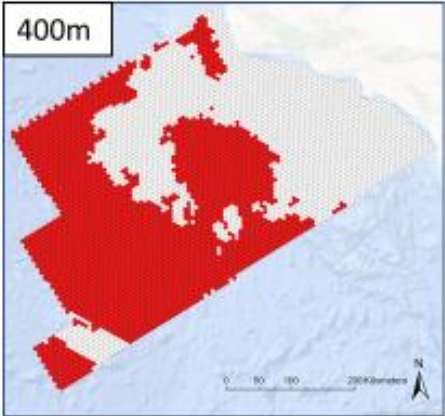
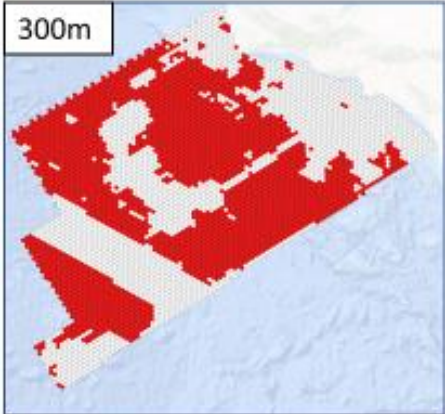
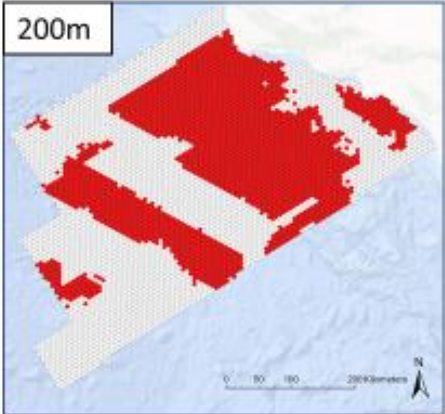
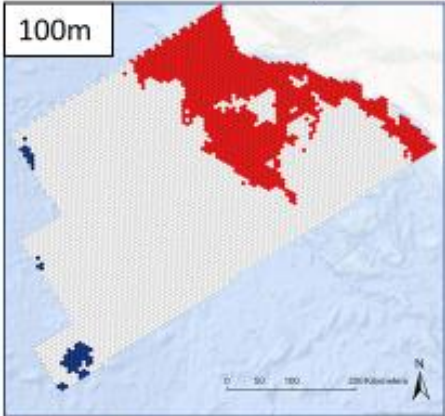
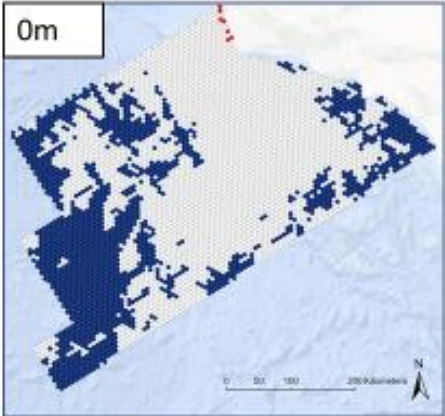


Temperature Trends 1985-2018, 3-year bins



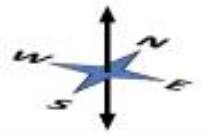
Nitrate Trends 1968-2018, 5-year bins

- Increasing
- Decreasing
- No significant trend

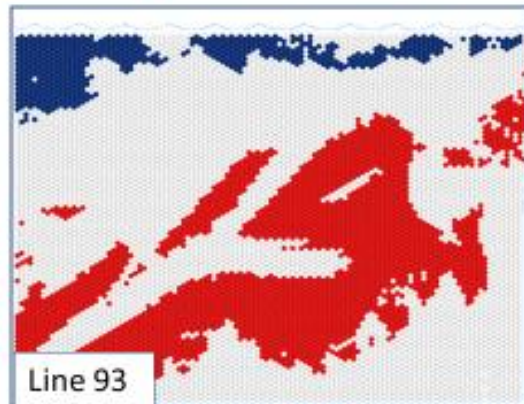
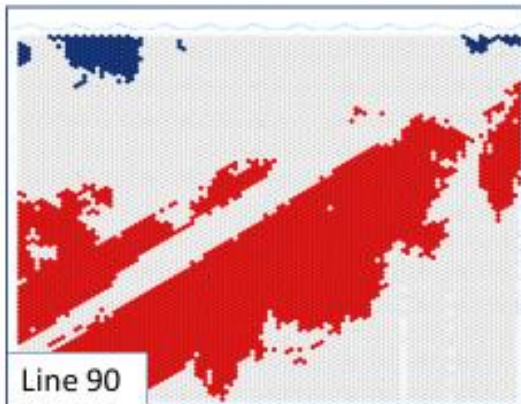
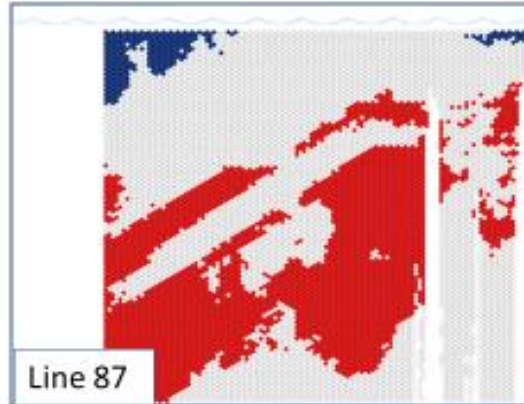
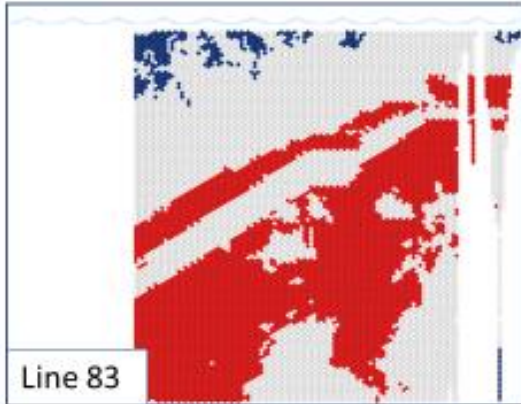
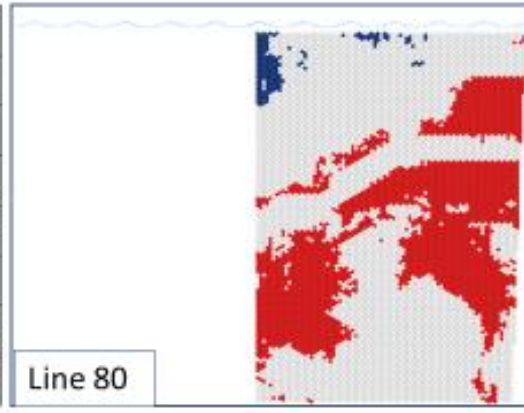
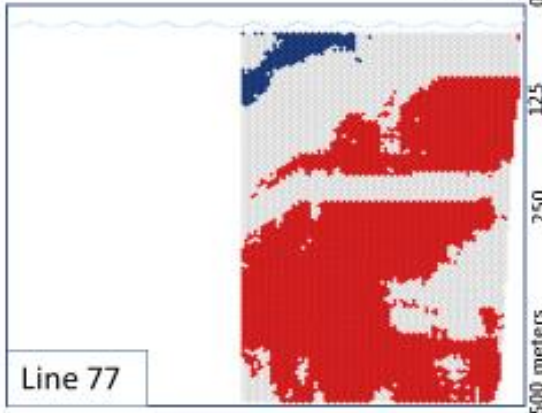


Nitrate Trends 1968-2018, 5-year bins

700 kilometers 350 175 0
CA coast

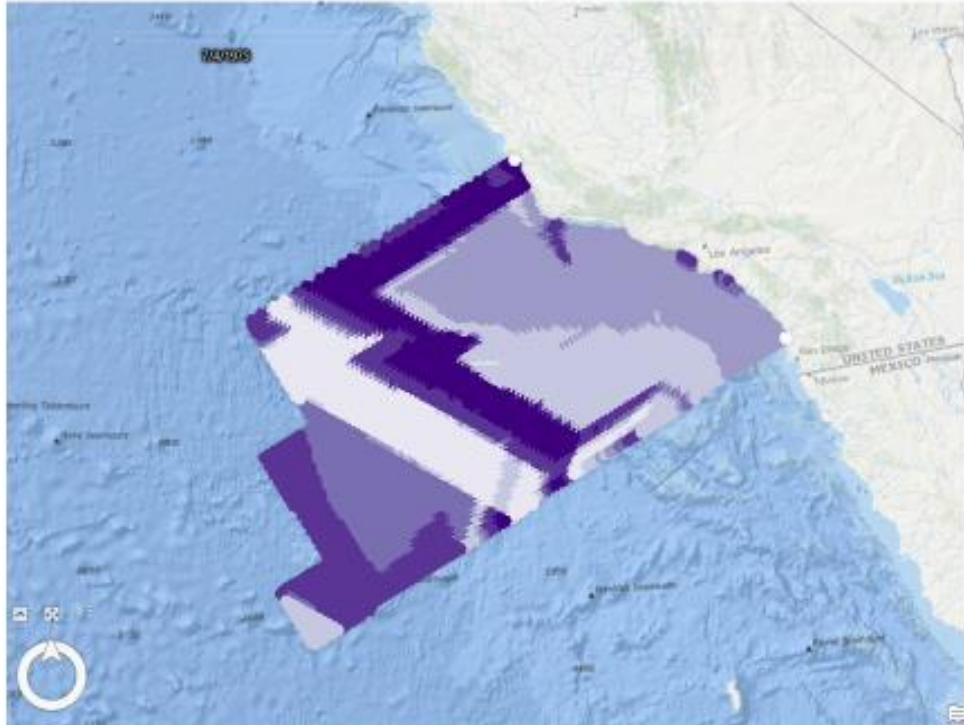


- Increasing
- Decreasing
- No significant trend



Appendix C Anomalous Nitrate Data

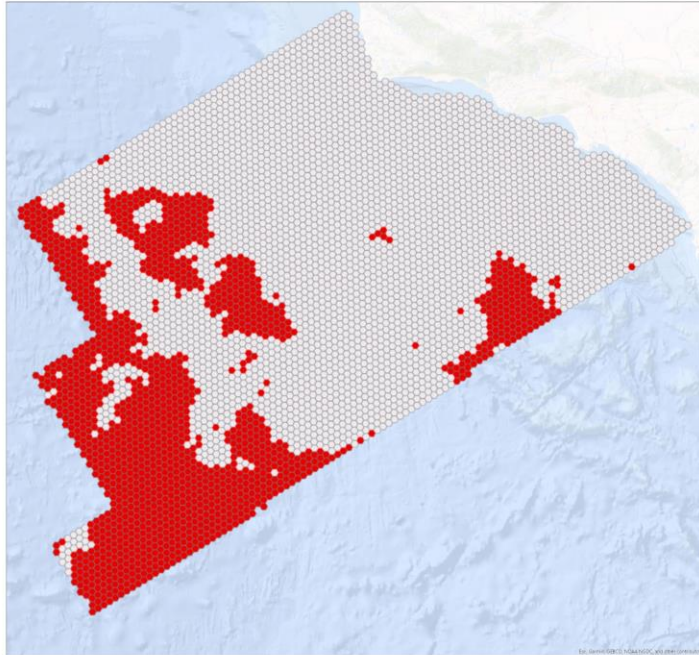
1975 Nitrate measurements –
source of error



Appendix D Results with “Filmstrips”

Temperature 1969--2018, Horizontal Cross Sections

0 m



(Left) Temperature trend over time, defined by Mann Kendall statistic

-  Increasing
-  Decreasing
-  No significant trend

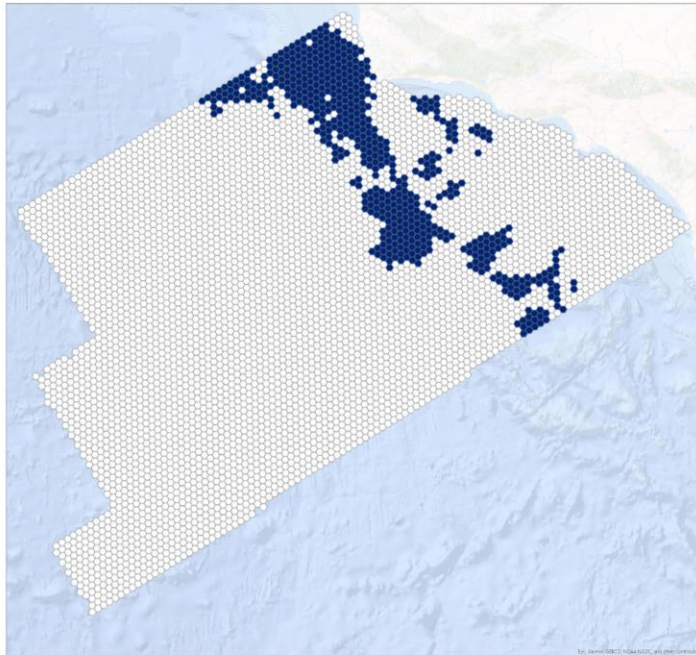
(Below) Temperature (°C)

-  ≤ 3.00
-  ≤ 6.00
-  ≤ 9.00
-  ≤ 12.00
-  ≤ 15.00
-  ≤ 18.00
-  ≤ 21.00



1968 —————> 2018
Time (5-year means)

100m



(Left) Temperature trend over time, defined by Mann Kendall statistic

-  Increasing
-  Decreasing
-  No significant trend

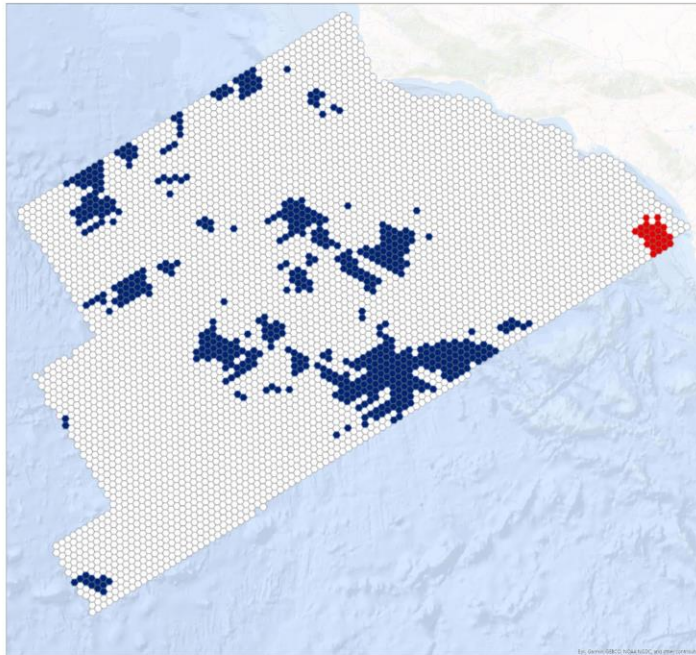
(Below) Temperature (°C)

-  ≤ 3.00
-  ≤ 6.00
-  ≤ 9.00
-  ≤ 12.00
-  ≤ 15.00
-  ≤ 18.00
-  ≤ 21.00



1968  2018
Time (5-year means)

200m

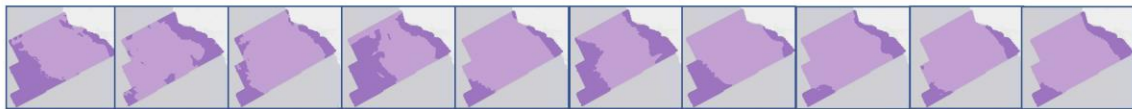


(Left) Temperature trend over time, defined by Mann Kendall statistic

-  Increasing
-  Decreasing
-  No significant trend

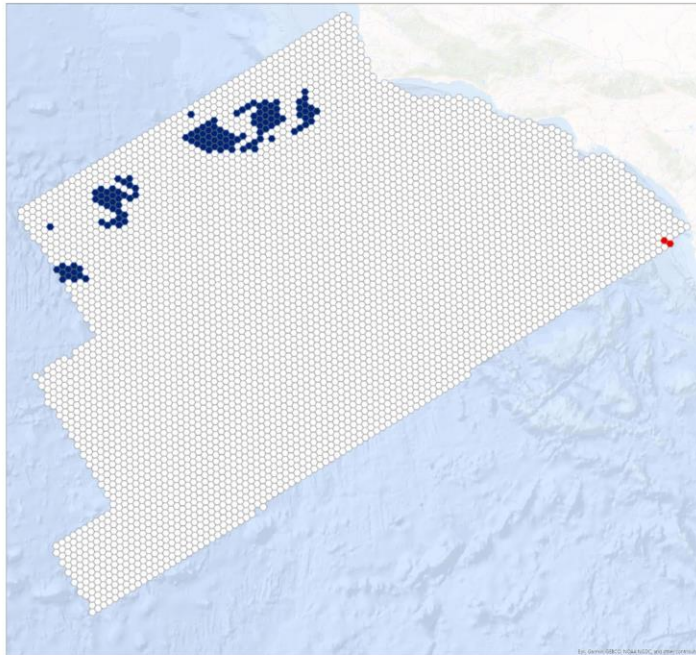
(Below) Temperature ($^{\circ}\text{C}$)

-  ≤ 3.00
-  ≤ 6.00
-  ≤ 9.00
-  ≤ 12.00
-  ≤ 15.00
-  ≤ 18.00
-  ≤ 21.00



1968  2018
Time (5-year means)

300m

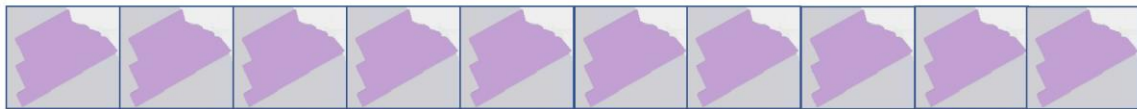


(Left) Temperature trend over time, defined by Mann Kendall statistic

-  Increasing
-  Decreasing
-  No significant trend

(Below) Temperature (°C)

-  ≤ 3.00
-  ≤ 6.00
-  ≤ 9.00
-  ≤ 12.00
-  ≤ 15.00
-  ≤ 18.00
-  ≤ 21.00

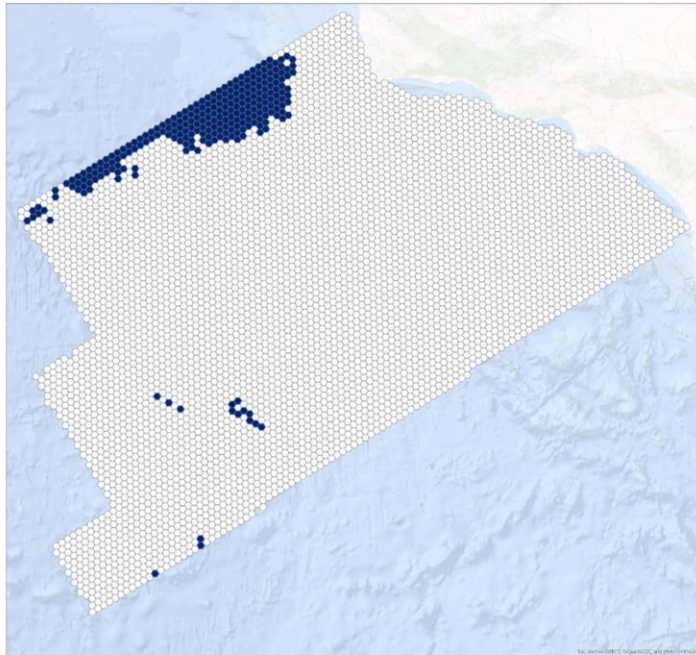


1968

Time (5-year means)

2018

400m

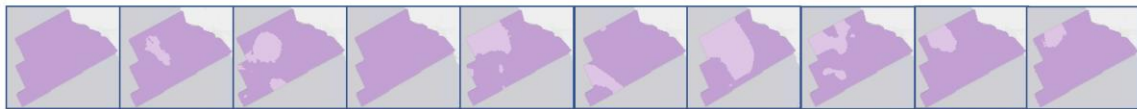


(Left) Temperature trend over time, defined by Mann Kendall statistic

-  Increasing
-  Decreasing
-  No significant trend

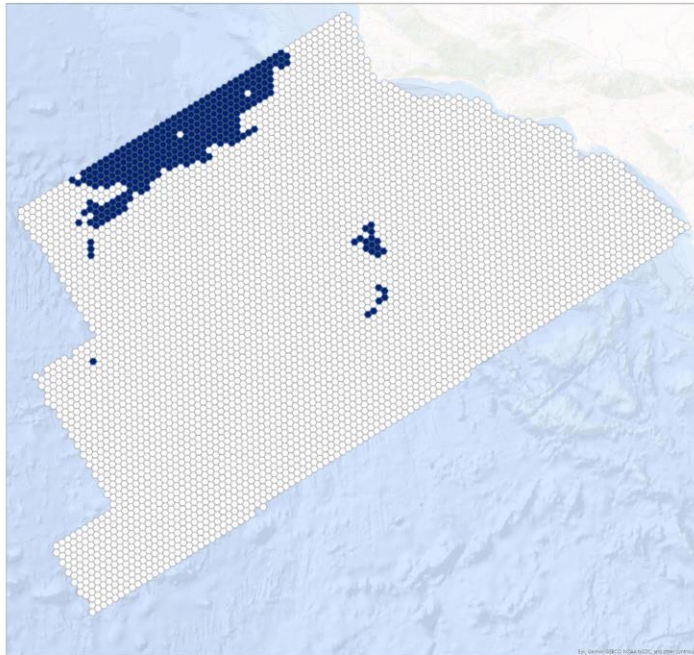
(Below) Temperature ($^{\circ}\text{C}$)

-  ≤ 3.00
-  ≤ 6.00
-  ≤ 9.00
-  ≤ 12.00
-  ≤ 15.00
-  ≤ 18.00
-  ≤ 21.00



1968  2018
Time (5-year means)

500m



(Left) Temperature trend over time, defined by Mann Kendall statistic

-  Increasing
-  Decreasing
-  No significant trend

(Below) Temperature ($^{\circ}\text{C}$)

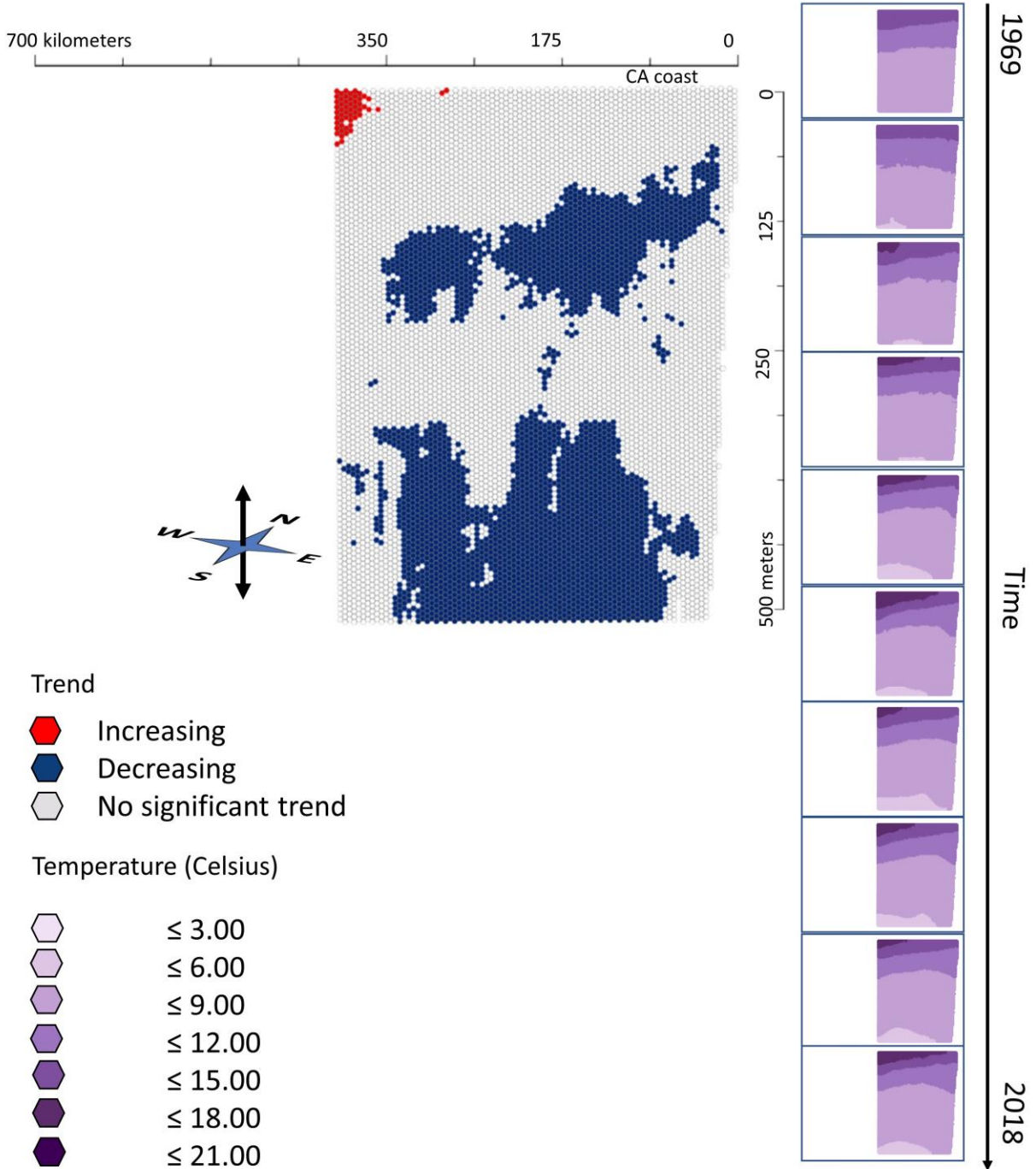
-  ≤ 3.00
-  ≤ 6.00
-  ≤ 9.00
-  ≤ 12.00
-  ≤ 15.00
-  ≤ 18.00
-  ≤ 21.00



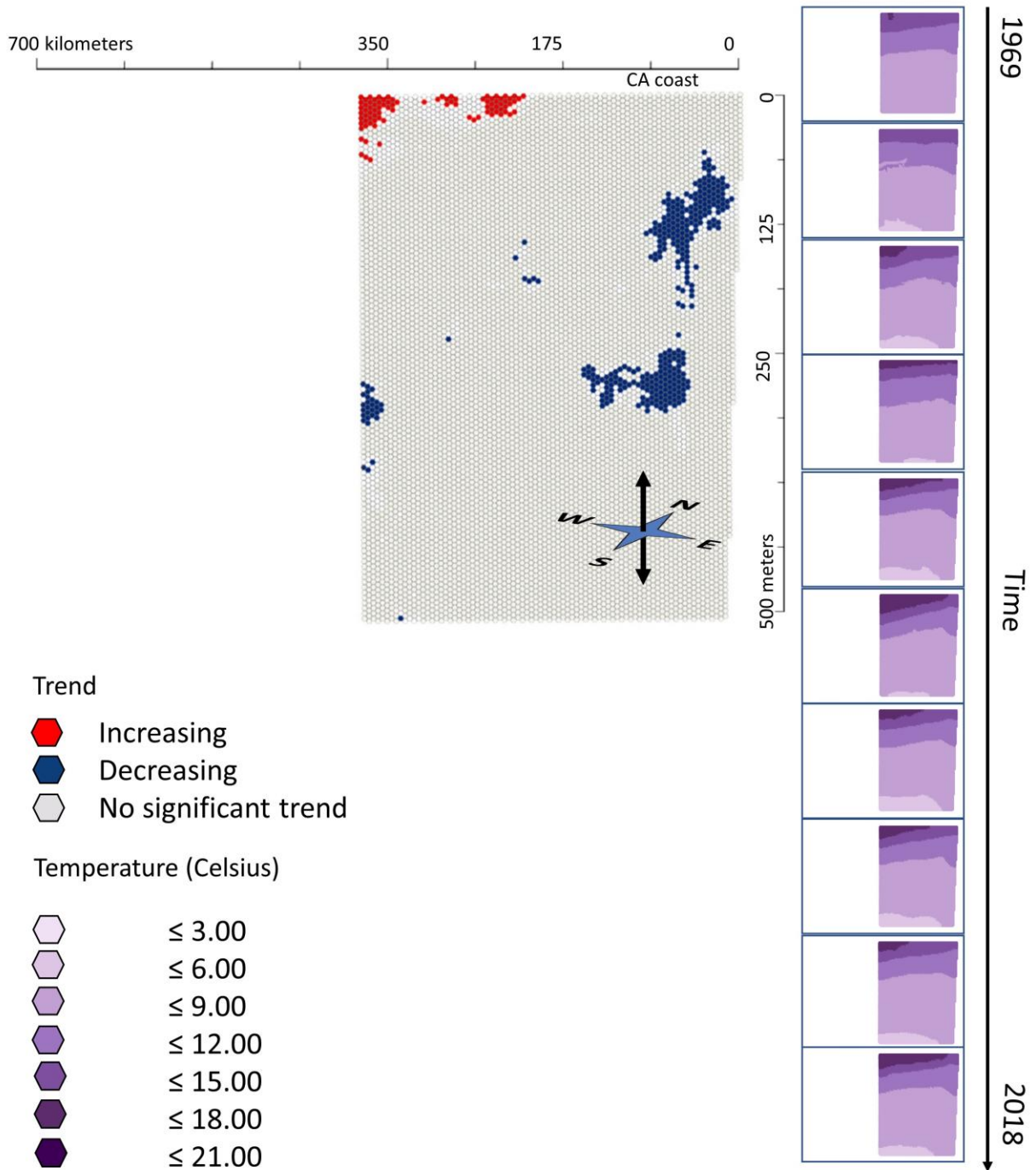
1968  2018
Time (5-year means)

Temperature 1969--2018 Vertical Cross Sections

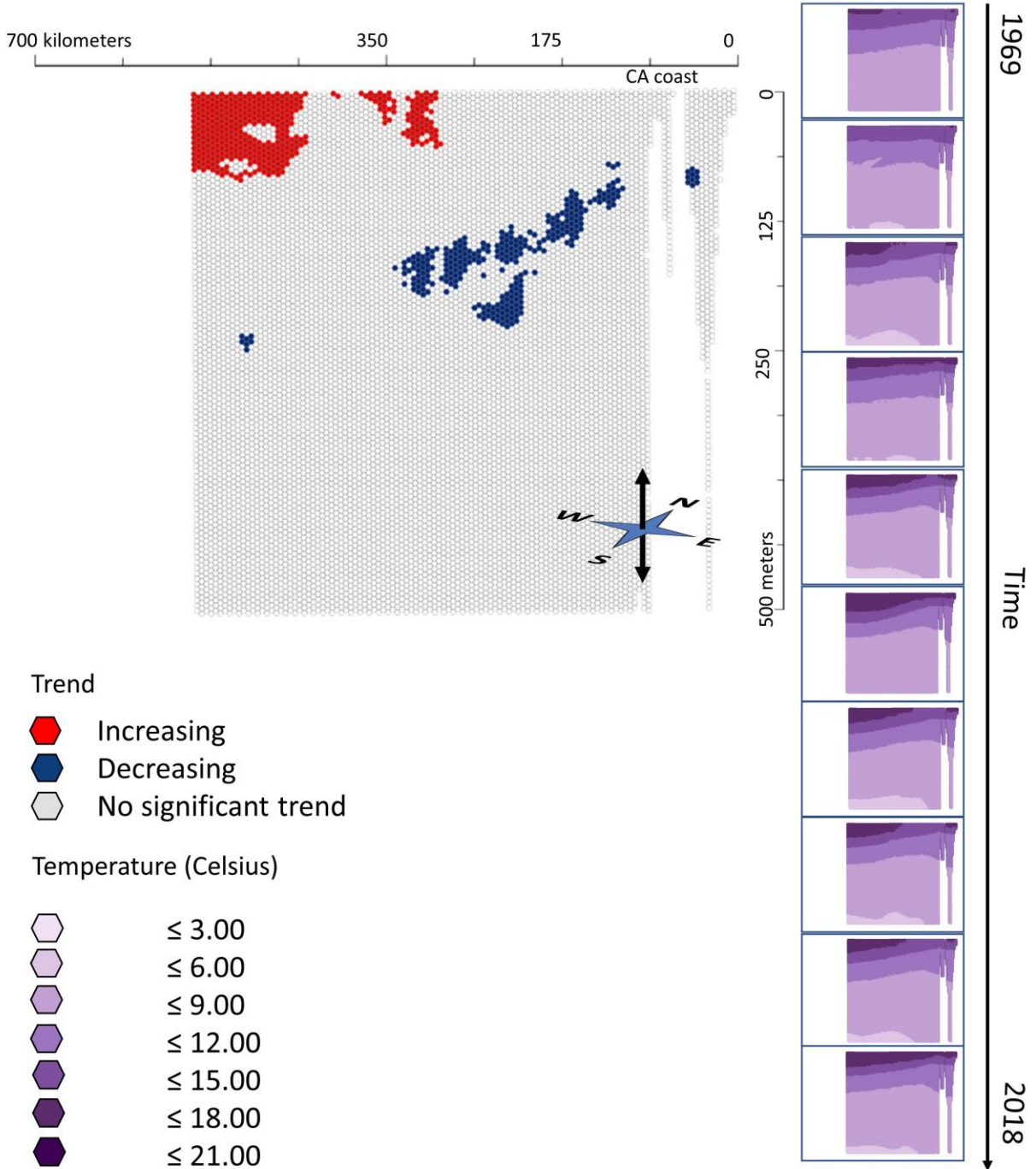
Line 77



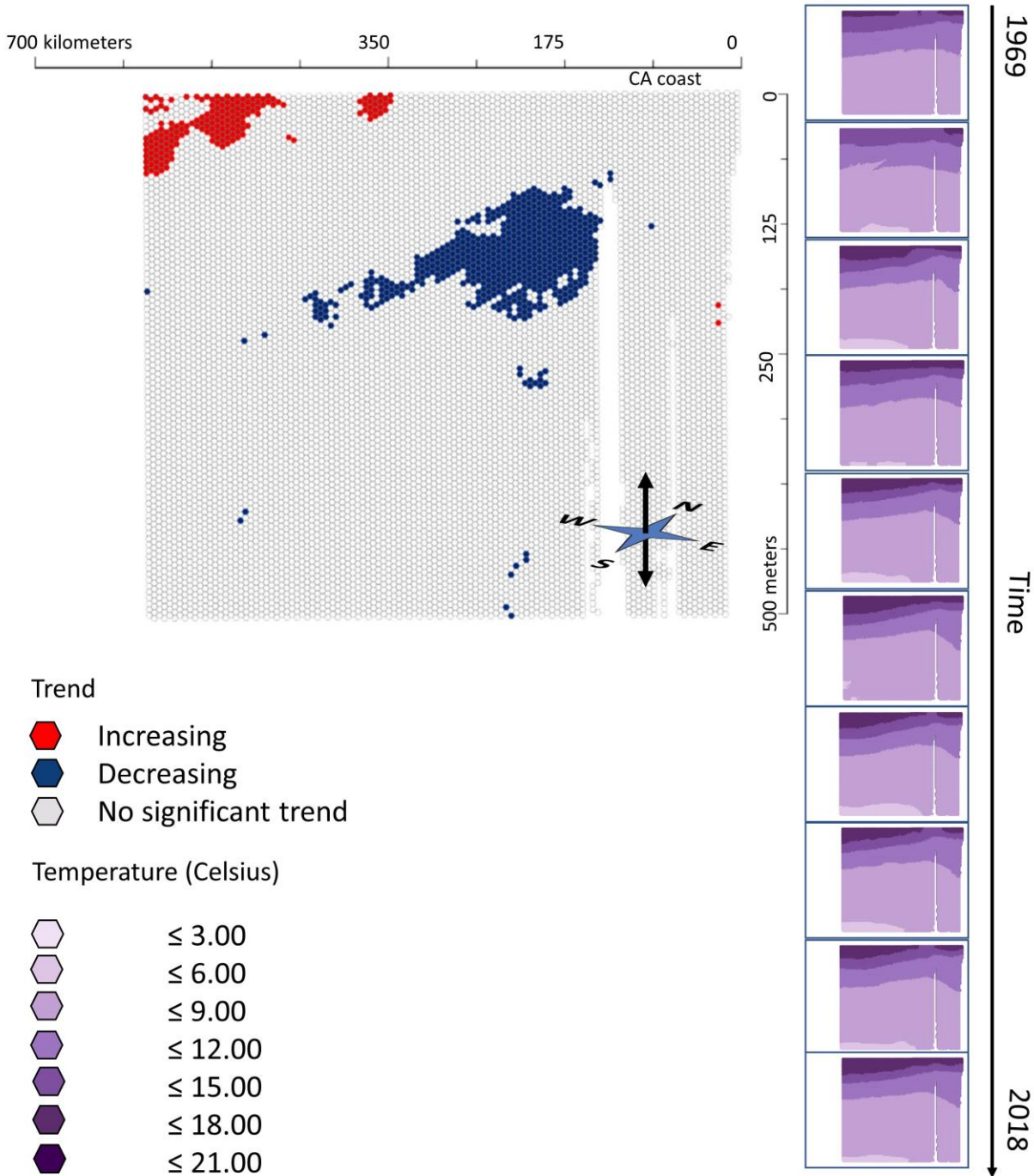
Line 80



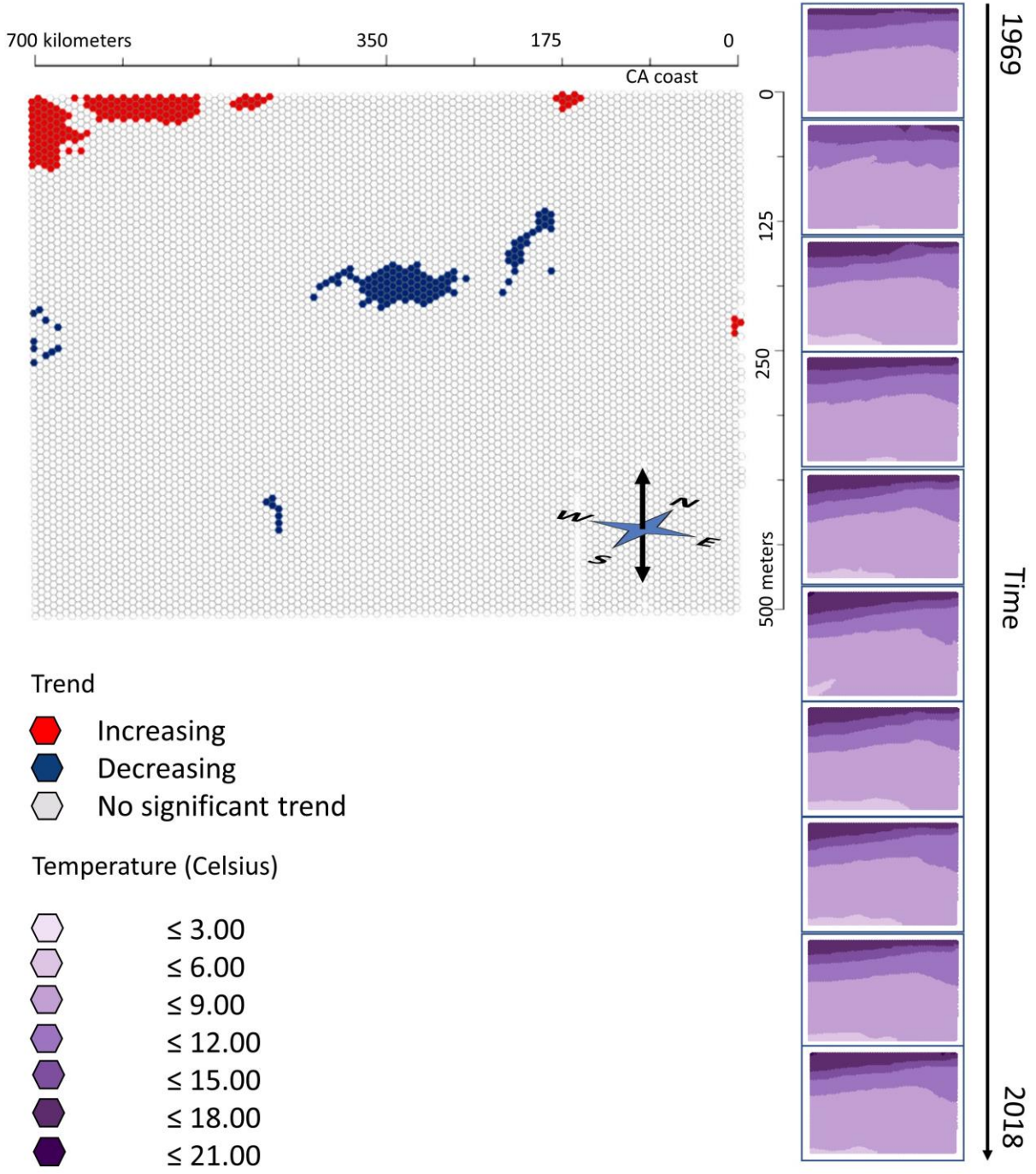
Line 83



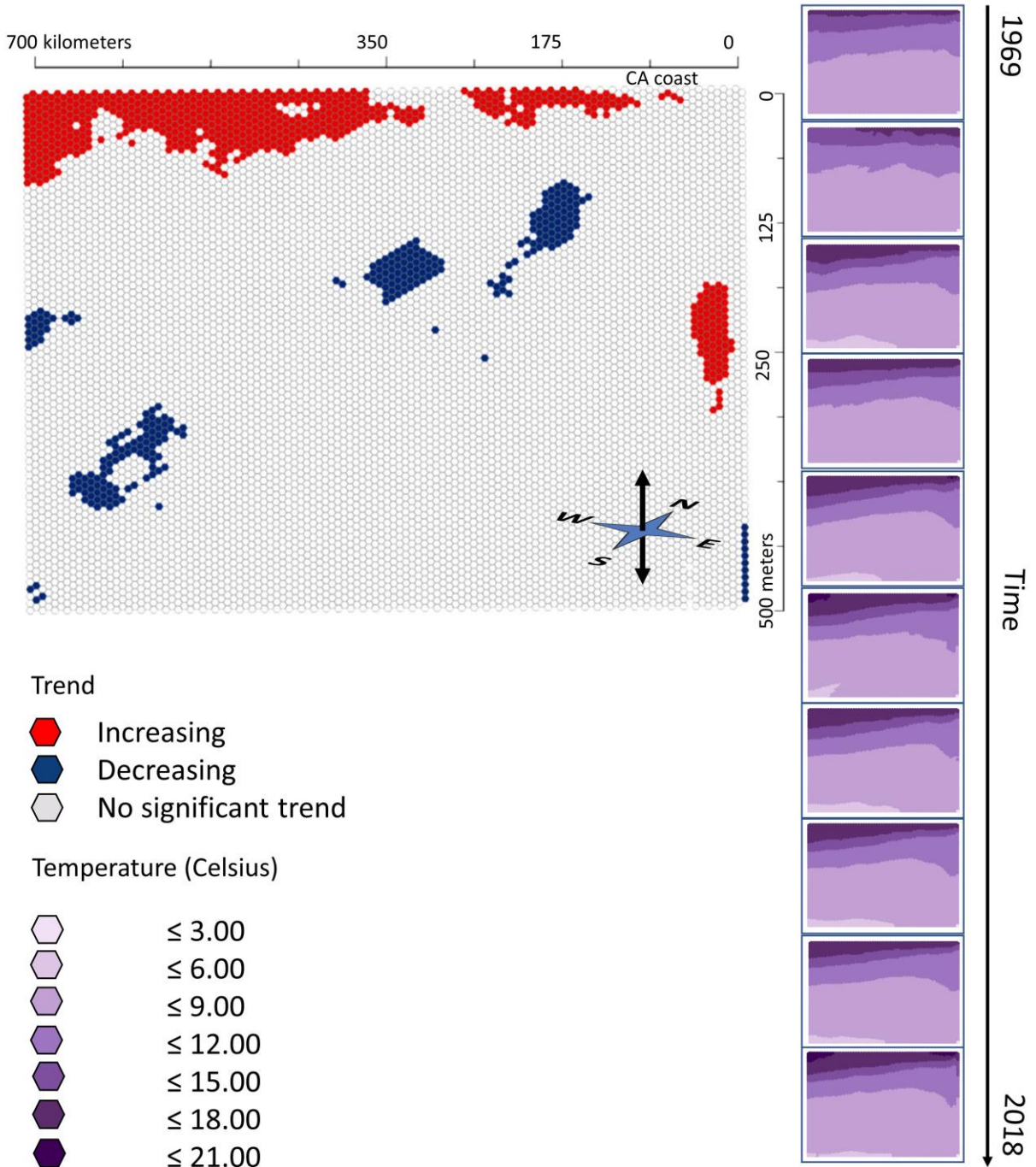
Line 87



Line 90

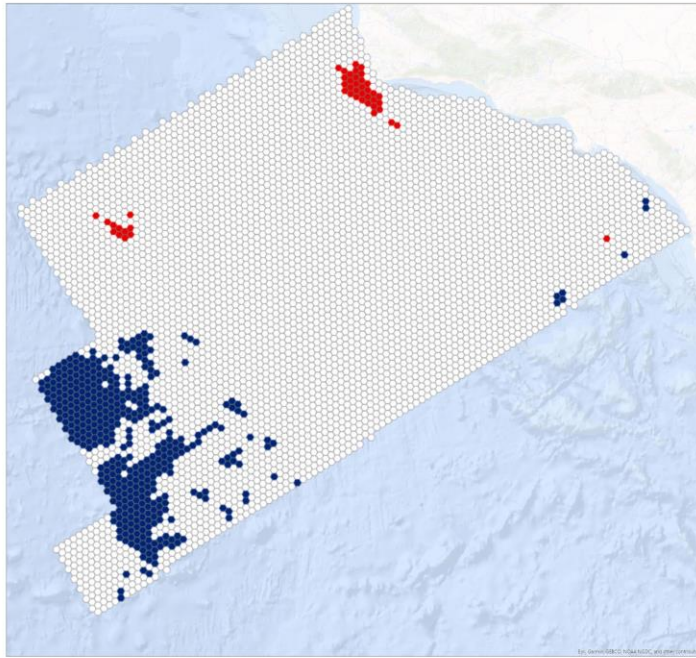


Line93



Nitrate 1985=-2017, Horizontal Cross Sections

0 m



(Left) Temperature trend over time, defined by Mann Kendall statistic

- Red hexagon: Increasing
- Blue hexagon: Decreasing
- White hexagon: No significant trend

(Below) Nitrate (micromol/liter)

- White hexagon: ≤ 6.00
- Light purple hexagon: ≤ 12.00
- Medium purple hexagon: ≤ 18.00
- Dark purple hexagon: ≤ 24.00
- Very dark purple hexagon: ≤ 30.00
- Black hexagon: ≤ 36.00
- Black hexagon: ≤ 42.00

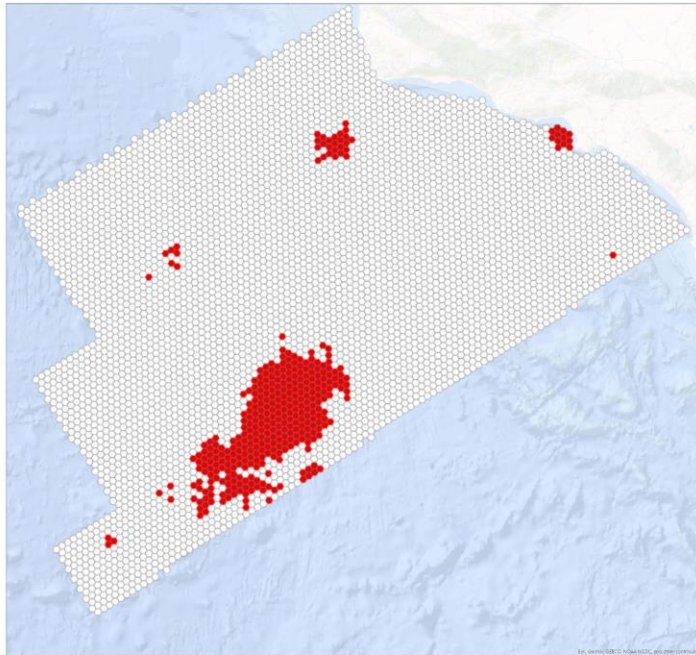


1985

Time (3-year means)

2017

100m



(Left) Temperature trend over time, defined by Mann Kendall statistic

-  Increasing
-  Decreasing
-  No significant trend

(Below) Nitrate (micromol/liter)

-  ≤ 6.00
-  ≤ 12.00
-  ≤ 18.00
-  ≤ 24.00
-  ≤ 30.00
-  ≤ 36.00
-  ≤ 42.00

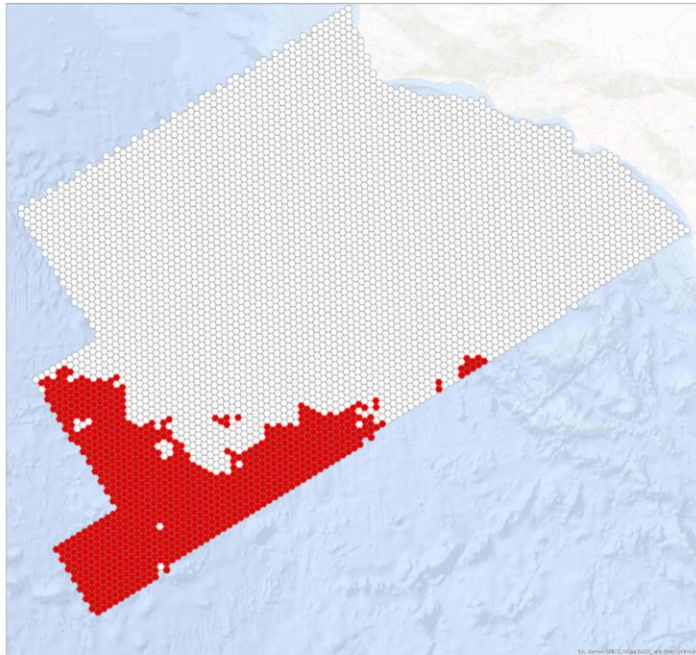


1985

Time (3-year means)

2017

200m



(Left) Temperature trend over time, defined by Mann Kendall statistic

-  Increasing
-  Decreasing
-  No significant trend

(Below) Nitrate (micromol/liter)

-  ≤ 6.00
-  ≤ 12.00
-  ≤ 18.00
-  ≤ 24.00
-  ≤ 30.00
-  ≤ 36.00
-  ≤ 42.00

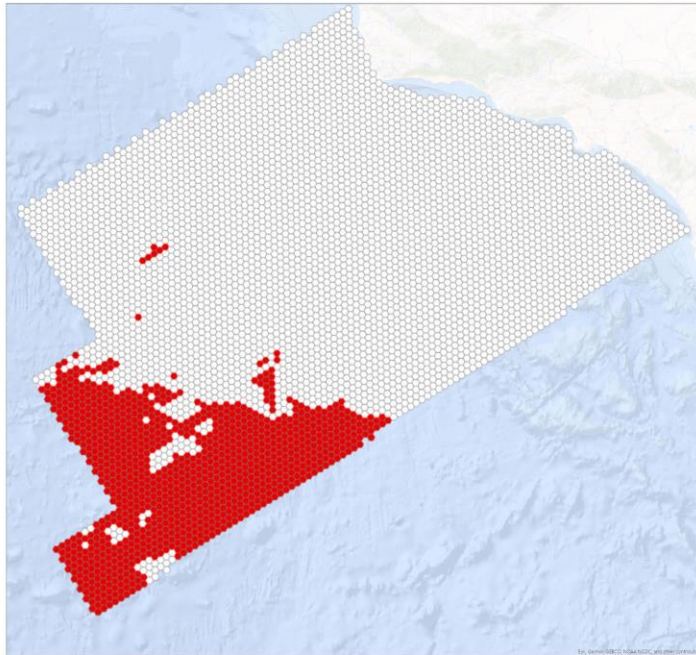


1985

Time (3-year means)

2017

300m



(Left) Temperature trend over time, defined by Mann Kendall statistic

-  Increasing
-  Decreasing
-  No significant trend

(Below) Nitrate (micromol/liter)

-  ≤ 6.00
-  ≤ 12.00
-  ≤ 18.00
-  ≤ 24.00
-  ≤ 30.00
-  ≤ 36.00
-  ≤ 42.00

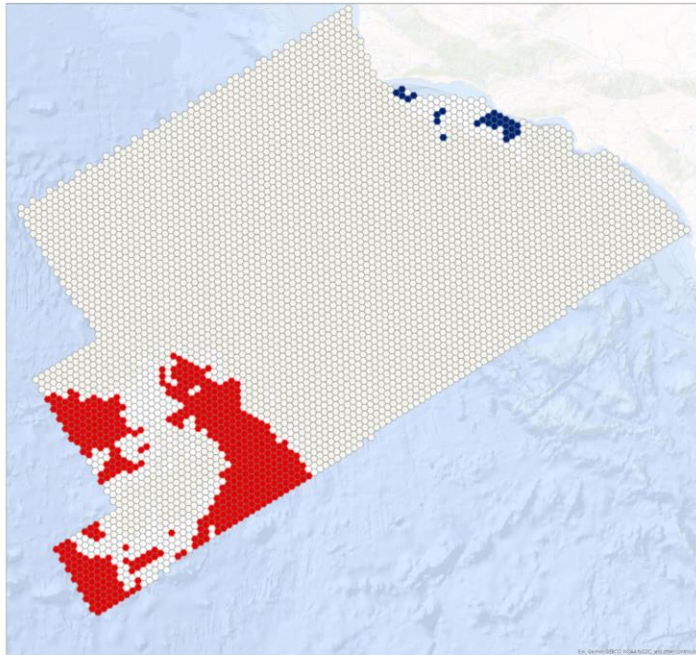


1985

Time (3-year means)

2017

400m



(Left) Temperature trend over time, defined by Mann Kendall statistic

-  Increasing
-  Decreasing
-  No significant trend

(Below) Nitrate (micromol/liter)

-  ≤ 6.00
-  ≤ 12.00
-  ≤ 18.00
-  ≤ 24.00
-  ≤ 30.00
-  ≤ 36.00
-  ≤ 42.00

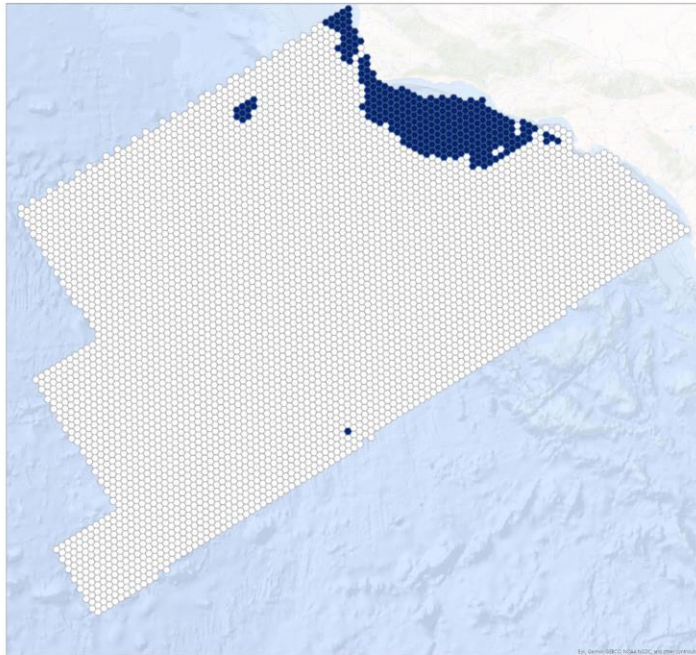


1985

Time (3-year means)

2017

500m



(Left) Temperature trend over time, defined by Mann Kendall statistic

-  Increasing
-  Decreasing
-  No significant trend

(Below) Nitrate (micromol/liter)

-  ≤ 6.00
-  ≤ 12.00
-  ≤ 18.00
-  ≤ 24.00
-  ≤ 30.00
-  ≤ 36.00
-  ≤ 42.00



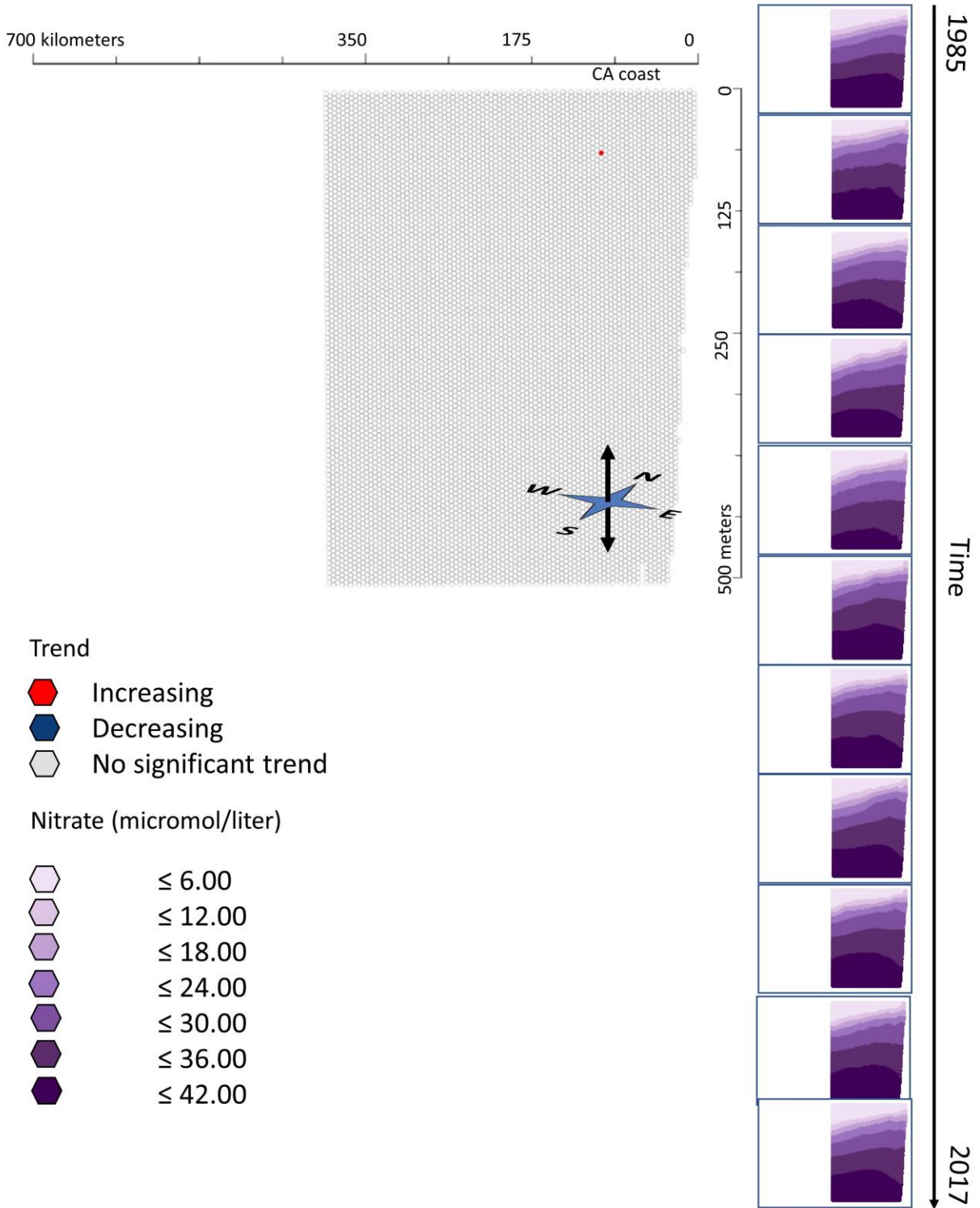
1985

Time (3-year means)

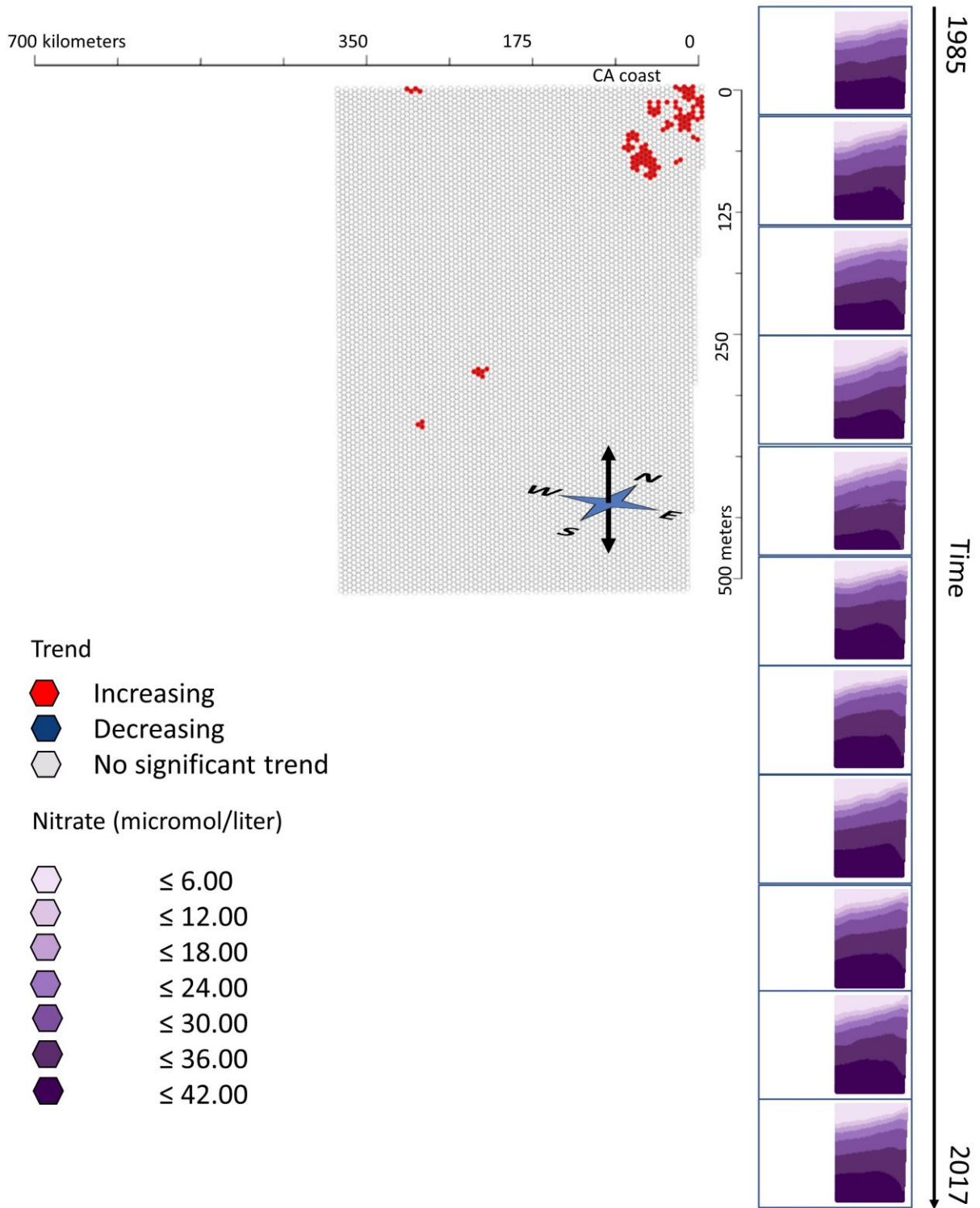
2017

Temperature 1985--2017 Vertical Cross Sections

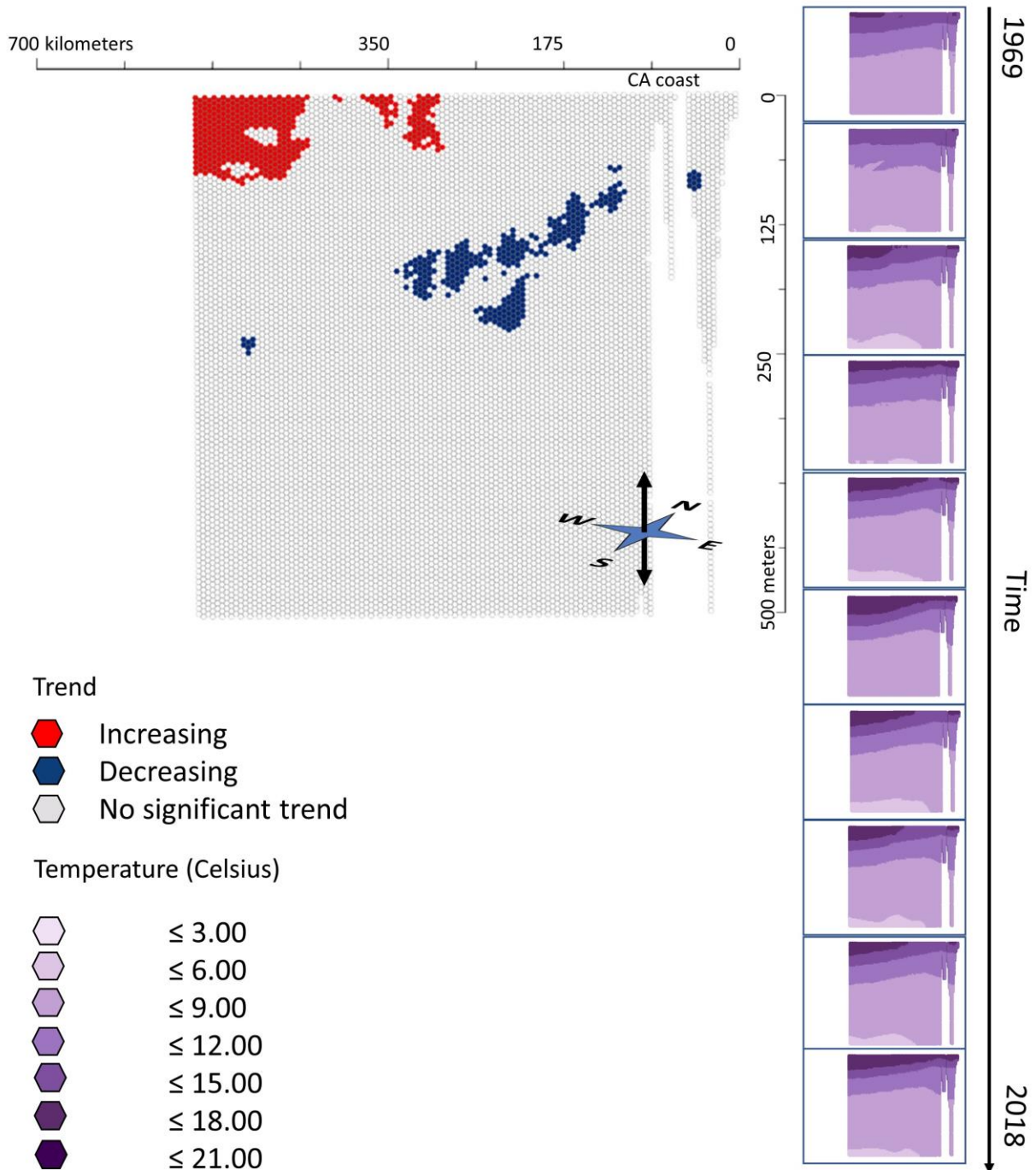
Line 77



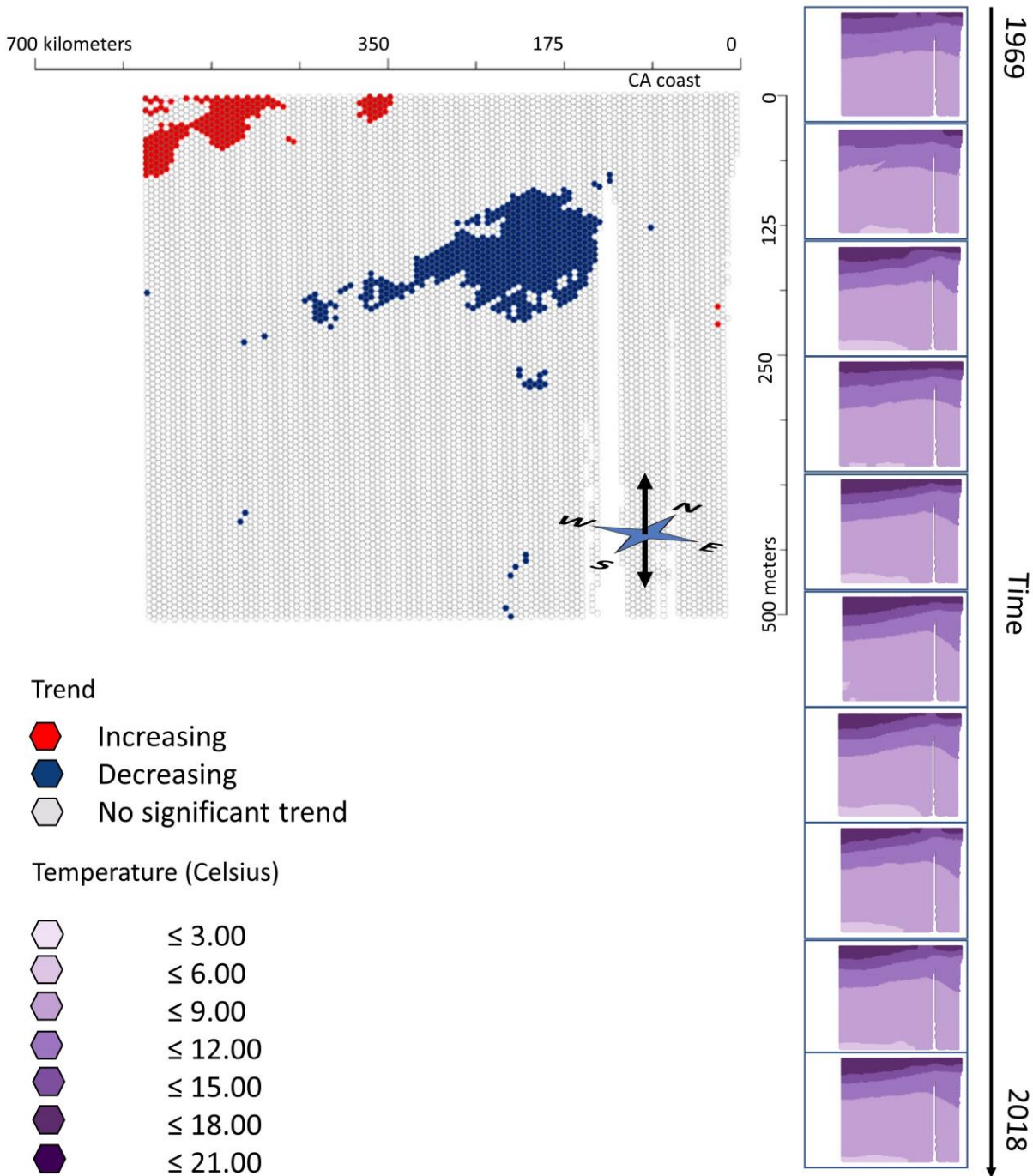
Line 80



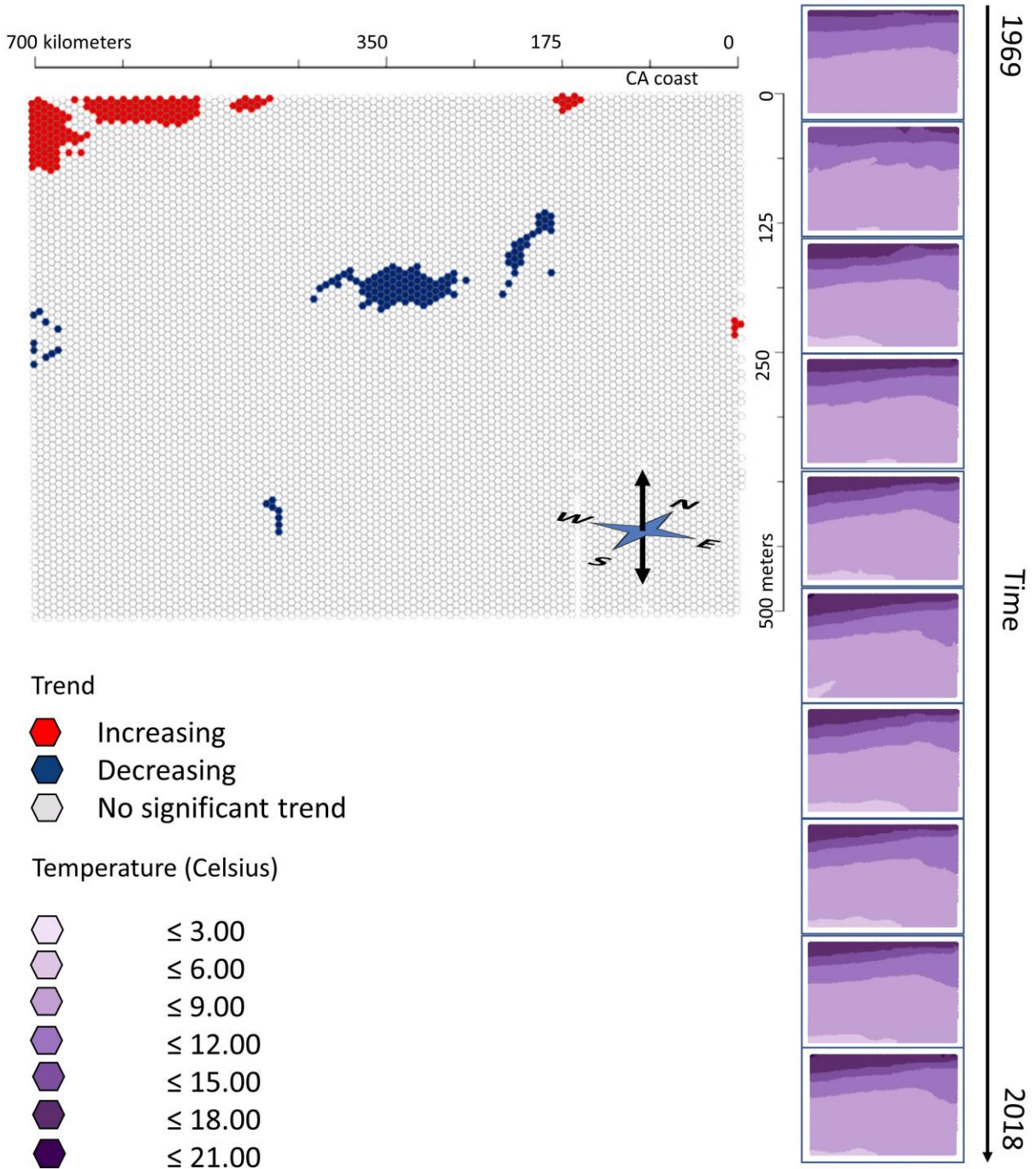
Line 83



Line 87



Line 90



Line93

